(NASA-CR-137531) ANALYTICAL MODELING OF INTUMESCENT COATING THERMAL PROTECTION SYSTEM IN A JP-5 FUEL FIRE ENVIRONMENT Final Report (Aerotherm Corp.) 87 p HC $7.50 CSCL 11C G3/18

N74-29016

Unclas 42955

Aerotherm Final Report 74-101

ANALYTICAL MODELING OF INTUMESCENT COATING THERMAL PROTECTION SYSTEM IN A JP-5 FUEL FIRE ENVIRONMENT

by

Kimble J. Clark
Allen B. Shimizu
Kurt E. Suchsland
Carl B. Moyer

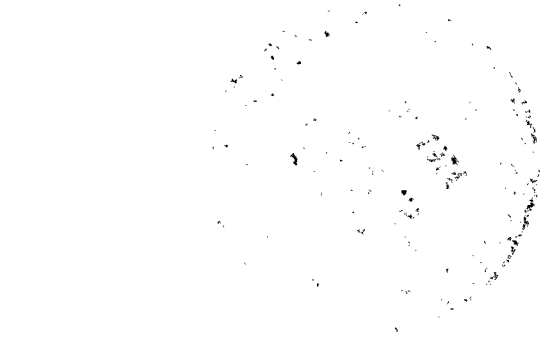

AEROTHERM
ACUREX Corporation

CR 137531
AVAILABLE TO THE PUBLIC

Aerotherm Project 7080

June 1974

Aerotherm Final Report 74-101

ANALYTICAL MODELING OF INTUMESCENT COATING THERMAL PROTECTION SYSTEM IN A JP-5 FUEL FIRE ENVIRONMENT

by

Kimble J. Clark
Allen B. Shimizu
Kurt E. Suchsland
Carl B. Moyer

Prepared for

National Aeronautics and Space Administration
Ames Research Center
Moffett Field, California 94035

Chemical Research Projects Office
S. R. Riccitiello
D. E. Cagliostro

Contract NAS2-7709

TABLE OF CONTENTS

LIST OF FIGURES

LIST OF FIGURES (Continued)

LIST OF TABLES

LIST OF SYMBOLS

GENERAL

A	area	ft^2
B_i	pre-exponential factor, Equation (2-14)	sec^{-1}
B'	$\dot{m}/\rho_e u_e C_M = (\dot{m}_g + \dot{m}_c)/\rho_e u_e C_M$	---
B'_c	dimensionless char rate, $\dot{m}_c/\rho_e u_e C_M$	---
B'_g	dimensionless pyrolysis gas rate $\dot{m}_g/\rho_e u_e C_M$	---
C_H	heat transfer Stanton number	---
C_M	mass transfer Stanton number	---
C_p	specific heat	Btu/lb°F
E_a	activation energy, Equation (2-14)	Btu/lb mol
E_f	local swell factor, Equation (3-1)	---
$E_{f_{max}}$	maximum expansion factor, Equation (3-1)	---
F	view factor	---
H_r	recovery enthalpy, $h_e + u_e^2/2$	Btu/lb
h	enthalpy (sensible plus chemical)	Btu/lb
h^T	enthalpy of formation at temperature T	Btu/lb
Δh_p	heat of formation of the virgin plastic	Btu/lb
Δh_c	heat of formation of the char	Btu/lb
$\bar{h}$	defined as $(\rho_p h_p - \rho_c h_c)/(\rho_p - \rho_c)$	Btu/lb

LIST OF SYMBOLS (CONTINUED)

$\tilde{j}_k$	total diffusional mass flux of element k regardless of molecular configuration	---
K_i	mass fraction of species i in a mixture	---
$\tilde{K}_k$	total mass fraction of element k regardless of molecular configuration	---
k	thermal conductivity	Btu/ft-°F-sec
$\dot{m}$	mass flow rate per unit area from surface	lb/ft^2sec
$\dot{m}_c$	mass flow rate of char from surface per unit surface area	lb/ft^2sec
$\dot{m}_g$	mass flow rate of pyrolysis gases out of surface per unit surface area	lb/ft^2sec
n	expansion exponent, Equation (3-1)	---
n_i	decomposition reaction order for i^{th} component, Equation (2-14)	---
P	static pressure	lb/ft^2
$\dot{q}_{chem}$	chemical energy rate term defined in Equation (2-15)	Btu/ft^2sec
$\dot{q}_{cond}$	rate of energy conduction into the ablating material	Btu/ft^2sec
$\dot{q}_{rad\ in}$	rate of radiant energy input to the ablating surface	Btu/ft^2sec
$\dot{q}_{rad\ out}$	rate of radiant energy emission from the ablating surface, equal to $F\sigma\varepsilon T_w^4$	Btu/ft^2sec
$\dot{q}_{sen}$	convective flux term defined in Equation (2-15)	Btu/ft^2sec
R	universal gas constant	Btu/lb mol °R

$\dot{s}$	surface recession rate due to thermochemical ablation	ft/sec
T	temperature	°R
u_e	velocity of gases at edge of boundary layer	ft/sec
v	convective velocity normal to surface	ft/sec
x	coordinate normal to ablating surface, fixed to receding surface, also virgin plastic mass fraction defined by Equation (2-12)	ft, ---
y	coordinate normal to ablating surface, origin fixed in space relative to back wall	ft

GREEK

α	absorptivity	---
Γ	volume fraction of resin in plastic, see Equation (2-13)	ft^3/resin/ ft^3material
θ	time	sec
ρ	density	lb/ft^3
ρ_o	initial density	lb/ft^3 resin or lb/ft^3 reinforcement
ρ_r	residual density in charred material	lb/ft^3 resin or lb/ft^3 reinforcement
σ	Stefan-Boltzmann constant	$Btu/ft^2\ sec°R^4$

SUBSCRIPTS

A	denotes one pyrolyzing component of resin

LIST OF SYMBOLS (CONCLUDED)

B	denotes second pyrolyzing component of resin
b	denotes backwall
C	denotes reinforcement
c	denotes char
e	denotes outer edge of boundary layer
f	denotes flame
g	denotes pyrolysis gas
i,j	species indexes
k	element index
o	original, initial
p	denotes virgin plastic
r	denotes residual density
w	denotes wall (heated surfaces)

SECTION 1

INTRODUCTION

Intumescent paints provide one promising method for temporary protection of surfaces exposed to heating from fires. These paints intumesce, or swell, when heated to temperatures in the range 350 to 500°F. Depending on the heating rate and other factors, a coating of intumescent paint can attain a final swelled thickness of five to 50 times its original, undecomposed thickness. The swelled, decomposed coating is low in density and thermal conductivity, so that it provides an effective insulation layer over the heat sensitive article.

Intumescent paints are currently being considered for protection of steel casings which contain explosive material. The goal here is to increase the reaction time, should the casing be exposed to a fire environment created by a nearby accident involving aviation fuel or other flammable substances. Reaction will occur when the backwall temperature of the steel casing exceeds some threshold value, typically 800-1000°R. A 0.060 inch bare steel plate, insulated at the backwall and exposed to a typical fire heat flux of 15 Btu/ft^2sec, will reach a backwall temperature of 1000°R in only 20 seconds. Application of a 0.080 inch intumescent coating can extend this time to 2-3 minutes. Such an increase in reaction time can be extremely beneficial in providing additional time for removal of the explosive item from the scene of the fire.

The Chemical Research Projects Office of NASA Ames has pioneered in the development of intumescent paints and rigid and semirigid foams for application as thermal protection systems (References 1, 2, 3, 4). Of particular interest in this study is Coating 313 (Reference 1) developed at CRPO, as applied to an explosive-containing steel casing for protection from JP-5 fuel fires. At present, two methods of utilization of Coating 313 are being considered: application directly to the steel substrate, and application over an intermediate inert insulation layer which is first bonded to the steel substrate. A major design question to be answered in this application is the following. Given the thermochemical properties of coating 313, the reaction temperature of the explosive material, and the impinging heat flux; what is the optimum combination of coating and insulation (if used) thicknesses which will provide maximum reaction time?

The purpose of the present study has been to develop an analytical tool for studying and predicting the thermochemical response of Coating 313 when exposed to a fuel fire environment. To achieve this objective, the existing Aerotherm Charring Material Thermal Response and Ablation (CMA) computer program has been modified to treat swelling materials. The modified code is now designated Aerotherm Transient Response of Intumescing Materials (TRIM) code. In addition, thermophysical property data for Coating 313 have been analyzed and reduced for use in the TRIM code, an input data sensitivity study has been performed, and performance tests of Coating 313/steel substrate models have been carried out. The end product of the study is a reliable computational model, the TRIM code, which has been thoroughly validated for Coating 313.

The remainder of this report has been divided into sections which are arranged to correspond to the chronological order in which the actual tasks were executed:

- Generation of Input Data
- Development of Swell Model and Implementation in Trim Code
- Sensitivity Study
- Acquisition of Experimental Data
- Comparisons of Predictions with Data
- Predictions with Intermediate Insulation

SECTION 2

GENERATION OF INPUT DATA

In order to carry out an analysis of the thermochemical response of a material which decomposes and ablates when exposed to a high-temperature environment, Aerotherm has developed a three-step calculation procedure. This procedure has been developed and refined over the past eight years at Aerotherm and applied successfully to many thermochemical ablation problems involving heat shields, nosetips, rocket nozzle throat inserts, etc. The present study represents the first time Aerotherm's calculation procedure has been applied to the intumescent paint problem.

The three basic steps involved in carrying out the analysis are the following (see Figure 2-1).

1. Calculate the heating environment
   a. Temperature, pressure, chemical composition
   b. Heat and mass transfer coefficients
   c. Radiation heat flux
2. Calculate a matrix of possible surface state solutions, satisfying simultaneously both mass balance and chemical equilibrium constraints
3. Solve the material indepth mass and energy balance equations, utilizing the solutions of 2 and a surface energy balance as the exposed-surface boundary conditions

2.1 COMPUTER CODES AND INPUT DATA REQUIREMENTS

The following discussion does not include detailed derivations of the various governing equations involved in the three-step analysis procedure, although most of these equations are presented, because such derivations are beyond the scope of this report. The derivations and more complete discussions of the theories can be found in the cited references.

Two environments are of interest in the present study:

- JP-5 Fuel Fire
- NASA Ames CRPO T-3 Facility

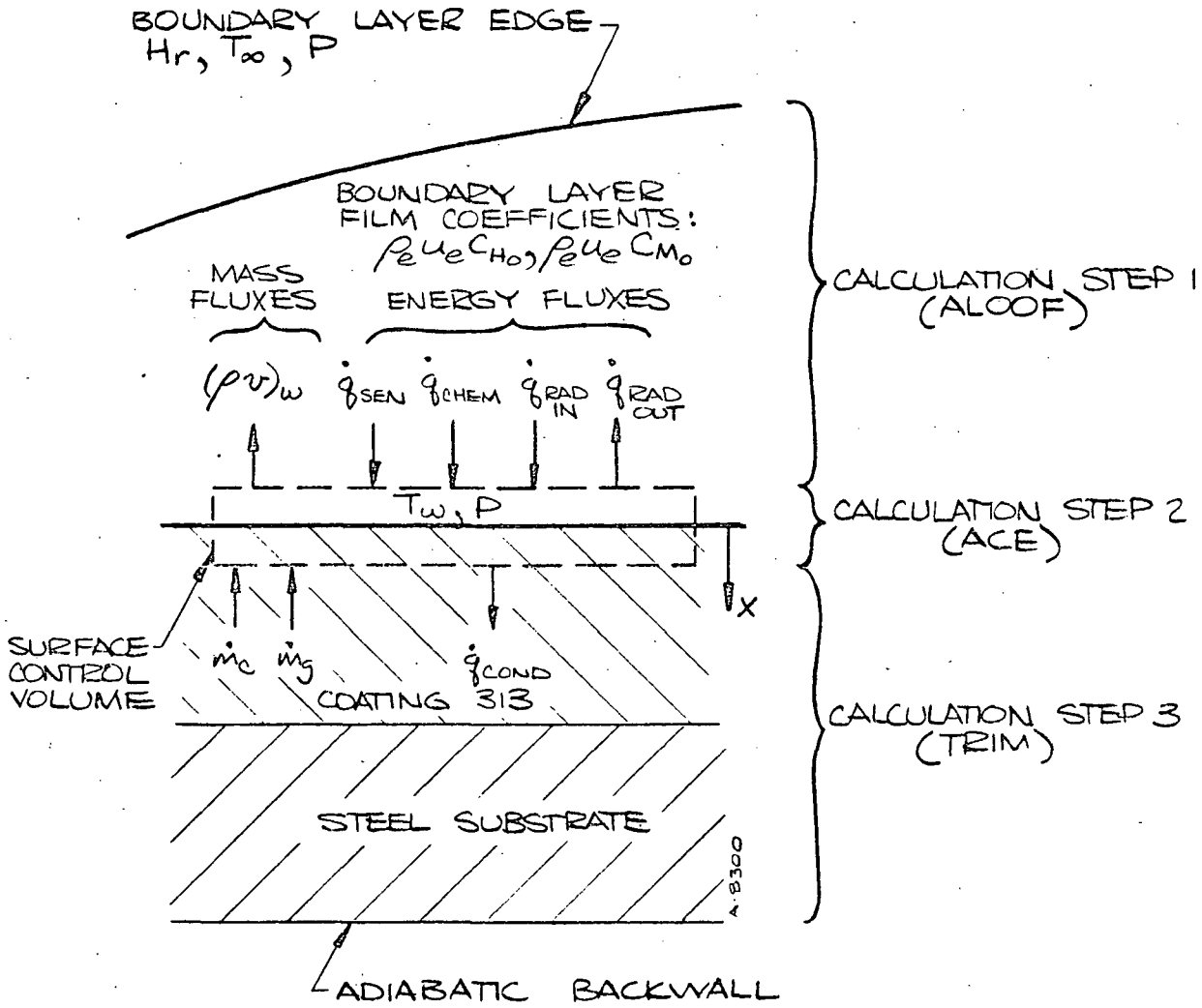

Figure 2-1. Schematic of Calculation Procedure for Predicting Material Thermochemical Response

As mentioned in Section 1, the JP-5 fuel fire environment is of concern in the eventual application of Coating 313. The thermochemical environment provided by the T-3 facility is also of interest, since tests of Coating 313 were carried out in the facility during the subject research program. In fact, it will be shown below that these two environments are essentially equivalent.

For either heating source, certain properties of the environment near the heated surface must be determined. These include temperature, convective velocity, and chemical composition. To determine the properties of a free-burning JP-5 fuel fire, the Aerotherm Large Open Pool Fire (ALOOF) code was used. The fire model used in this code is thoroughly documented in Reference 5, and the actual property values computed for this study are presented in the next subsection. Essentially, the ALOOF code solves one-dimensional conservation of mass, momentum, and energy equations for a free-burning fire, subject to the constraints of chemical equilibrium. The major energy loss in the fire column is radiation, and the rate of air entrainment is specified by a correlation based upon turbulent, strongly-buoyant fire plumes.

To determine the characteristics of the T-3 Facility environment, simple control volume mass and energy balance calculations on the furnace were carried out. These calculations are discussed in detail in Reference 6 and summarized in the following subsection. These environment calculations comprise the first step of the overall material response calculation procedure, as indicated in Figure 2-1.

Once the environment has been defined, the second step is to perform the surface state calculations. The Aerotherm Chemical Equilibrium (ACE) code was used for these calculations. The ACE code and underlying theory are described in detail in References 7 and 8. A second Aerotherm chemistry code which has wider circulation than the ACE code is the Aerotherm Equilibrium Surface Thermochemistry (EST) computer program, documented in Reference 9. Although the EST code has fewer options than the ACE code, it still has all the computational features necessary for the present study.

The ACE code solves an open system mass balance for a control volume attached to the heated surface (Figure 2-1), under the constraint that the mixture of ablation products and boundary layer gases immediately above the surface be in chemical equilibrium. Specifically, the elemental mass balance takes the form:

$$\tilde{j}_{k_w} + (\rho v)_w \tilde{K}_{k_w} = \dot{m}_g \tilde{K}_{k_g} + \dot{m}_c \tilde{K}_{k_c} \qquad (2\text{-}1)$$

where the elemental diffusive flux is

$$\tilde{j}_{k_w} = \rho_e u_e C_M (\tilde{K}_{k_w} - \tilde{K}_{k_e}) \tag{2-2}$$

Combining Equations (2-1) and (2-2) and normalizing with the mass transfer coefficient gives

$$(\tilde{K}_{k_w} - \tilde{K}_{k_e}) + \frac{(\rho v)_w}{\rho_e u_e C_M} \tilde{K}_{k_w} = B'_g \tilde{K}_{k_g} + B'_c \tilde{K}_{k_c} \tag{2-3}$$

where

$$B'_g = \frac{\dot{m}_g}{\rho_e u_e C_M} \quad , \quad B'_c = \frac{\dot{m}_c}{\rho_e u_e C_M} \tag{2-4}$$

The global surface mass balance is obtained by summing equation (2-1) over all elements in the system:

$$(\rho v)_w = \dot{m}_g + \dot{m}_c \tag{2-5}$$

which can be normalized to obtain

$$B' = \frac{(\rho v)_w}{\rho_e u_e C_M} = B'_g + B'_c \tag{2-6}$$

The first step of the overall calculation procedure, the environment definition, provides the elemental mass fractions at the boundary layer edge, $\tilde{K}_{k_e}$, and the static pressure, P. Then, if B'_g and B'_c are specified, and if thermochemical data for all candidate species are available, equations (2-3) and (2-6) can be solved, in conjunction with equilibrium law-of-mass-action equations for each possible chemical reaction, to yield the elemental mass fractions $\tilde{K}_{k_w}$ and all other mixture thermodynamic properties for the gas mixture adjacent to the surface. When this is done for a range of values of B'_g and B'_c, the second step of the calculation procedure is complete. The result is a matrix of surface state solutions which is used in the third and final step of the procedure.

In the present study, it was necessary to carry out the first and second steps of the calculation procedure only once. Having thus established the matrix of boundary conditions for the exposed surface, for the JP-5 fuel fire environment and restricting the surface to be Coating 313, it is not necessary to repeat these calculations each time the third step - the final material response prediction - is carried out (until another heating environment is tested).

The final step of the calculation process utilizes the TRIM code developed in the present study. As described in Section 3 below, the TRIM code is a modified version of the Aerotherm Charring Material Thermal Response and Ablation (CMA) code. The CMA code and underlying theory are documented in References 10 and 11. In a coordinate system attached to the exposed surface (which can be receding due to thermochemical ablation), the in-depth energy balance solved is the following:

$$\rho C_p \frac{\partial T}{\partial \theta}\Big)_x = \frac{1}{A} \frac{\partial}{\partial x} \left(kA \frac{\partial T}{\partial x}\Big)_\theta - \bar{h} \frac{\partial \rho}{\partial \theta}\Big)_x + \frac{\partial}{\partial x} (\rho h)_\theta \dot{s} + \frac{\dot{m}}{A} \frac{\partial h_g}{\partial x}\Big)_\theta + h_g \frac{\partial \rho}{\partial \theta}\Big)_y \qquad (2\text{-}7)$$

where

$$\bar{h} = \frac{\rho_p h_p - \rho_c h_c}{\rho_p - \rho_c} \qquad (2\text{-}8)$$

and

$$\dot{m} = - \int_y^{y_b} A \frac{\partial \rho}{\partial \theta}\Big)_y dy \qquad (2\text{-}9)$$

The terms in equation (2-7) represent, from left to right, the sensible energy accumulation, the net conduction, the chemical energy accumulation, net energy convected as a consequence of coordinate motion, net energy convected by the pyrolysis gases passing through, and the energy convected away by pyrolysis gases generated at the point. Coordinate x is attached to the surface with motion $\dot{s}$, coordinate y is referenced to the laboratory system, and subscripts p and c refer to virgin and fully-charred materials, respectively. A derivation of equation (2-7) is provided in Reference 11.

The net conduction term is equation (2-7) has been the major focus in the development of the TRIM code via modifications of the CMA code. A discussion of the alterations to this term required to treat the intumescing or swelling coating is postponed to Section 3, since the primary purpose of this section is to describe the overall computational procedure and input/output data flow. At this point, it suffices to say that a char swell model is required to properly treat the conduction term.

All in-depth material thermodynamic and transport properties are assumed to be a weighted average of the same properties for the virgin and fully-charred materials, which are input as functions of temperature. Thus,

$$C_p = x\, C_{p_p} + (1 - x) C_{p_c} \tag{2-10}$$

$$k = x\, k_p + (1 - x) k_c \tag{2-11}$$

where

$$x = \frac{\rho_p}{\rho_p - \rho_c}\left(1 - \frac{\rho_c}{\rho}\right) \tag{2-12}$$

The indepth solid material enthalpy h is obtained by integrating equation (2-10) over temperature, and adding the char and virgin material heats of formation, Δh_c and Δh_p. The pyrolysis gas enthalpy h_g is obtained from a separate ACE calculation.

The local instantaneous density ρ in equation (2-12) is assumed to be composite density given by

$$\rho = \Gamma(\rho_A + \rho_B) + (1 - \Gamma)\rho_c \tag{2-13}$$

Equation (2-13) is based upon the premise that many decomposing, char-forming materials appear to behave as three independently pyrolyzing components: a two-component resin filler, A and B, and a reinforcing material, C. The resin volume fraction Γ is presumed to be a known quantity. Each of the three components is allowed to decompose according to the following relation:

$$\left(\frac{\partial \rho_i}{\partial \theta}\right)_y = -B_i \exp(-E_{a_i}/RT)\,\rho_{o_i}\left(\frac{\rho_i - \rho_{r_i}}{\rho_{o_i}}\right)^{n_i} \tag{2-14}$$

The quantities B_i, E_{a_i}, n_i, ρ_{o_i}, and ρ_{r_i}; i = A, B, C, are input to the computer program.

In the TRIM code, the indepth energy and mass balance equations, equations (2-7) and (2-14), are solved subject to the following surface energy balance boundary condition (see Figure 2-1):

$$\underbrace{\rho_e u_e C_H (H_r - h_{e_w})}_{\dot{q}_{sen}} + \underbrace{\rho_e u_e C_M \left[\sum_i (K_{i_e} - K_{i_w}) h_i^{T_w} - B' h_w \right]}_{\dot{q}_{chem}} + \dot{m}_c h_c + \dot{m}_g h_g \tag{2-15}$$

$$+ \underbrace{\alpha_w \dot{q}_{rad}}_{\substack{\dot{q}_{rad} \\ in}} - \underbrace{F\sigma\varepsilon_w T_w^4}_{\substack{\dot{q}_{rad} \\ out}} - \dot{q}_{cond} = 0$$

Recall that $\rho_e u_e C_H$, $\rho_e u_e C_M$, H_r, K_{i_e}, P, and $\dot{q}_{rad}$ are determined from the environment definition calculations carried out in the first step of the overall procedure; and that h_{e_w}, $h_i^{T_w}$, K_{i_w}, and T_w are determined as functions of B'_c, B'_g, and P from the ACE calculations in step two.

So far only the response of the decomposing material, such as Coating 313 or other intumescing materials, has been discussed. The TRIM code, of course, also includes provisions for treating the thermal response of the nondecomposing backup materials which, in this study, are an inert intermediate insulation and the steel substrate. In passing from one material to the next, the conduction heat flux must be continuous. The governing equations of the overall composite of coating/insulation/substrate are solved subject to a specified backwall boundary condition, which is an adiabatic wall in all cases of interest here. The only backup material thermophysical properties required are density, specific heat, and thermal conductivity as functions of temperature.

The TRIM code provides numerous output quantities. A major portion of the output is identical to that provided by the CMA code and is therefore discussed in Reference 10. Of primary interest here are the temperature profile from exposed surface to backwall, and the density profile in the decomposing material (Coating 313).

In the preceding paragraphs, the standard Aerotherm calculation procedure for analyzing material thermochemical response has been briefly outlined. Appendix A presents a flowchart illustrating the interrelationships of the computer codes involved and the input and output data associated with each code.

2.2 INPUT DATA FOR THE COATING 313/JP-5 FUEL FIRE PROBLEM

As described in Section 2.1, the first step in the material response analysis is to define the environment. The fuel fire environment used in this study was taken from Reference 5, in which the ALOOF code was utilized. These calculations assume the fuel composition and heat of formation to be that of JP-4 fuel. In this work, it is assumed that the fuel composition and heat of formation for JP-5 fuel, the fuel of interest here, are similar to those for JP-4 fuel. It appears that the major difference between these two fuels is the minimum flash point, which is -20°F for JP-4 and 140°F for JP-5 (Reference 12). This effects mainly ignition characteristics, and would not be expected to significantly influence the steady-state combustion characteristics. In addition, the fire base diameter was taken as 30 ft, the fuel burning rate was 0.0149 lbm/ft^{2}sec, the entrainment coefficient was 0.17, the static pressure was one atmosphere, and the flame emissivity was unity.

The resulting calculated environment is typical of large, free-burning aviation fuel fires; flame temperature of 2390°R, air/fuel ratio of 7.3, and maximum upward convective velocity of 50 ft/sec. Corresponding to this environment, the following TRIM input quantities were calculated:

- $\dot{q}_{rad}$ = 15.52 Btu/ft^{2}sec
- H_r = -281 Btu/lbm (JANAF (Reference 13) Thermochemical base state)
- $\rho_e u_e C_H$ = 0.00761 lbm/ft^{2}sec

The convection heat transfer coefficient $\rho_e u_e C_H$ was estimated using a correlation available in Reference 14 for the average transfer coefficient over a cylinder in crossflow. A cylinder diameter of one foot was assumed; and flame properties computed by ACE were utilized in the correlations.

For the T-3 furnace environment, the calculations of Reference 6 were utilized. From known values of the furnace operating parameters, including fuel flowrate, furnace wall area and temperature, and flame temperature, a system energy balance was solved to obtain the air/fuel ratio and, thus, the flame chemical composition. The flame temperature has been measured and found to be 2000-2150°F. The wall temperature is somewhat lower, measurements falling in the range 1700-1900°F. The nominal fuel flowrate is 0.9 gal/hr. Inserting these values into the energy balance and estimating the conduction loss through the walls of the furance, the air/fuel mass ratio was calculated to be 10.0. As in the actual free-burning fire, this is a fuel-rich ratio, since the stoichiometric air/fuel mass ratio for JP-4 fuel is 14.6.

Using the above properties of the T-3 furnace environment, the following TRIM input quantities were calculated:

- $\dot{q}_{rad}$ = 10.4 - 14.8 Btu/ft^{2}sec
- H_r = -445 Btu/lbm (JANAF Thermochemical base state)
- $\rho_e u_e C_H$ = 0.00057 lbm/ft^{2}sec

The radiation heat flux range corresponds to the wall temperature range 1700-1900°F, since essentially all of the radiation comes from the furnace walls. Negligible radiation is emitted from the combustion gases because the path length is relatively short - on the order of one foot. The convection heat transfer coefficient $\rho_e u_e C_H$ was estimated for the top of the furnace where the model is located. A flat-plate correlation from Reference 15 was used, in conjunction with flame properties calculated by ACE.

As discussed in Section 2.1, the second step in the calculation procedure utilizes the ACE code. The edge-gas temperature, pressure, and composition are provided by the ALOOF or T-3 Facility calculations just described. The virgin material and char elemental compositions for Coating 313 were provided by NASA Ames CRPO (Reference 16). The pyrolysis gas composition was calculated from the known virgin and char elemental compositions and the specification that 54% by mass of the char is comprised of virgin material, and all Si in the virgin material remains in the char. Table 2-1 summarizes the elemental compositions for the virgin material, char, and pyrolysis gas.

As indicated in Appendix A, the elemental compositions of the edge gas, char, and pyrolysis gas are input to the ACE code, along with an array of values of B'_g and B'_c and the thermochemical state of the edge gas ($\tilde{K}_{k_e}$, P, T_e). In addition, thermochemical data for 128 molecular species containing one or more of the elements C, H, O, N, S, and Si were input to the code. For the fuel-rich environments of both the free-burning fire and the T-3 facility, the equilibrium calculations indicate that char consumption (B'_c) is negligible for all surface temperatures of interest. That is, negligible amounts of carbon oxides are formed, and carbon sublimation is also negligible for the low surface temperature regime of interest ($T_w \leq 2500°R$). Figure 2-2 presents a plot of h_w versus T_w for various values of the pyrolysis gas evolution rate, B'_g, where

$$h_w = \sum_i K_{i_w} h_i^{T_w} \qquad (2\text{-}16)$$

TABLE 2-1
COATING 313 ELEMENTAL COMPOSITIONS

Element	Mass Fractions		
	Virgin Material	Char	Pyrolysis Gas
C	0.3660	0.5994	0.1282
H	0.0510	0.0213	0.0839
O	0.3129	0.1650	0.4782
N	0.1090	0.1020	0.1194
S	0.1230	0.0627	0.1902
Si	0.0421	0.0496	0.0000

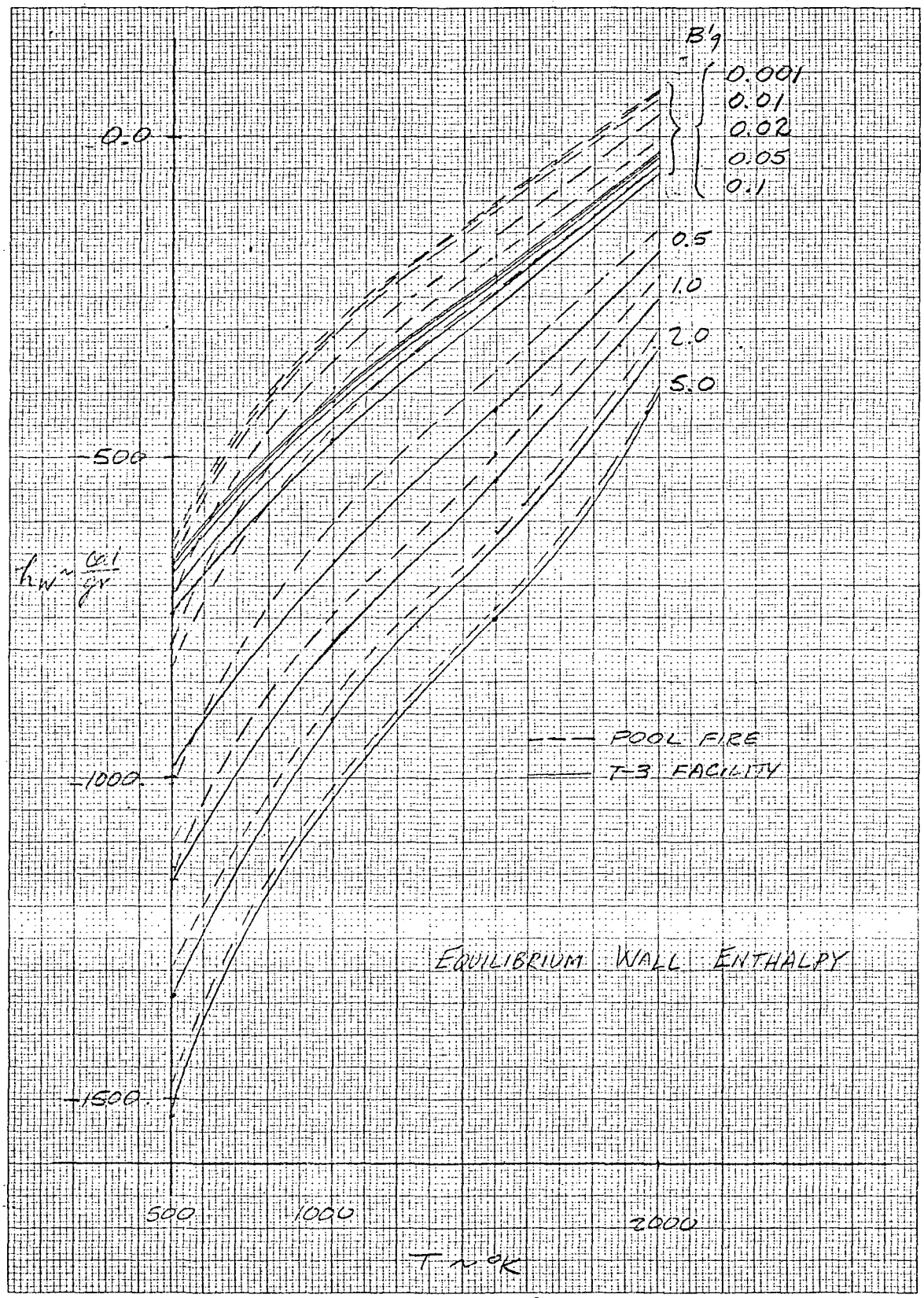
B'g
0.001
0.01
0.02
0.05
0.1
0.5
1.0
2.0
5.0
0.0
-500
-1000
-1500
$h_w \sim \frac{cal}{gr}$
POOL FIRE
T-3 FACILITY
EQUILIBRIUM WALL ENTHALPY
500
1000
2000
T ~ °K

Figure 2-2

Examination of this plot reveals that the difference between the h_w curves for the two environments considered is small, which is a result of the similar air/fuel ratios. In addition, calculations carried out for both environments indicated that convection heat transfer rarely exceeded 1.5 to 2.0 Btu/ft^{2}sec, which is considerably smaller than the radiation heat flux in either case. Thus, the two environments are essentially equivalent in terms of both total heat flux and chemistry.

ACE is also used to compute the equilibrium pyrolysis gas enthalpy as a function of temperature, for input to the TRIM code. Figure 2-3 presents $h_g(T)$, using the pyrolysis gas elemental composition presented in Table 2-1.

The final input data to be discussed are those required by the TRIM code. The major effort here was in the reduction of TGA data provided by CRPO for Coating 313, to obtain the material decomposition kinetics constants (input data catagory 1 in Figure 2-2). TGA data for two temperature rise rates, 6°C per minute and 10°C per minute, were provided.

It was obvious from these TGA's that a number of reactions are required to describe decomposition. Reference 1 indicates the decomposition steps for the 313 intrumescent agent. CMA, from which TRIM derives, allows only three reactions. Therefore, the TGA was divided into three reactions which either ignored or attempted to lump reactions together.

The 6°C/min heating rate TGA for Coating 313 in N_2 was used for the correlation - see Figure 2-4. The quantities $\partial\rho_i/\partial\theta$, ρ_i, ρ_{r_i}, and ρ_{o_i} were determined for each of the three reactions, assuming the resin volume fraction to be 0.50 (Equation 2-13). Using a temperature in the middle range of each reaction as a reference, the value of $\Delta\ell n(-\partial\rho_i/\partial\theta)$, $\Delta\ell n(\rho_i-\rho_{r_i}/\rho_{o_i})$, and $\Delta(1/T)$ were found at the various temperatures and

$$\frac{\Delta\ell n\left(-\frac{\partial\rho_i}{\partial\theta}\right)}{\Delta\ell n\left(\frac{\rho_i - \rho_{r_i}}{\rho_{o_i}}\right)}$$

was plotted versus

$$\frac{\Delta\left(\frac{1}{T}\right)}{\Delta\ell n\left(\frac{\rho_i - \rho_{r_i}}{\rho_{o_i}}\right)}.$$

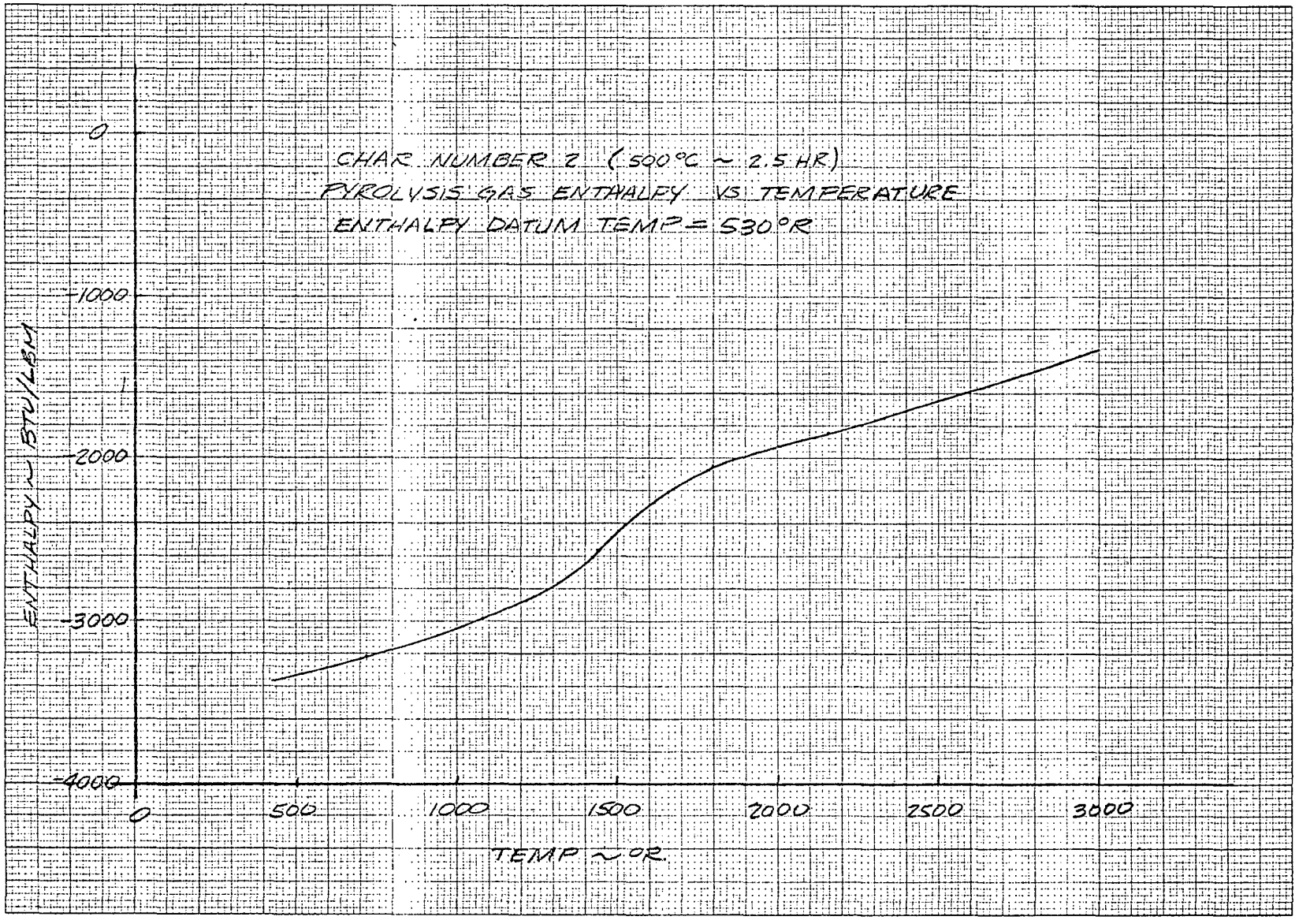
CHAR NUMBER 2 (500°C ~ 2.5 HR)
PYROLYSIS GAS ENTHALPY VS TEMPERATURE
ENTHALPY DATUM TEMP = 530°R
ENTHALPY ~ BTU/LBM
0
-1000
-2000
-3000
-4000
0
500
1000
1500
2000
2500
3000
TEMP ~ °R

Figure 2-3

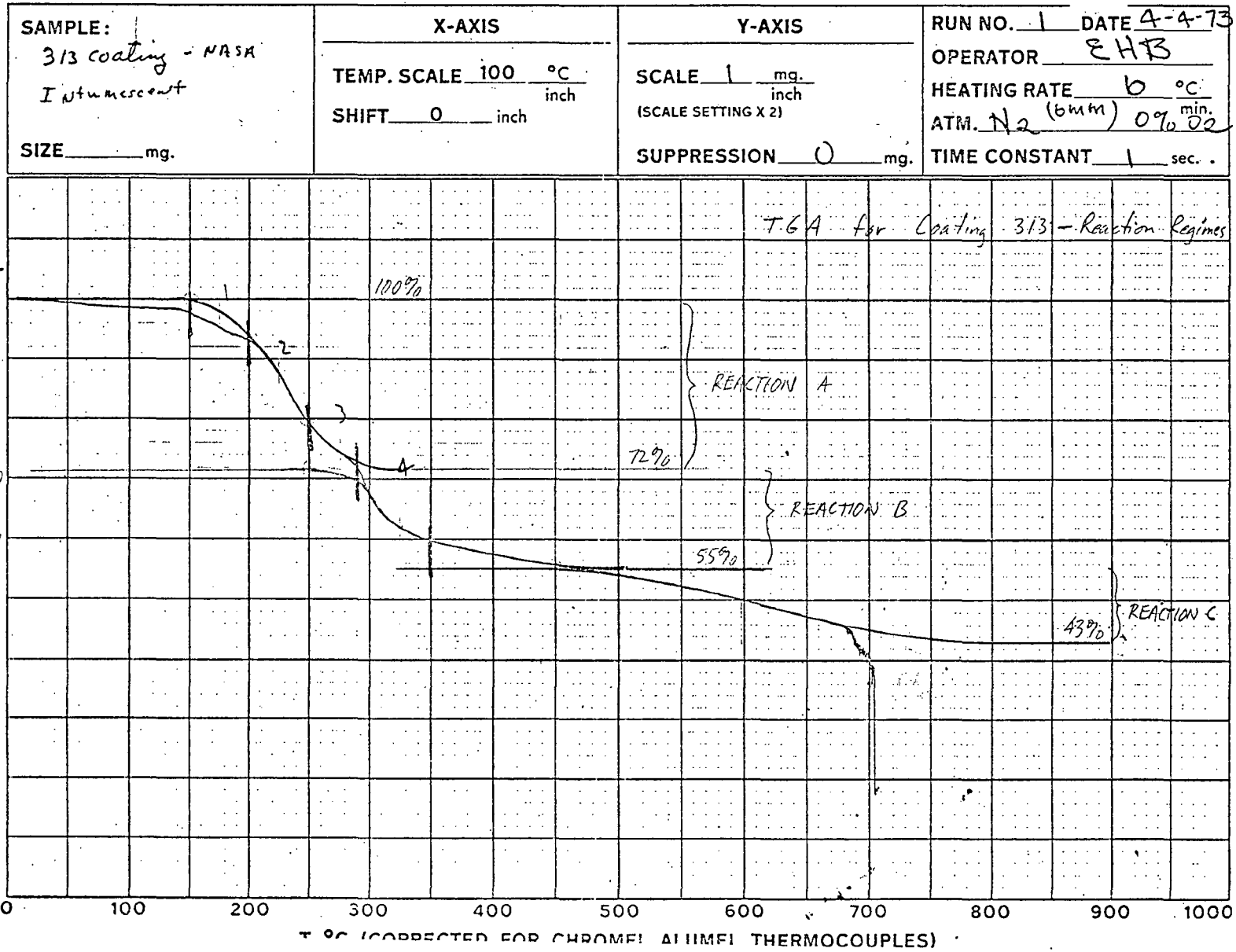
SAMPLE:
313 coating - NASA
Intumescent
SIZE mg.
X-AXIS
TEMP. SCALE 100 °C / inch
SHIFT 0 inch
Y-AXIS
SCALE 1 mg. / inch
(SCALE SETTING X 2)
SUPPRESSION 0 mg.
RUN NO. 1 DATE 4-4-73
OPERATOR EHB
HEATING RATE 6 °C / min.
ATM. N2 (6 mm) 0% O2
TIME CONSTANT 1 sec.
T.G.A. for Coating 313 - Reaction Regimes
100%
72%
55%
43%
REACTION A
REACTION B
REACTION C
WEIGHT, mg.
100
90
80
70
60
50
40
30
20
10
0
0
100
200
300
400
500
600
700
800
900
1000
T °C (CORRECTED FOR CHROMEL ALUMEL THERMOCOUPLES)

Figure 2-4

The slope of the resulting line is (-E/R) and the intercept is n_i for the decomposition equation in TRIM (Equation (2-14)).

Due to the problem of attempting to fit two reactions into one, the above plot for the second reaction was not linear and there was a large amount of scatter. Thus, the lower two temperature data points alone were used in determining E_{a_i} and n_i. Values of B_i were calculated for several points in each reaction and an average value of B_i was used for each.

In order to validate the decomposition kinetics constants backed out from the above analysis of the TGA data, two CMA runs were executed which simulated the actual TGA experiment. This was done by specifying a temperature rise rate in the code equal to that in the TGA experiment and assuming that the thermal conductivity of the hypothetical one-dimensional slab of Coating 313 was infinitely high, so that uniform temperatures would prevail at any instant in time. Figure 2-5 illustrates the predictions with the two TGA's in nitrogen. Both predictions match the data well, with the 10°C per minute prediction fitting the corresponding data better than the 6°C per minute case, which was the TGA actually used to determine the decomposition parameters.

It should be pointed out that the densities ρ_{o_i} and ρ_{r_i} used in the decomposition model were assumed to be directly proportional to the weights reported in the TGA plots. In other words, swelling or expansion of the sample was not considered in the analysis of the TGA data, so the densities ρ_{o_i}, i = B, C, and ρ_{r_i}, i = A, B, C, thus determined are higher than the actual values. In Section 3, it is pointed out that use of these "unexpanded" densities in the TRIM code is permissible, since the only term in the indepth energy equation depending upon length changes in the decomposing material is the thermal conduction term.

Table 2-2 summarizes the decomposition kinetics constants derived from the analysis of the Coating 313 TGA data.

The heats of formation of the virgin material and char, Δh_p and Δh_c, were calculated from combustion bomb data supplied by CRPO. There was some uncertainty as to what the products were in the combustion bomb experiment. CRPO indicated that no liquid H_2O was present when the combustion bomb was opened. Therefore hydrogen was assumed to go to H_2O vapor. Carbon was naturally considered as going to CO_2. There apparently was some sulfur and nitrogen remaining in the SiO_2(solid) residual. The heats of combustion provided from the actual experiment were modified in a manner which accounted for the change in the heat of combustion if the remaining sulfur went to H_2SO_4(g) and the remaining nitrogen went to HNO_3(g). According to CRPO, these modifications were small compared to the original values of the heat of combustion.

SAMPLE: 313 coating - NASA Intumescent

SIZE _____ mg.

X-AXIS

TEMP. SCALE 100 °C / inch

SHIFT 0 inch

Y-AXIS

SCALE 1 mg. / inch

(SCALE SETTING X 2)

SUPPRESSION 0 mg.

RUN NO. 1 DATE 4-4-73

OPERATOR EHB

HEATING RATE 6 °C / min.

ATM. N_2 (6mm) 0% O_2

TIME CONSTANT 1 sec.

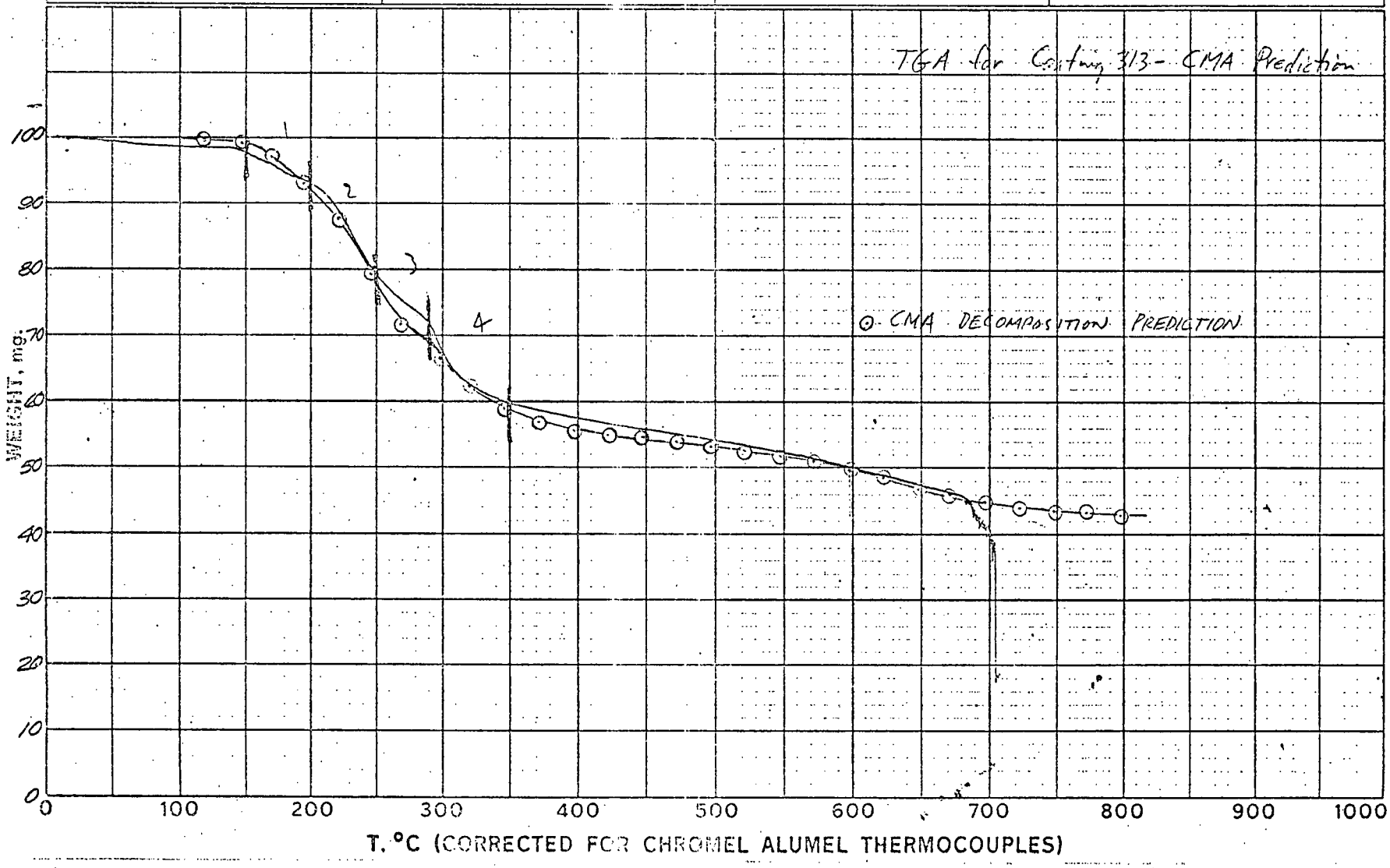

Figure 2-5

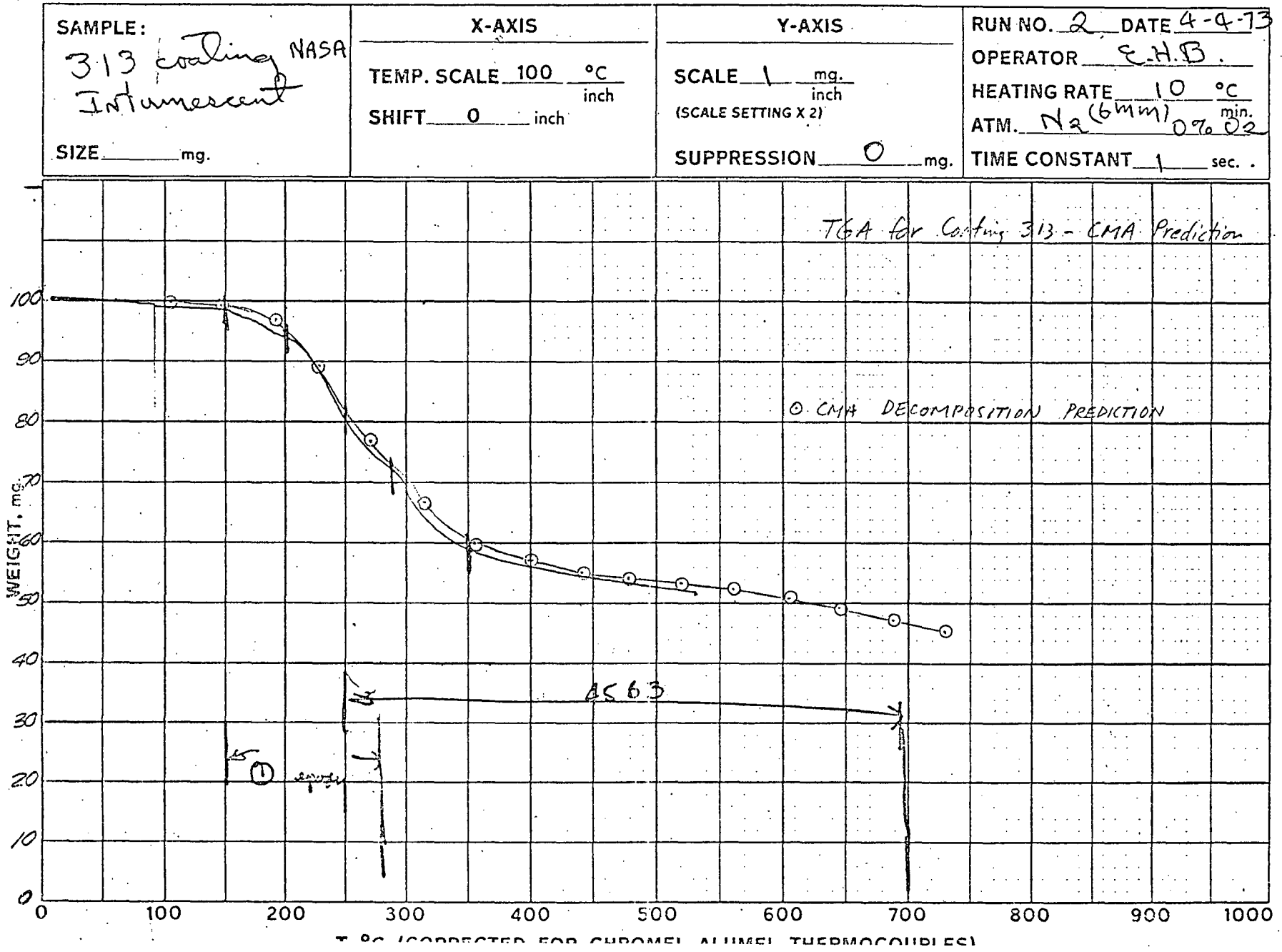

Figure 2-5. Concluded

TABLE 2-2
DECOMPOSITION KINETICS CONSTANTS FOR COATING 313 (SEE EQUATION (2-14))

Reaction	ρ_{o_i} (lbm/ft^3)	ρ_{r_i} (lbm/ft^3)	B_i (sec^{-1})	E_{a_i} (°R)	n_i (-)
A	48.90	0	800.0	11,550.0	1.0
B	29.69	0	690,000.0	20,130.0	2.0
C	96.05	75.10	5.0	13,800.0	1.0

Γ = 0.50 (see Equation (2-13))

There was some question as to whether S went to SO_2 or H_2SO_4(g) and whether N went to N_2 or HNO_3(g). To shed some light on this, ACE was run at 301°K and 700°K at 100 atm for several oxygen/fuel ratios. The ACE calculations indicated that H_2SO_4 (g & l) is the dominant sulfur product at equilibrium; however, equilibrium favors N_2(g) over HNO_3. Thus the heat of formation was determined in two ways: 1.) assuming N_2(g) for the product, and 2.) assuming HNO_3(g) for the product. Normalizing the mass fractions of the elemental composition to unity the heats of formation were calculated to be:

Nitrogen Product	Δh_p, cal/gm	Δh_c, cal/gm
N_2(g)	-968.	-2338.
HNO_3(g)	-1105.	-2467.

Evidently, the fate of the nitrogen makes minor differences in the answer. It should be noted that the nominal value of -2400 cal/gm for Δh_c seems rather low. The Δh_p value corresponding to the N_2(g) product was utilized in the TRIM predictions.

Specific heat data were supplied by CRPO (Reference 17) and were obtained through a differential scanning calorimeter experiment. Specific heat values were reported for the virgin coating and two chars, a pre-char at 350°C (Char #1) and a pre-char (Char #2) at 500°C. Figure 2-6 shows the specific heats for virgin and chars #1 and #2 as a function of temperature. Reference 17 discusses the uncertainty of the virgin Cp above 170°C and, therefore, Figure 2-6 shows an estimated specific heat for the virgin coating above this temperature. The sensitivity of this Cp difference was determined to be negligible based on two calculations where backwall temperature was compared; therefore the reported values of Cp were used for all subsequent calculations. Chars #1 and #2 exhibited similar specific heats, but Reference 17 cast some doubt on the accuracy of the Char #1 reported values since reactions were noted during DSC testing. For this reason, the Char #2 sample was prepared and tested and it is these reported values which are used throughout this modelling program.

The thermal conductivity of the virgin coating was supplied directly through CRPO, as was the thermal diffusivity for the char. Figure 2-7 shows the virgin conductivity curve which was supplied. The char thermal diffusivity was given as 0.0095 (cgs units), and conductivity was calculated from the aforementioned specific heats and density. From examination of the conductivity curves in Figure 2-7, it is apparent that, in view of the uncertainty levels

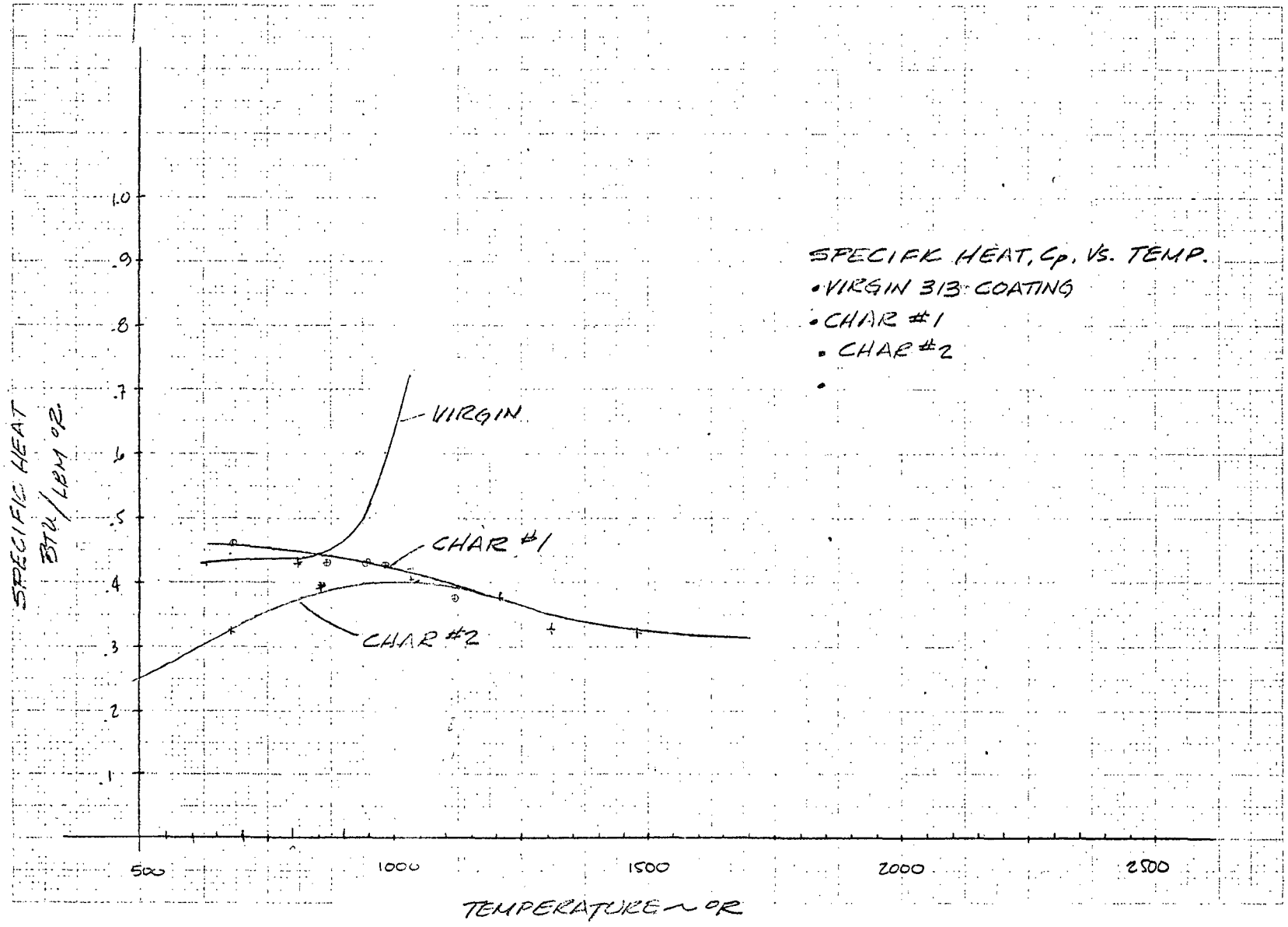
SPECIFIC HEAT, Cp, VS. TEMP.
• VIRGIN 313 COATING
• CHAR #1
• CHAR #2
SPECIFIC HEAT BTU/LBM °R
1.0
.9
.8
.7
.6
.5
.4
.3
.2
.1
VIRGIN
CHAR #1
CHAR #2
500
1000
1500
2000
2500
TEMPERATURE ~ °R

Figure 2-6

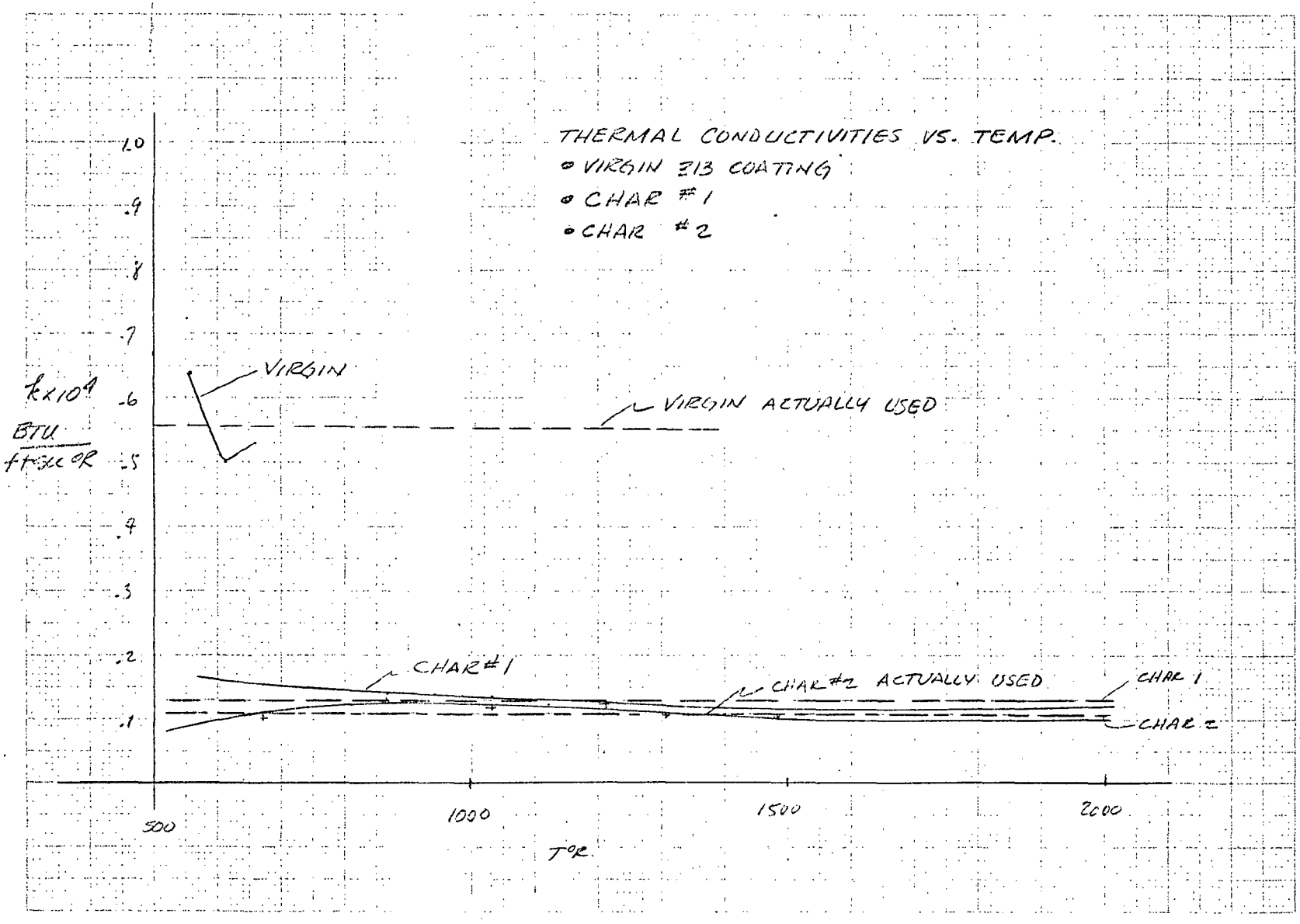
THERMAL CONDUCTIVITIES VS. TEMP.
• VIRGIN Z13 COATING
• CHAR #1
• CHAR #2
1.0
.9
.8
.7
k x 10⁴
.6
BTU / ft sec °R
.5
.4
.3
.2
.1
VIRGIN
VIRGIN ACTUALLY USED
CHAR #1
CHAR #2 ACTUALLY USED
CHAR 1
CHAR 2
500
1000
1500
2000
T °R

Figure 2-7

associated with the experimental data, the thermal conductivities for virgin and char may be considered constant and temperature independent. Figure 2-7 also shows the conductivity actually used for subsequent calculation prior to the conductivity sensitivity studies (Section 6).

The emissivity (= absorbtivity) of the char and virgin coating were supplied by CRPO as 1.0 and 0.8. Actual emissivity for partially decomposed material is computed as a weighted average in a manner similar to the local thermal conductivity calculations (Equation (2-11)).

Table 2-3 summarizes the thermophysical properties used for the virgin and charred forms of Coating 313. As described in Section 6, the value for the char thermal conductivity was eventually doubled, based on comparison with experimental data obtained during the program.

All calculations in this study have been carried out using a steel substrate or a layer of thermal insulation and a steel substrate. Nominal literature values were chosen for their thermophysical values and these are tabulated in Table 2-3. Steel and insulation properties were obtained from References 18 and 19. Subsequent validation of the steel properties was made by comparison to T-3 test facility back-wall response of an uncoated steel test sample (Section 6). The insulation properties used correspond to a general class of semi-refractory insulation comprised of alumina-silica, asbestos fibers, and binder.

For all calculations performed here, the backside of the steel substrate was assumed to be insulated.

Finally, the char swell model, which is the only remaining input data for TRIM yet to be described, is discussed in the following section.

TABLE 2-3
THERMOPHYSICAL PROPERTIES OF VIRGIN AND CHARRED COATING 313, INERT INSULATION, AND STEEL

AEROTHERM CHARRING MATERIAL THERMAL RESPONSE AND ABLATION PROGRAM

Virgin Temperature (Density = 87.320 lb/cu ft) (deg R)	Specific Heat (Btu/lb-deg)	Conductivity (Btu/ft-sec-deg)	Sensible Enthalpy (Btu/lb)	Emissivity
500.00	.4200	.0000555	-12.75	.8000
600.00	.4300	.0000555	29.75	.8000
700.00	.4300	.0000555	72.75	.8000
800.00	.4400	.0000555	116.25	.8000
900.00	.4800	.0000555	162.25	.8000
1000.00	.6300	.0000555	217.75	.8000
Char Temperature (Density = 37.548 lb/cu ft) (deg R)	**Specific Heat (Btu/lb-deg)**	**Conductivity (Btu/ft-sec-deg)**	**Sensible Enthalpy (Btu/lb)**	**Emissivity**
500.00	.2500	.0000110	-8.25	1.0000
600.00	.3000	.0000110	19.25	1.0000
700.00	.3300	.0000110	50.75	1.0000
800.00	.3700	.0000110	85.75	1.0000
900.00	.3900	.0000110	123.75	1.0000
1000.00	.4000	.0000110	163.25	1.0000
1250.00	.3600	.0000110	258.25	1.0000
1500.00	.3200	.0000110	343.25	1.0000
4000.00	.3200	.0000110	1143.25	1.0000
Insulation Temperature (Density = 45.000 lb/cu ft) (deg R)	**Specific Heat (Btu/lb-deg)**	**Conductivity (Btu/ft-sec-deg)**		
500.00	.2500	.0000030		
1000.00	.2500	.0000210		
1500.00	.2500	.0000280		
4000.00	.2500	.0000280		
Steel Temperature (Density = 490.000 lb/cu ft) (deg R)	**Specific Heat (Btu/lb-deg)**	**Conductivity (Btu/ft-sec-deg)**		
500.00	.1000	.0104000		
1000.00	.1300	.0083000		
1500.00	.1800	.0062500		
1750.00	.2100	.0054200		
2000.00	.1600	.0047200		
3000.00	.1600	.0034700		
4000.00	.1600	.0034700		

SECTION 3

DEVELOPMENT OF SWELL MODEL AND IMPLEMENTATION IN TRIM CODE

With the exception of the swell model, all input and output data associated with the computer codes used in this study are discussed in the previous section. In this section, the swell model and its relation to the indepth energy balance are described. In addition, the incorporation of the swell model into the Aerotherm Charring Material Thermal Response and Ablation (CMA) code is described. This particular version of CMA, with the specialized capability of treating swelling materials, is now designated as the Aerotherm Transient Response of Intumescing Materials (TRIM) code.

3.1 DERIVATION OF THE SWELL MODEL

The swell model used in this study is based upon a relatively small amount of experimental data and, therefore, should be viewed only as a temporary model which should be updated as more experimental swell data become available. Such data is currently being collected at NASA Ames CRPO for Coating 313. In the interim, however, the swell model postulated here has proven to be quite useful in correlating backwall temperature data obtained in this study. The model has the distinct advantage that it is conceptually and mathematically simple and, thus, easy to implement in a calculational procedure.

In Reference 4, the process of intumescing is associated with the steepest portion of a TGA trace for a typical intumescent coating. In the previous section of this report, the TGA trace for Coating 313 is discussed. There it is shown how the three-component decomposition model used in TRIM is related to the TGA curve. In particular, the total weight-loss curve is broken up into three decomposition reactions, and the steepest portion of the curve is identified with reaction B (see Equation 2-13). The swell model postulated here is based upon the following criteria:

1. At any point indepth where $\rho_B = \rho_{o_B}$, swelling or intumescing has not been initiated
2. At any point indepth where $\rho_B = \rho_{r_B}$, swelling is complete

In the finite-difference formulation used to treat the indepth energy equation, the above criteria are applied to each fixed-mass node. At a given instant in time, each node has a uniform average density. If $(\rho_B)_{Node} = \rho_{o_B}$, then the node thickness is its original, input thickness. If $(\rho_B)_{Node} = \rho_{r_B}$, then the node thickness is given by its original value times some input expansion factor, the latter typically being between 5 and 50.

A number of choices are available for specifying the material swelling for intermediate densities, i.e. $\rho_{r_B} < \rho_B < \rho_{o_B}$. Either linear or nonlinear variations are possible, the choice being dictated by experimental data if available. A general function which covers a number of possibilities is the following:

$$E_f(y,\theta) = E_{f_{max}} - (E_{f_{max}} - 1.0)\left(\frac{\rho_B(y,\theta) - \rho_{r_B}}{\rho_{o_B} - \rho_{r_B}}\right)^n \qquad (3\text{-}1)$$

where E_f is the instantaneous swell factor, by which the original node thickness is multiplied, and $E_{f_{max}}$, an input quantity, is the maximum swell factor any node can reach upon becoming fully decomposed. For linear expansion, the exponent n is unity. For nonlinear expansion in which the major portion of the expansion occurs when the material is only slightly decomposed, n is greater than unity. In contrast, for nonlinear expansion in which most of the expansion occurs only after the material is almost fully decomposed, n is less than unity. Figure 3-1 illustrates the dependence of the variation in E_f on the value of n, when $E_{f_{max}} = 10.0$.

The swell factor as defined in Equation 3-1 depends explicitly only on $\rho_B(y,\theta)$. However, since $\rho_B(y,\theta)$ is a function of both depth from the surface and time, the swelling process is implicitly linked to the overall transient thermochemical response of the material.

The final question which must be addressed is related to the effect swelling nodes have on the finite-difference formulation of the indepth energy equation, Equation (2-7), since this equation was originally derived for nodes of fixed dimension (Reference 11). Examination of Equation (2-7) reveals that only one term is independent of the nodal mass, that being the net conduction term $1/A\ \partial/\partial x\ (kA\ \partial T/\partial x)_\theta$. All other terms contain material density ρ in some fashion, either linearly or as a derivative with respect to space or time. If the entire equation were multiplied by a nodal volume, then the nodal density-volume product would be equivalent to nodal mass. But nodal mass is conserved,

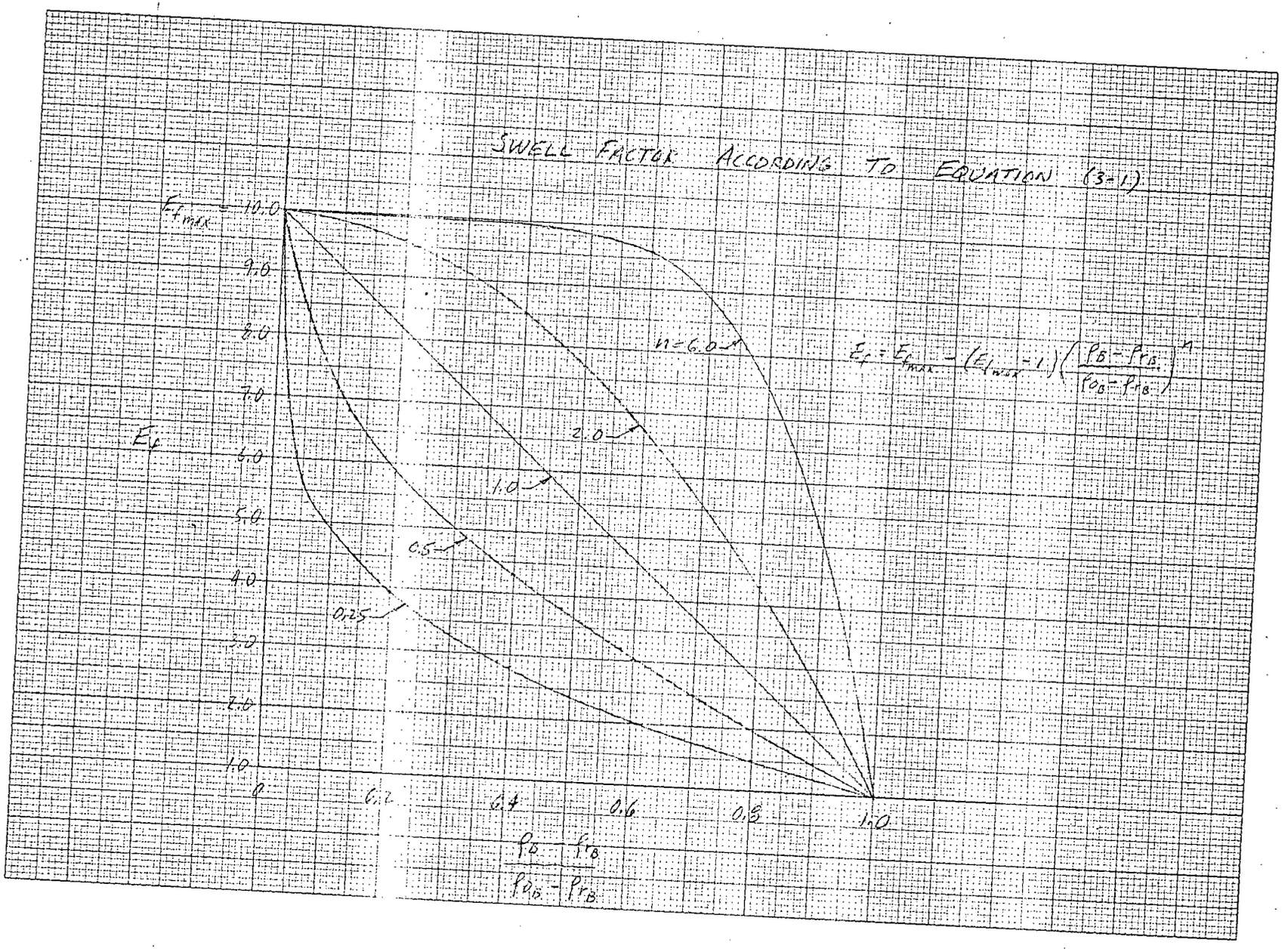
SWELL FACTOR ACCORDING TO EQUATION (3-1)
$E_{f_{max}}$
10.0
9.0
8.0
7.0
6.0
5.0
4.0
3.0
2.0
1.0
0
E_f
m=6.0
2.0
1.0
0.5
0.25
$E_f = E_{f_{max}} - (E_{f_{max}} - 1)\left(\frac{P_D - P_{r_B}}{P_{D_0} - P_{r_B}}\right)^m$
0.2
0.4
0.6
0.8
1.0
$\frac{P_D - P_{r_B}}{P_{D_0} - P_{r_B}}$

Figure 3-1

regardless of the length variation of the node, by virtue of Equation (2-13). This means that for a node of instantaneous fixed mass, an increase in nodal size dictates a decrease in nodal density. Thus, all terms in the energy equation, with the exception of the thermal conduction term, are independent of nodal expansion. A more rigorous discussion of this fact is presented in Appendix B. Modification of the conduction term to account for nodal expansion is described below.

3.2 IMPLEMENTATION OF THE SWELL MODEL IN THE TRIM CODE AND MISCELLANEOUS CODE FEATURES

As already pointed out in the introduction to this section, the swell model modifications were carried out on the existing CMA code, and the new code resulting therefrom is now designated the TRIM code. The alterations to the existing CMA code were of two types: expansion factor modelling and input/output related user conveniences. The code changes associated with the swell model included operations on the thermal conductivity term and the inclusion of a new subroutine, PAINT. The subroutine calculates the expansion factor of each node based on local density, and input values of maximum expansion factor and non-linear expansion exponent, according to Equation (3-1). Examination of the equation shows $E_f = 1$ when $\rho_B = \rho_{OB}$ and $E_{f_{max}}$ when $\rho_B = \rho_{rB}$. Additionally, the subroutine includes the entire program common block in anticipation of future updating of the expansion model.

The modification of the conduction term consists of dividing the instantaneous value of the nodal thermal conductivity by the instantaneous value of the nodal expansion factor E_f. This operation, in effect, reduces the conduction heat flux in the material which occurs by virtue of the reduction in temperature gradient associated with material expansion.

Input/output modifications have been made to facilitate the most simplified code operation possible. Input changes consist of reading values of $E_{f_{max}}$ and n for the swell model; reading flame temperature and emissivity which calculates radiative heat input based on $\dot{q}_{rad} = \varepsilon\sigma T_f^4$, and a nodal thickness generator which greatly simplifies the usually tedious task of nodal layout, especially in experimentation where thickness variation is the rule. New output features are a surface expansion and expansion rate calculation at each printed output and, more importantly, a summary output which collects various quantities such as backwall temperature (in both °C and °F), radiation heat flux absorbed by the surface, and flame temperature, all as a function of time. A more detailed discussion of the input/output provided by the TRIM code is provided in Reference 20.

SECTION 4

SENSITIVITY STUDY

In the course of preparing the input data for the TRIM code (see Section 2), it became apparent that certain input thermochemical properties for Coating 313, such as heat of formation, activation energy, thermal conductivity, etc., have rather large associated uncertainties. For this reason, the sensitivity study described in this section was carried out. In this task, various input data were varied about their nominal values in order to determine what impact such perturbations would have on predicted backwall temperature histories. For several data parameters, the impact was rather substantial, indicating that the values of these parameters should be known with minimum uncertainty. On the other hand, large variations in other input data parameters had very little effect on the predicted backwall temperature history, indicating that highly-accurate estimations of those particular properties really are not necessary.

Table 4-1 summarizes the cases considered in the sensitivity study. For all cases, the nominal radiation heat flux to the exposed surface was specified to be 10.5 Btu/ft^{2}sec. The convective heat flux depends upon the instantaneous wall enthalpy (see Equation (2-15)), but was always less than 0.3 Btu/ft^{2}sec. These levels of radiative and convective heat fluxes correspond to nominal operating conditions in the NASA Ames CRPO T-3 Facility. In addition, the backwall was assumed to be adiabatic in all cases.

The sensitivity study concentrated on investigating the effects of uncertainties in the following parameters:

1. Maximum swell factor, $E_{f_{max}}$
2. Char heat of formation, Δh_c
3. Reaction B activation energy, E_{a_B}
4. Initial coating thickness
5. Substrate thickness
6. Nonlinear expansion

TABLE 4-1

COMPILATION OF SENSITIVITY CALCULATIONS

$\dot{q}_{rad}$ = 10.5 Btu/ft^{2}sec

$\dot{q}_{conv} \leq$ 0.3 Btu/ft^{2}sec

Adiabatic Backwall

Run #	$E_{f_{max}}$	E_{a_B}(°R)	Δh_f (Btu/lbm)	Coating Response Mode	Coating(in) Thickness	Steel (in) Substrate Thickness	Expansion Mode
1	1	20130	-4208.5	decomposing	0.040	0.0625	linear
2	10	↓	↓	↓	↓	↓	↓
3	50	↓	↓	↓	↓	↓	↓
4	1	↓	+4000	↓	↓	↓	↓
5	10	↓	↓	↓	↓	↓	↓
6	50	↓	↓	↓	↓	↓	↓
7	10	40260	-4208.5	↓	↓	↓	↓
8	↓	10065	-4208.5	↓	↓	↓	↓
9	↓	40260	+4000	↓	↓	↓	↓
10	↓	10065	+4000	↓	↓	↓	↓
*11	--	--	--	pure virgin	↓	↓	↓
*12	10	--	--	pure char	10 x 0.040	↓	↓
13	↓	20130	-4208.5	decomposing	0.020	↓	↓
14	↓	↓	-4208.5	↓	0.080	↓	↓
15	↓	↓	+4000	↓	0.020	↓	↓
16	↓	↓	+4000	↓	0.080	0.0625	↓
17	↓	↓	-4208.5	↓	0.040	0.1250	↓
18	↓	↓	-4000	↓	0.040	0.1250	↓
*19	--	--	--	none	0.000	0.0625	↓
*20	--	--	--	none	0.000	0.1250	↓
21	10	20130	-4208.5	decomposing	0.040	0.0625	nonlinear
22	10	20130	+4000	decomposing	0.040	0.0625	↓

*$\dot{q}_{conv}$ = 0.0

Initially, each of these quantities was judged either to have a large associated uncertainty or to have the potential for a large influence on the predicted backwall temperature history.

Figure 4-1 illustrates the effects of variations in $E_{f_{max}}$, where $1. \leq E_{f_{max}} \leq 50$. When $E_{f_{max}} = 1$, no expansion whatsoever is permitted. In the first set of curves of Figure 4-1, the char heat of formation is negative, -4208.5 Btu/lbm, while in the second set of curves it is positive, 4000 Btu/lbm. Recall that the negative value was deduced from heat-of-combustion data provided by CRPO. The negative char heat of formation, in conjunction with virgin material and pyrolysis gas heats of formation of -1743.Btu/lbm and -3300. Btu/lbm, respectively, implies that the overall virgin-to-char decomposition is exothermic. On the other hand, with the same values for virgin material and pyrolysis gas heats of formation, the positive char heat of formation of 4000 Btu/lbm implies an overall endothermic decomposition reaction. Whether the decomposition is exothermic or endothermic is strongly reflected in the predicted backwall temperature histories: the temperature is significantly lower for the energy-absorbing endothermic reaction. Figure 4-1 also illustrates that the principal effect of $E_{f_{max}}$ is in dictating the late-time backwall temperature level. Up to 50% reduction in late-time temperature is achieved by allowing a material expansion of 50 times its original thickness. However, almost as much protection is provided by a coating with $E_{f_{max}} = 10.0$. Early in time, $\theta \leq 30$-40 seconds, the prediction is fairly insensitive to the value of $E_{f_{max}}$.

Figure 4-2 illustrates the effects of varying the activation energy, E_{a_B} for the assumed intumescing reaction. Recall that the nominal value of 20130°R was deduced from the TGA data supplied by CRPO for Coating 313. Again, both positive and negative values of Δh_c were considered. Lowering the activation energy relative to the nominal value allows decomposition to occur earlier in time. For the negative Δh_c case, this causes the surface temperature to rise more rapidly which, in turn, makes reradiation more significant earlier in time with the net effect that less impinging energy is absorbed by the material. For the positive Δh_c case, energy is absorbed by decomposition earlier in time, so that less energy has reached the substrate at any given time. Raising E_{a_B} relative to its nominal value has the inverse effect, for both positive and negative Δh_c.

Figure 4-3 shows the difference in protection offered by the two extreme cases, a nondecomposing virgin coating and a fully precharred, expanded coating. For the precharred coating, $E_{f_{max}} = 10.0$. It is not surprising that the precharred coating drastically outperforms the decomposing coating. What is unexpected, at least at first glance, is the fact that the fully precharred coating even outperforms the decomposing coating of Run #5 (Figure 4-2), which has a positive

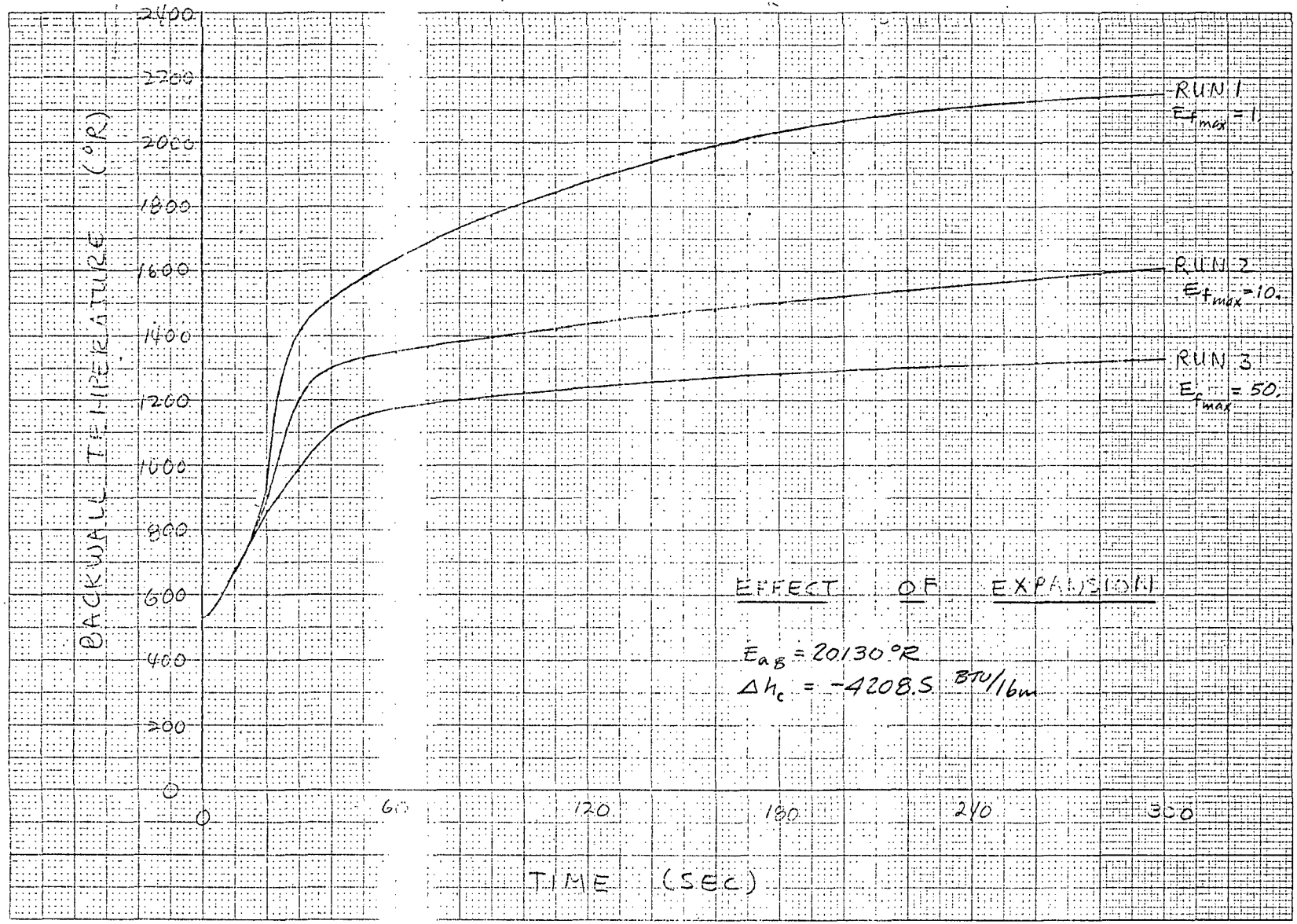
BACKWALL TEMPERATURE (°R)
2400
2200
2000
1800
1600
1400
1200
1000
800
600
400
200
0
0
60
120
180
240
300
TIME (SEC)
RUN 1
$E_{f_{max}} = 1.$
RUN 2
$E_{f_{max}} = 10.$
RUN 3
$E_{f_{max}} = 50.$
EFFECT OF EXPANSION
$E_{aB} = 20130°R$
$\Delta h_c = -4208.5$ BTU/lbm

Figure 4-1

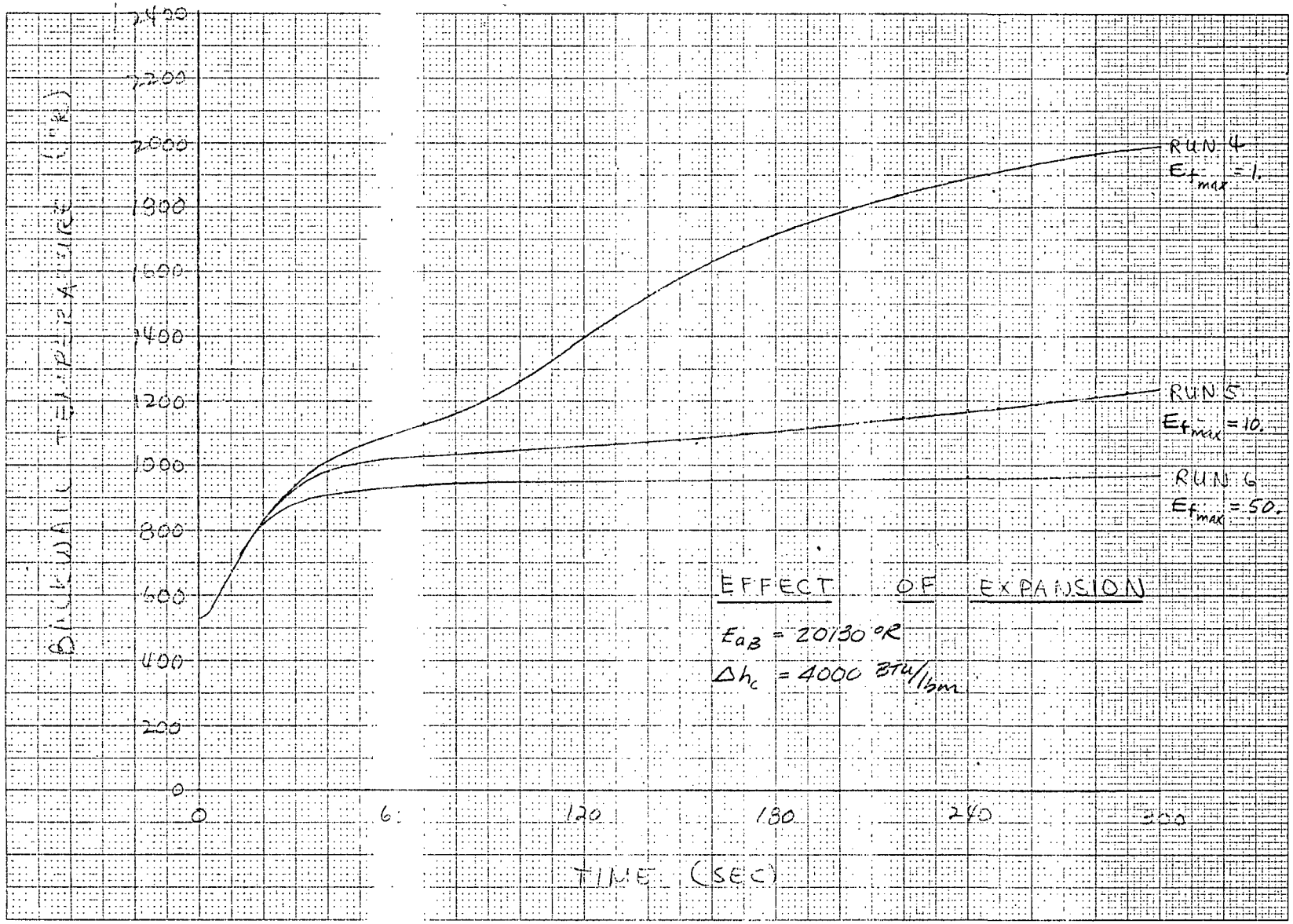

Figure 4-1. Concluded

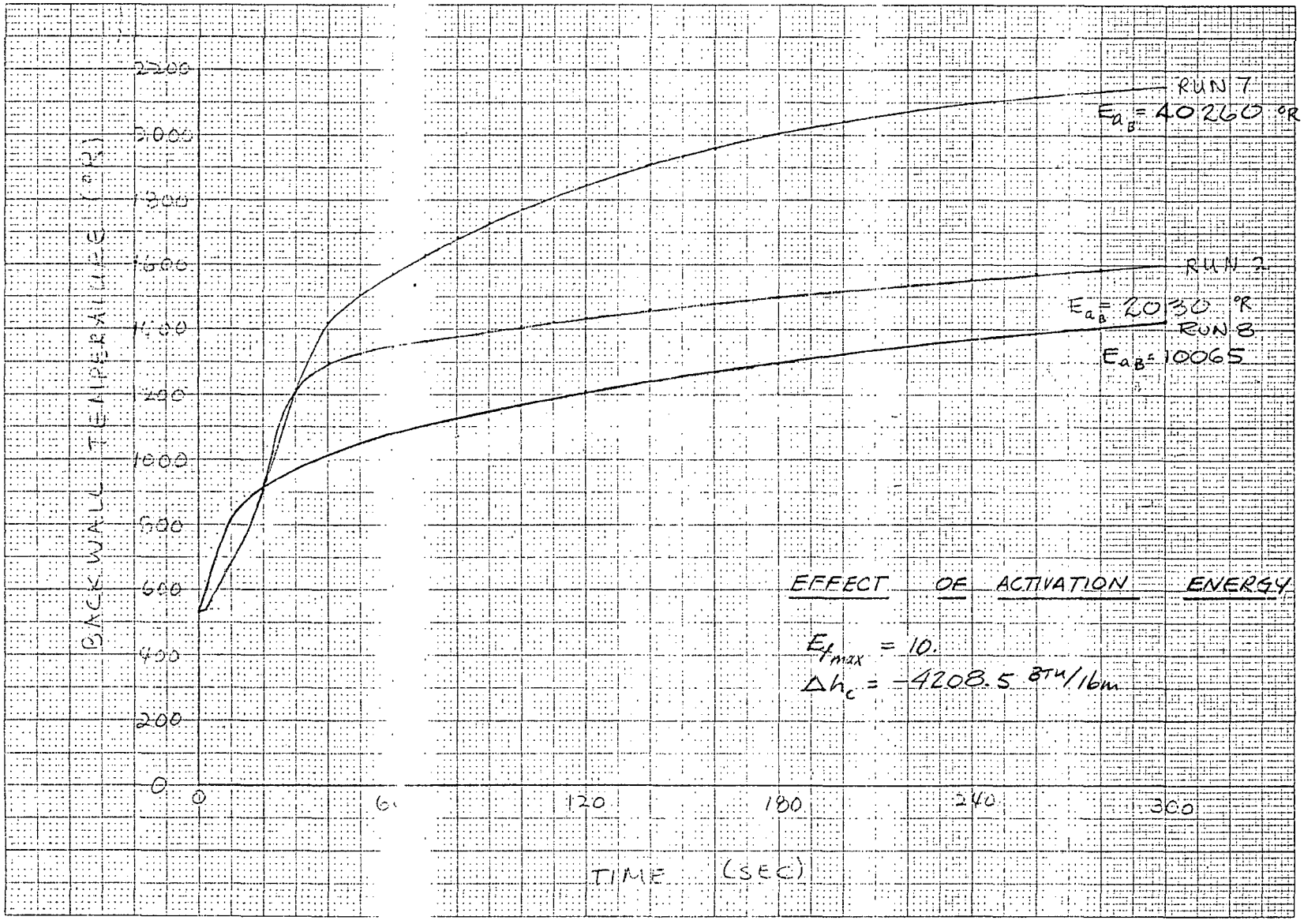
RUN 7
E_{a_B} = 40260 °R
RUN 2
E_{a_B} = 20300 °R
RUN 8
E_{a_B} = 10065
EFFECT OF ACTIVATION ENERGY
$E_{f_{max}}$ = 10.
Δh_c = -4208.5 BTU/lbm
BACK WALL TEMPERATURE (°R)
2200
2000
1800
1600
1400
1200
1000
800
600
400
200
0
0
60
120
180
240
300
TIME (SEC)

Figure 4-2

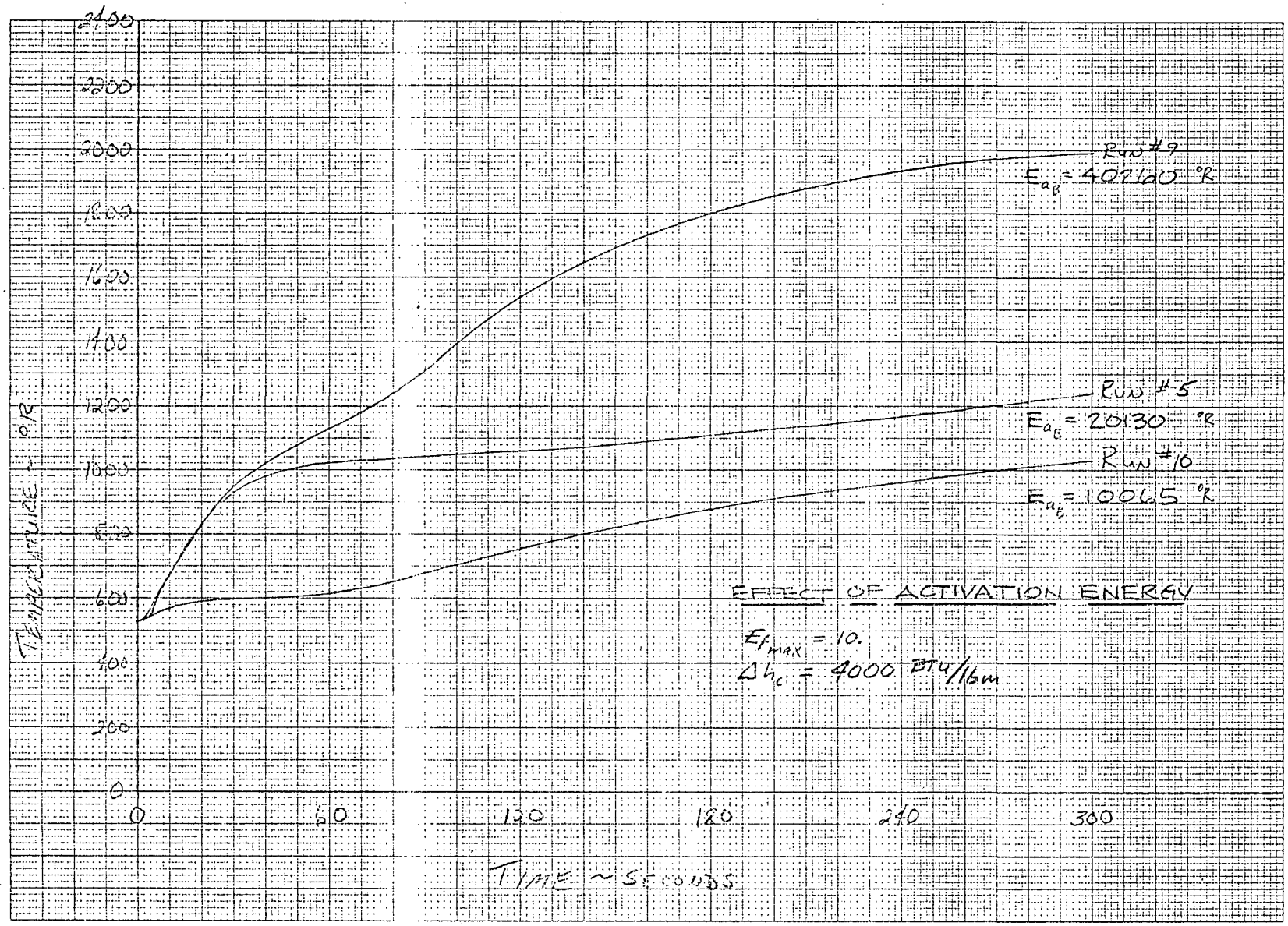

Figure 4-2. Concluded

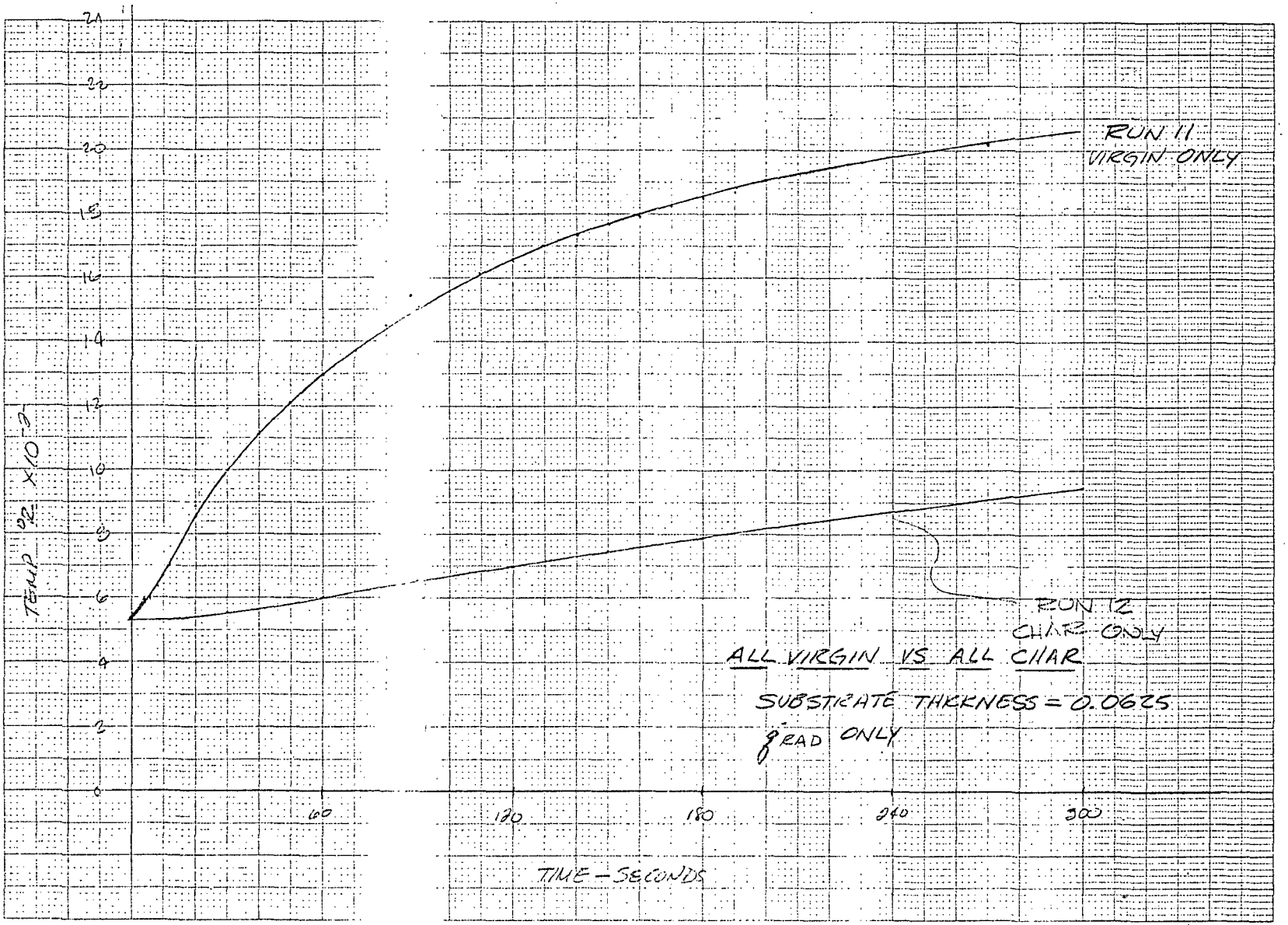
RUN 11
VIRGIN ONLY
RUN 12
CHAR ONLY
ALL VIRGIN VS ALL CHAR
SUBSTRATE THICKNESS = 0.0625
RAD ONLY
TEMP $\dot{Q}_R$ X10-9
TIME - SECONDS
0
2
4
6
8
10
12
14
16
18
20
22
60
120
180
240
300

Figure 4-3

Δh_c (Δh_c = 4000 Btu/lbm, E_{a_B} = 20130°R, $E_{f_{max}}$ = 10.0). A plausible explanation for this result is that the early-time surface reradiation, associated with the precharred coating and due to its low thermal conductivity even at the onset of heating, more than offsets the energy absorbed due to endothermic decomposition in Run #5.

Figure 4-4 shows the effect of initial coating thickness, for both positive and negative Δh_c. It is noteworthy that a 0.040 in. initial coating can reduce the late-time backwall temperature by up to 45%, but that doubling the initial coating to 0.080 inch thickness results in only a small increase in temperature reduction to 55%. This suggests that for the heating conditions considered the optimum initial coating thickness is somewhat less that 0.080 inch.

Figure 4-5 illustrates the effects of different steel substrate thickness for fixed coating properties. Due to the high thermal conductivity of the substrate, the differences in backwall temperature history are minimal. Due to the greater thermal capacity of the thicker substrate, its backwall temperature remains up to 200°F lower than that of the thinner substrate. These substrate thickness effects are further emphasized in Figure 4-6, which shows the response of an uncoated steel plate. In this case, differences in backwall temperature occur only during the first three minutes of heating, with the thicker substrate lagging due to its greater thermal inertia. After this time, however, a steady-state surface temperature and, hence, steady-state reradiation is reached. Due to the relatively high thermal conductivity of steel, the temperature profiles are relatively flat throughout the substrate, so that backwall temperature is then relatively insensitive to substrate thickness.

Figure 4-7 illustrates the effects of linear versus nonlinear intumescence. For linear intumescence, n= 1.0. For nonlinear intumescence, in which most of the material swelling occurs initially when only a slight state of decomposition has been reached, n = 6.0. Apparently, for all times and $E_{f_{max}}$ values of interest, nonlinear expansion with n = 6.0 does not lead to significant improvement in the performance of the coating.

Later in the program, after additional experimental data were acquired, the sensitivity of the predictions to variations in the char thermal conductivity was investigated. These additional data were obtained in experiments conducted with Coating 313 in the Ames T-3 facility. The purpose of the experiments was to gain additional information which could be used to reduce the uncertainties in the input data required by the TRIM code. The results of this investigation are reported in Section 6.

In summary, the primary conclusions to be drawn from the sensitivity study are the following:

1. The char heat of formation, h_c, and activation energy for the assumed intumescing reaction, E_{a_B}, influence strongly the predicted backwall temperature history.

2. For the heating conditions considered, a coating with $E_{f_{max}} = 10.0$ offers substantially more protection than one with $E_{f_{max}} = 1.0$, but only slightly less protection than one with $E_{f_{max}} = 50.0$. This suggests that the gains realized in increasing the intumescing quality of a coating begin to diminish once $E_{f_{max}} = 10.0$ is reached.

3. For the heating conditions considered, a coating with initial thickness of 0.080 in offers only slightly improved protection over one with an initial thickness of 0.040 in. This suggests that the optimum initial coating thickness is somewhat less than 0.080 in.

4. Both substrate thickness and nonlinearity of intumescence appear to have only small effects on the predicted backwall temperature history.

5. It appears desirable to design a coating which decomposes rapidly and has an endothermic decomposition. Endothermic decomposition absorbs a portion of the incident heat flux, and rapid decomposition minimizes the time to achieve significant surface reradiation which, in turn, minimizes the integrated energy conduction into the coating/substrate composite.

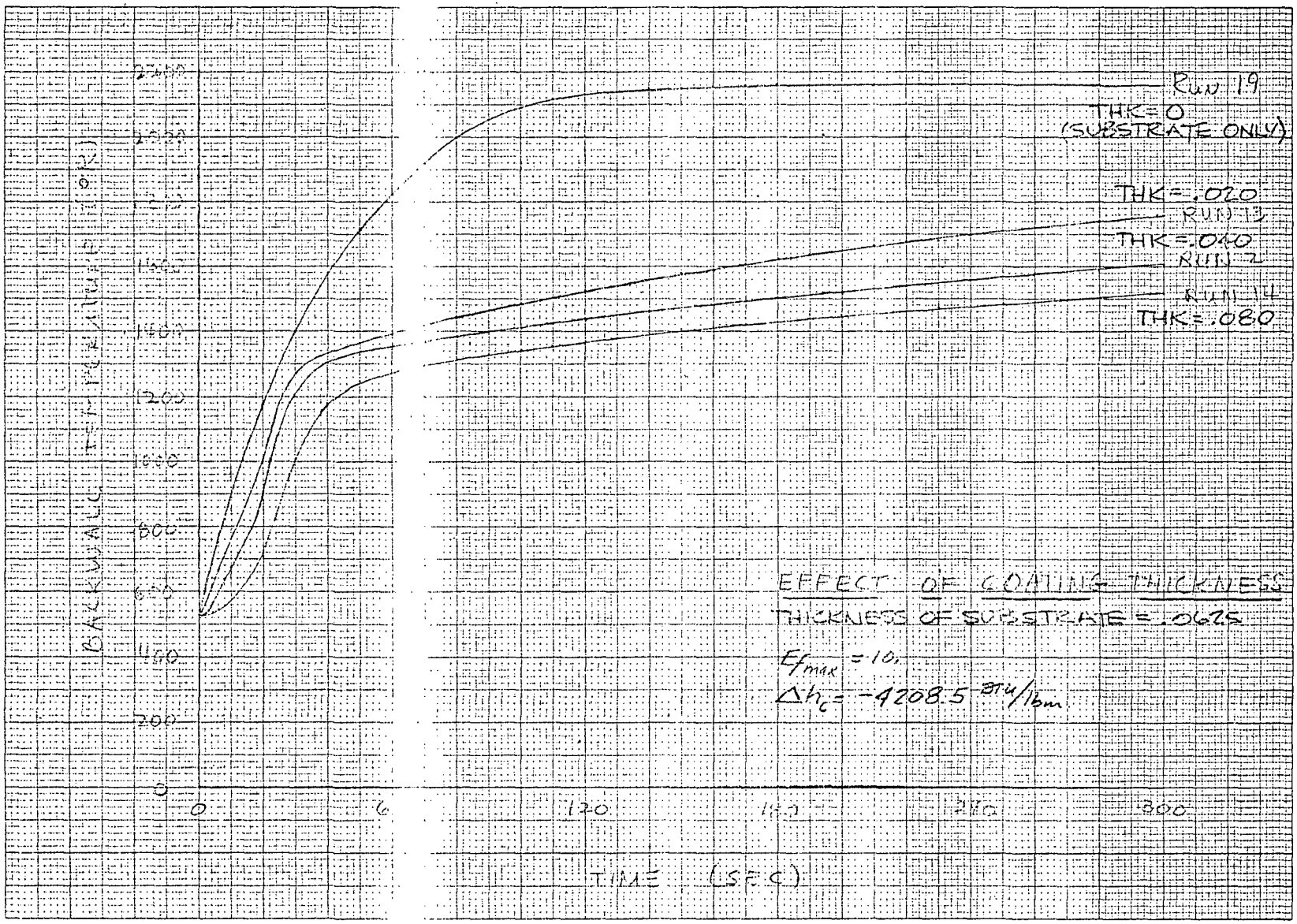
RUN 19
THK=0
(SUBSTRATE ONLY)
THK=.020
RUN 13
THK=.040
RUN 2
RUN 14
THK=.080
EFFECT OF COATING THICKNESS
THICKNESS OF SUBSTRATE = .0625
Ef_{max} = 10.
Δh_c = -4208.5 Btu/lbm
BACKWALL EFFLUENCE (BTU/FT²)
TIME (SEC)
0
120
200
300

Figure 4-4

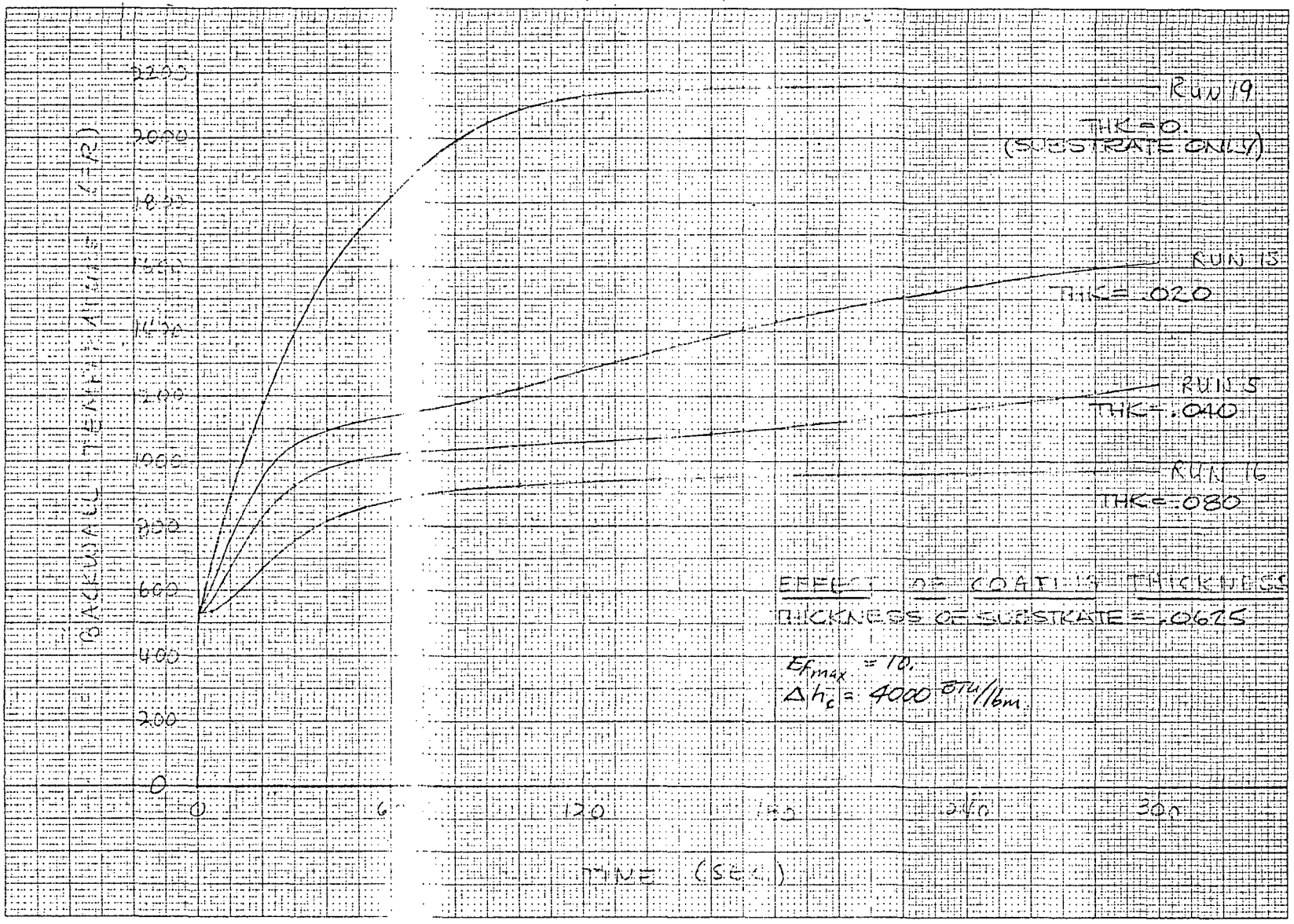

Figure 4-4. Concluded

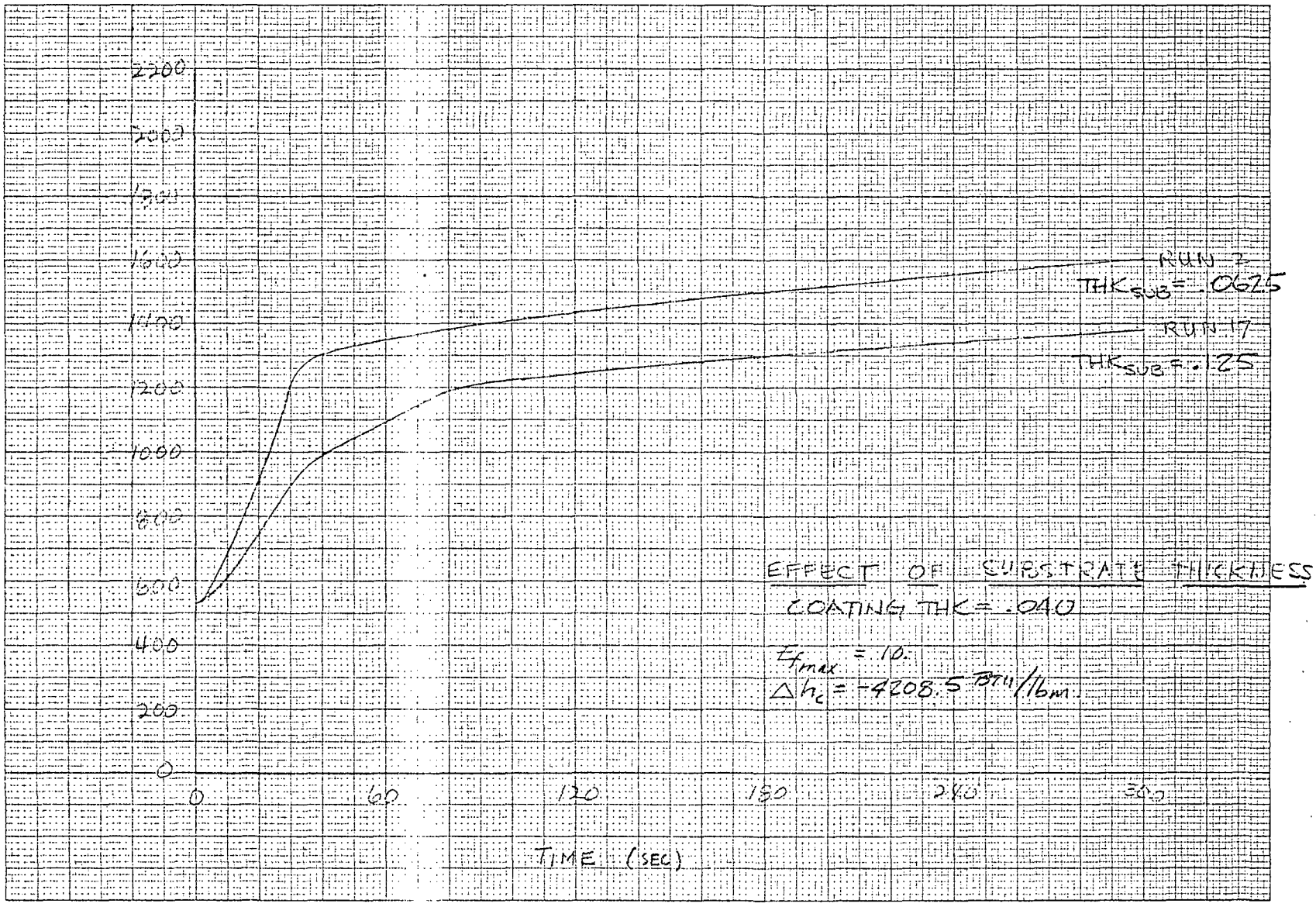
2200
2000
1800
1600
1400
1200
1000
800
600
400
200
0
0
60
120
180
240
300
TIME (SEC)
RUN 7
THK$_{SUB}$ = .0625
RUN 17
THK$_{SUB}$ = .125
EFFECT OF SUBSTRATE THICKNESS
COATING THK = .040
$F_{f_{max}}$ = 10.
Δh_c = -4208.5 BTU/lbm

Figure 4-5

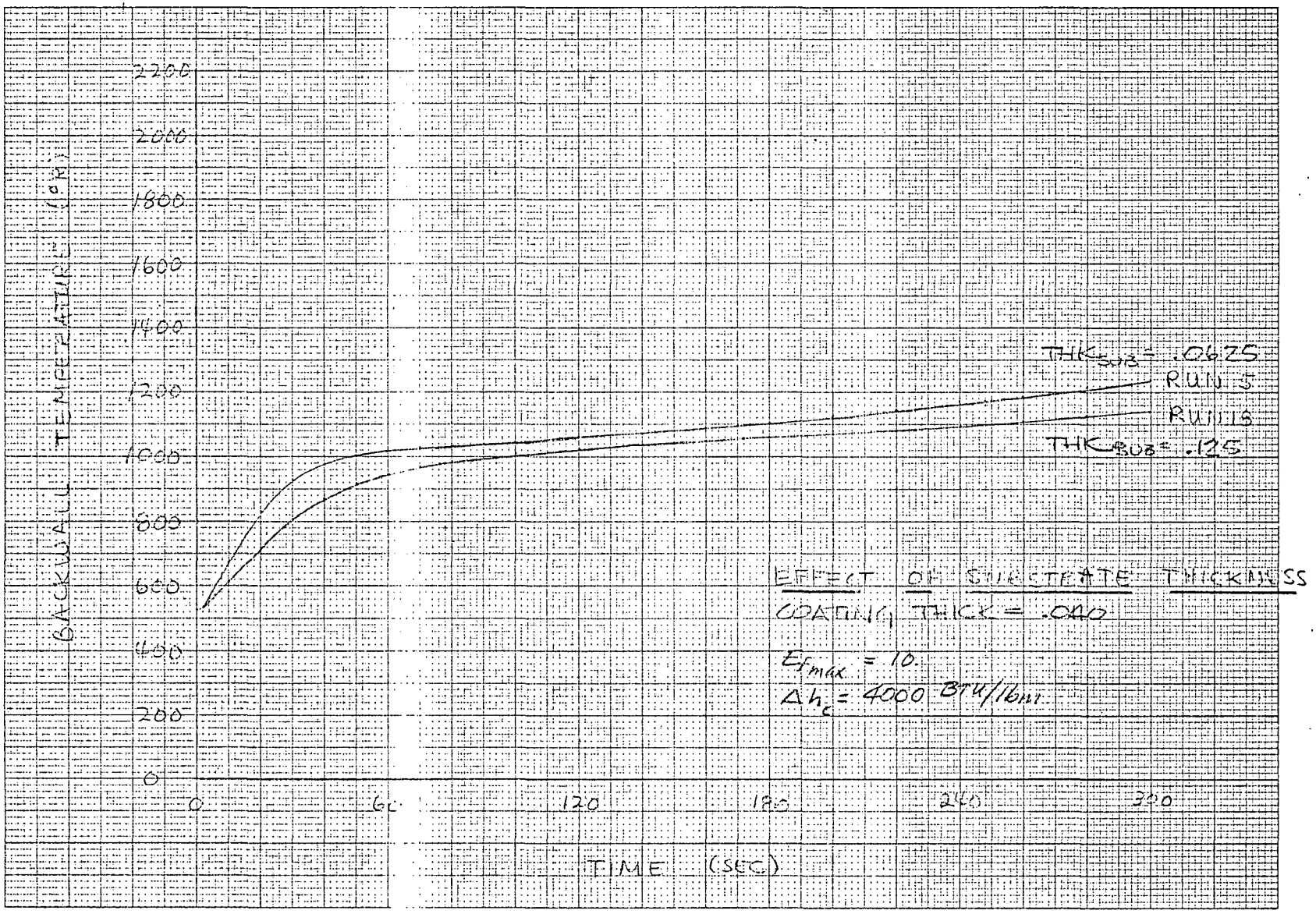

Figure 4-5. Concluded

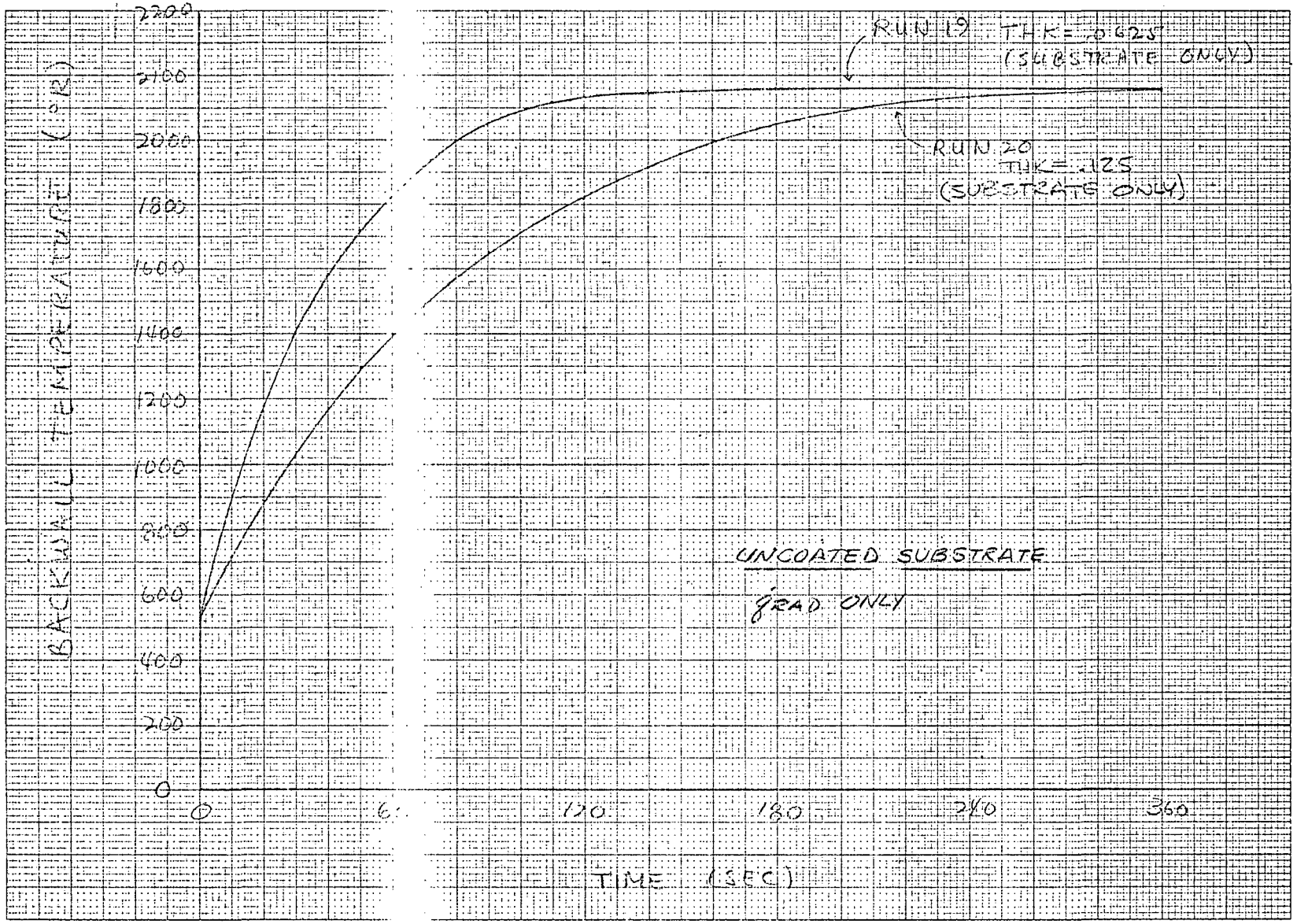
RUN 19 THK = .0625"
(SUBSTRATE ONLY)
RUN 20
THK = .125
(SUBSTRATES ONLY)
UNCOATED SUBSTRATE
GRAD ONLY
BACKWALL TEMPERATURE (°R)
2200
2000
1800
1600
1400
1200
1000
800
600
400
200
0
0
60
120
180
240
360
TIME (SEC)

Figure 4-6

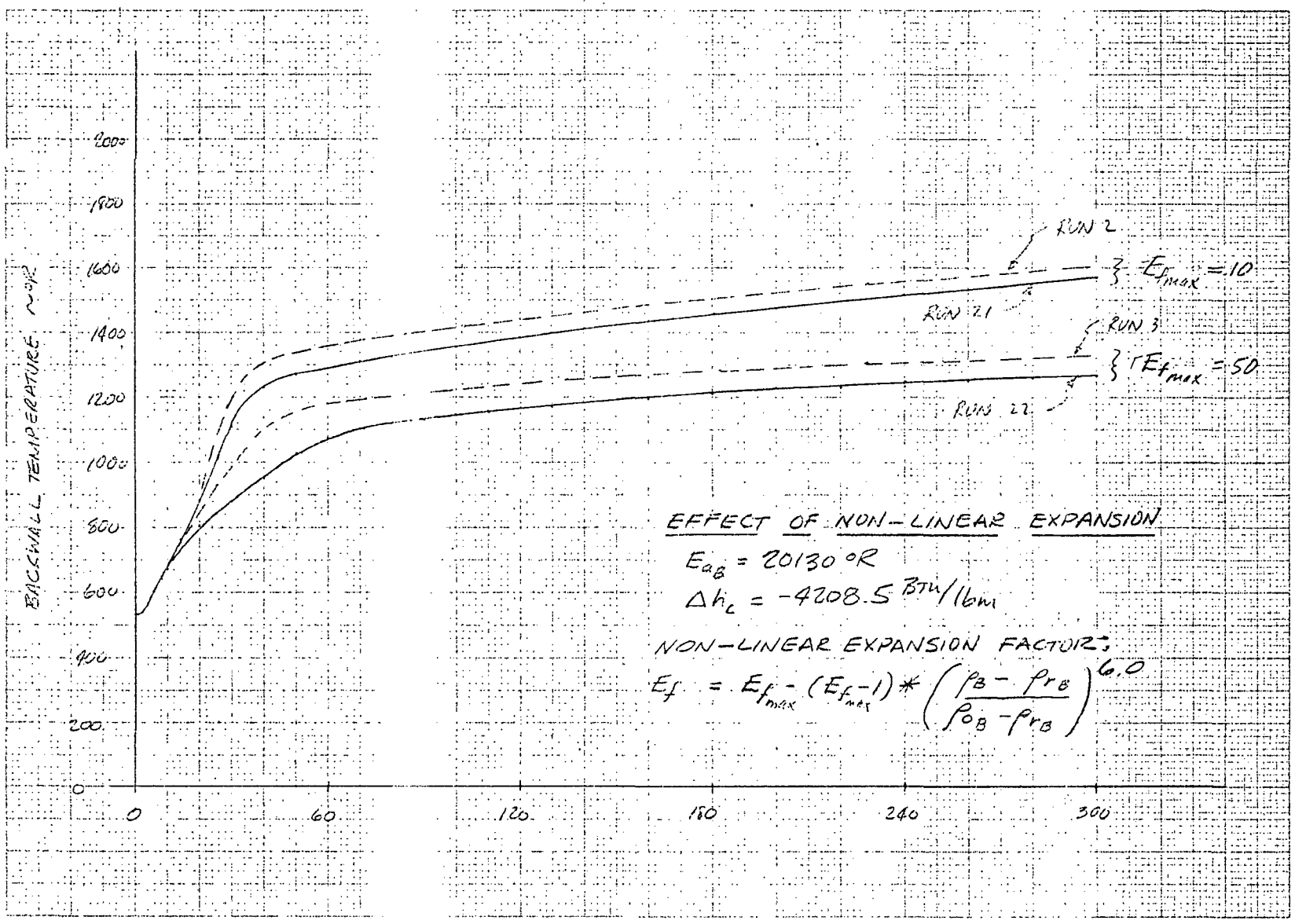
BACKWALL TEMPERATURE °R
2000
1800
1600
1400
1200
1000
800
600
400
200
0
0
60
120
180
240
300
RUN 2
RUN 21
RUN 3
RUN 22
$E_{f_{max}} = 10$
$E_{f_{max}} = 50$
EFFECT OF NON-LINEAR EXPANSION
$E_{a_B} = 20130\ ^\circ R$
$\Delta h_c = -4208.5\ BTU/lbm$
NON-LINEAR EXPANSION FACTOR:
$E_f = E_{f_{max}} - (E_{f_{max}} - 1) * \left(\frac{\rho_B - \rho_{r_B}}{\rho_{o_B} - \rho_{r_B}}\right)^{6.0}$

Figure 4-7

SECTION 5
ACQUISITION OF EXPERIMENTAL DATA

The purpose of the experimental program carried out in the present study was to obtain experimental data which could be used to validate the TRIM code. A number of models were tested in the NASA Ames CRPO T-3 Facility. The coating and substrate thicknesses of each model were carefully measured before each test. During testing, the total heat flux impinging on the model and the backwall temperature history were measured. Predictions of the backwall temperature history, for the measured thicknesses and heat fluxes associated with each model, were then attempted. These predictions and comparisons with data are discussed in Section 6 below.

Figure 5-1 presents a schematic of the Ames CRPO T-3 Facility. The facility is simply a fuel-oil fired furnace, and the associated heating and thermochemical environment is discussed in detail in Section 2 above. All models were tested in "area 1" designated in the sketch.

Figure 5-2 depicts the models that were tested in the program. A 1.0 foot-square, 1.0 inch thick asbestos template was used to hold the actual model in position in area 1. The model consisted of a 3.0 inch square steel plate, with a 1.0 inch diameter disc mounted in the center. A single chromel/alumel thermocouple was mounted on the back side of the disc, at its center. The 1.0 inch disc was mounted in the plate with epoxy, and Coating 313 was then applied over the entire 3.0 inch x 3.0 inch surface. After drying and curing, the coating was machined to a precisely known thickness. The center disc was thermally isolated from the remainder of the coated model in order to prevent radial heat conduction in the vicinity where the thermocouple was mounted. By concentrating on the central portion of the model in this manner, edge effects associated with swelling were also eliminated. After each model was mounted in the asbestos template, additional asbestos insulation was positioned over the back side of the model to achieve an adiabatic backwall boundary condition.

Before and after each model was tested, the total heat flux at test area 1 was measured with a water-cooled calorimeter. During each test, the backwall temperature rise was continuously monitored. All data were recorded on a strip-chart recorder.

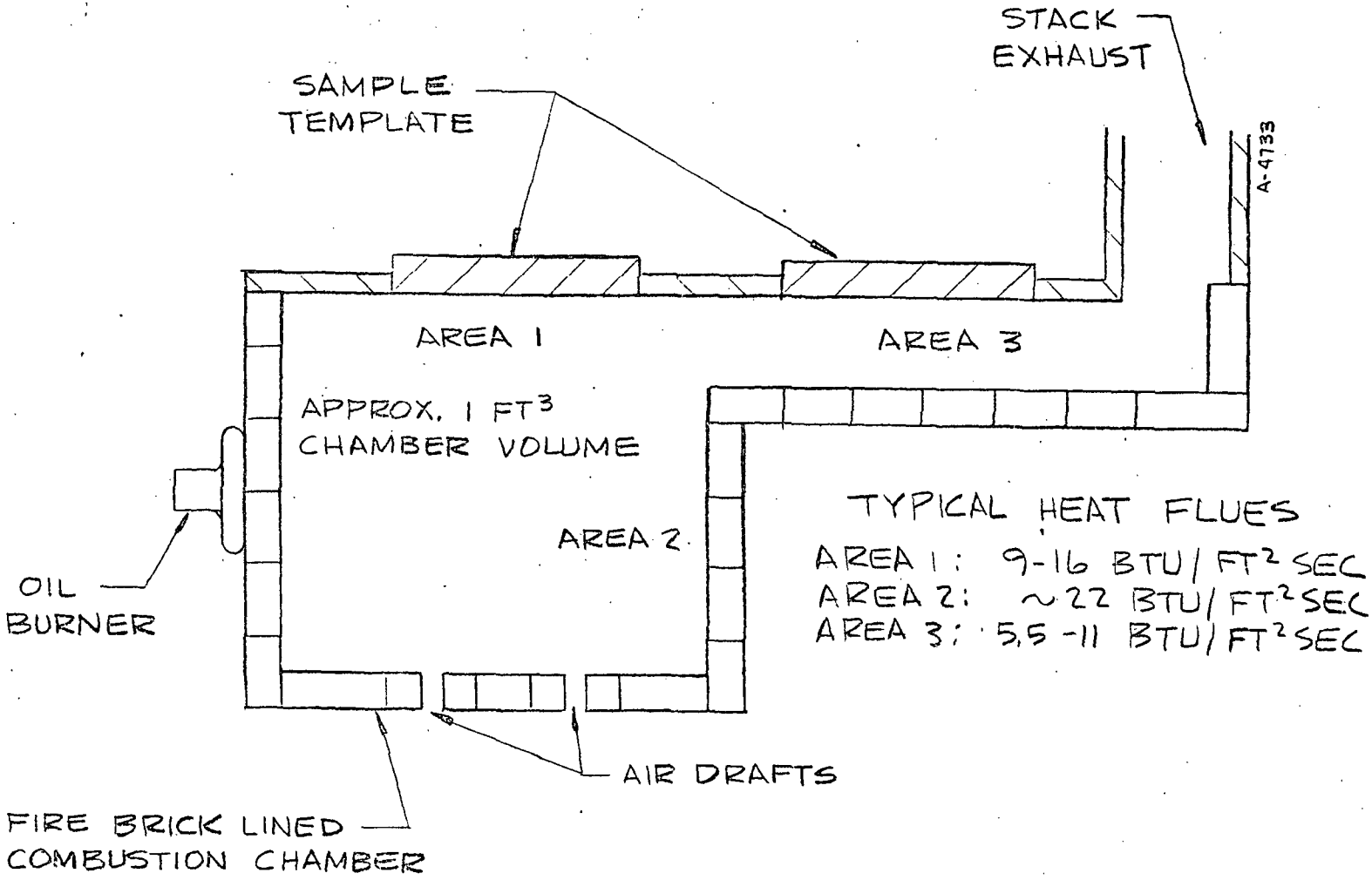

Figure 5-1. Schematic of NASA Ames CRPO T-3 Facility

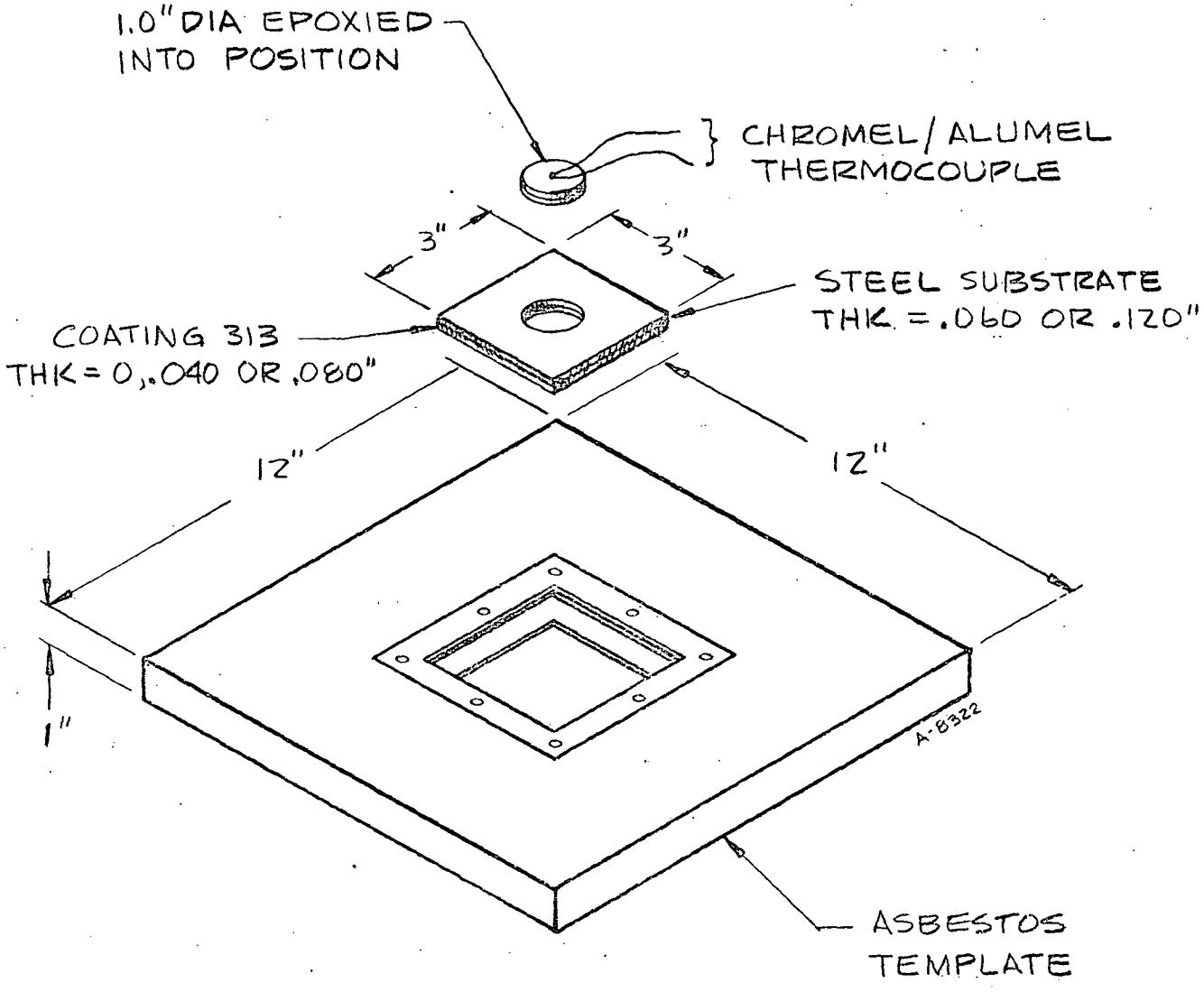

Figure 5-2. Schematic of the Coating 313/Steel Substrate Models Tested in the T-3 Facility

Table 5-1 presents a summary of the model coating/substrate configurations which were tested and Figures 5-3 through 5-7 show backwall temperature histories for these models.

Figure 5-3 presents the backwall temperature histories for the uncoated steel models. Two thicknesses were considered, 0.060 inch and 0.120 inch. The data appear to be fairly reproducible and consistant, with the temperature rise rate for the thinner model being somewhat higher than that for the thicker model. The measured heat flux after each test was always slightly lower than that measured before the test. This was due to the radiative loss experienced by the interior walls of the furance when the hatch at area 1 was opened to insert and remove the model.

Figures 5-4 to 5-7 present the measured backwall temperature histories for the coated models. These data are seen to be quite reproducible and self-consistant. The model with the thinnest coating and thinnest substrate (0.040 inch, 0.060 inch) experienced the highest temperature rise rate. The model with the thickest coating and thickest substrate (0.080 inch, 0.120 inch) had the lowest temperature rise rate. Intermediately, the model with 0.040/0.120 coating/substrate had a temperature rise rate which was higher than that for the 0.080/0.060 coating/substrate model.

The 0.060 inch uncoated substrate reached a backwall temperature of 1000°R in about 20 seconds. A 0.040 inch coating extended the time to 90 seconds, and a 0.080 inch coating extended the time to 140 seconds. The 0.120 inch uncoated substrate reached a backwall temperature of 1000°R in roughly 35 seconds. Coatings of 0.040 inch and 0.080 inch extended this time to 100 seconds and 220 seconds, respectively.

Test run 5a was a rerun of the model tested in run 5. In this precharred condition, the coating offered inferior protection to that provided by the initially undecomposed coating of run 5. This implies that decomposition of Coating 313 is accompanied by a highly endothermic reaction whose energy absorption more than offsets the improved early-time reradiation provided by a precharred coating. Note (Figure 5-5) that the departure of the temperature histories for runs 5 and 5a from one another occurs at about 900-950°R, which is approximately the temperature of intumescence for Coating 313 (see Figure 2-5).

Approximate measurements of the total post-test swell were made. They indicated that the final thickness of the charred coating was in general about five times the thickness of the virgin coating.

TABLE 5-1

SUMMARY OF T-3 TEST DATA

Test Run #	Model No.	Substrate Thickness (in)	Coating Thickness (in)
1	313-.062-1	0.060	0
2	313-.125-1	0.120	0
3	313-.062-3	0.060	0.080
4	313-.062-4	0.060	0.079
5	313-.062-5	0.060	0.040
5a	313-.062-5	0.060	charred
6	313-.062-6	0.060	0.038
7	313-.062-2	0.060	0
8	313-.125-2	0.120	0
9*	313-.125-3	0.120	0.041
10	313-.125-4	0.120	0.040
11	313-.125-5	0.120	0.085
12	313-.125-6	0.119	0.082

*Test terminated prematurely due to broken model thermocouple

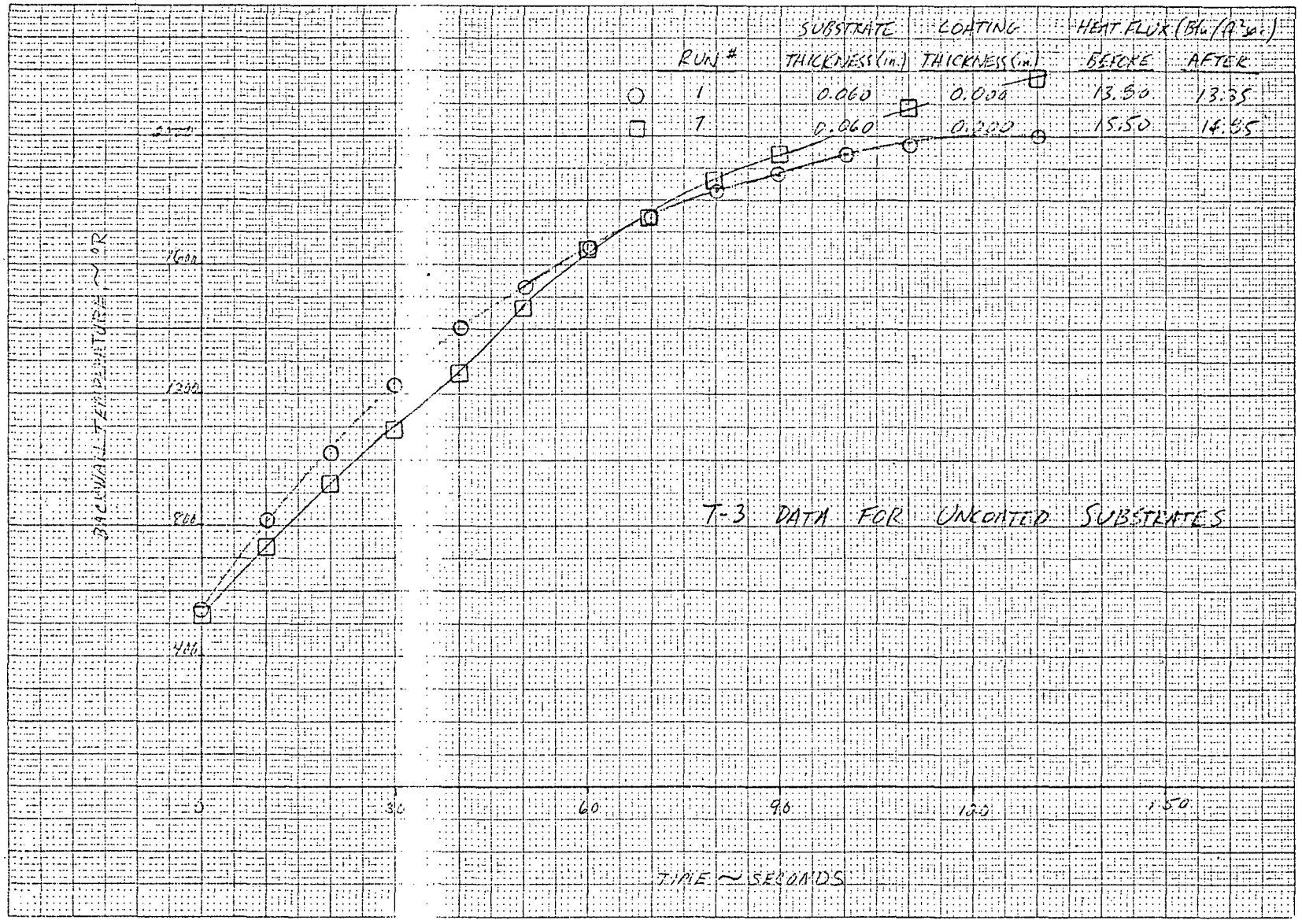
RUN #
SUBSTRATE THICKNESS (in.)
COATING THICKNESS (in.)
HEAT FLUX (Btu/ft²sec)
BEFORE
AFTER
1
0.060
0.004
13.30
13.35
7
0.060
0.020
15.50
14.55
T-3 DATA FOR UNCOATED SUBSTRATES
BACKWALL TEMPERATURE ~ °R
1600
1200
800
400
30
60
90
120
150
TIME ~ SECONDS

Figure 5-3

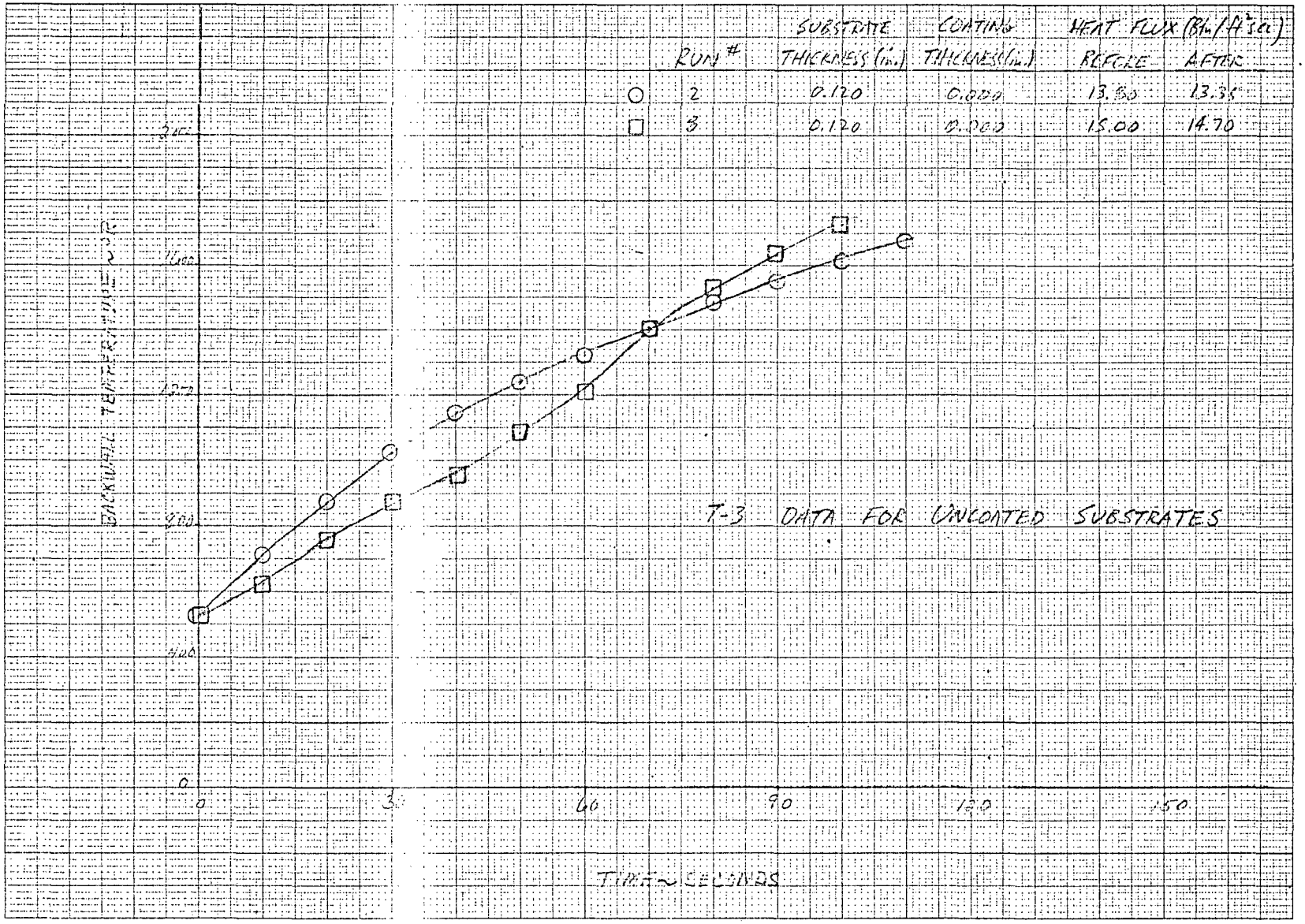

Figure 5-3. Concluded

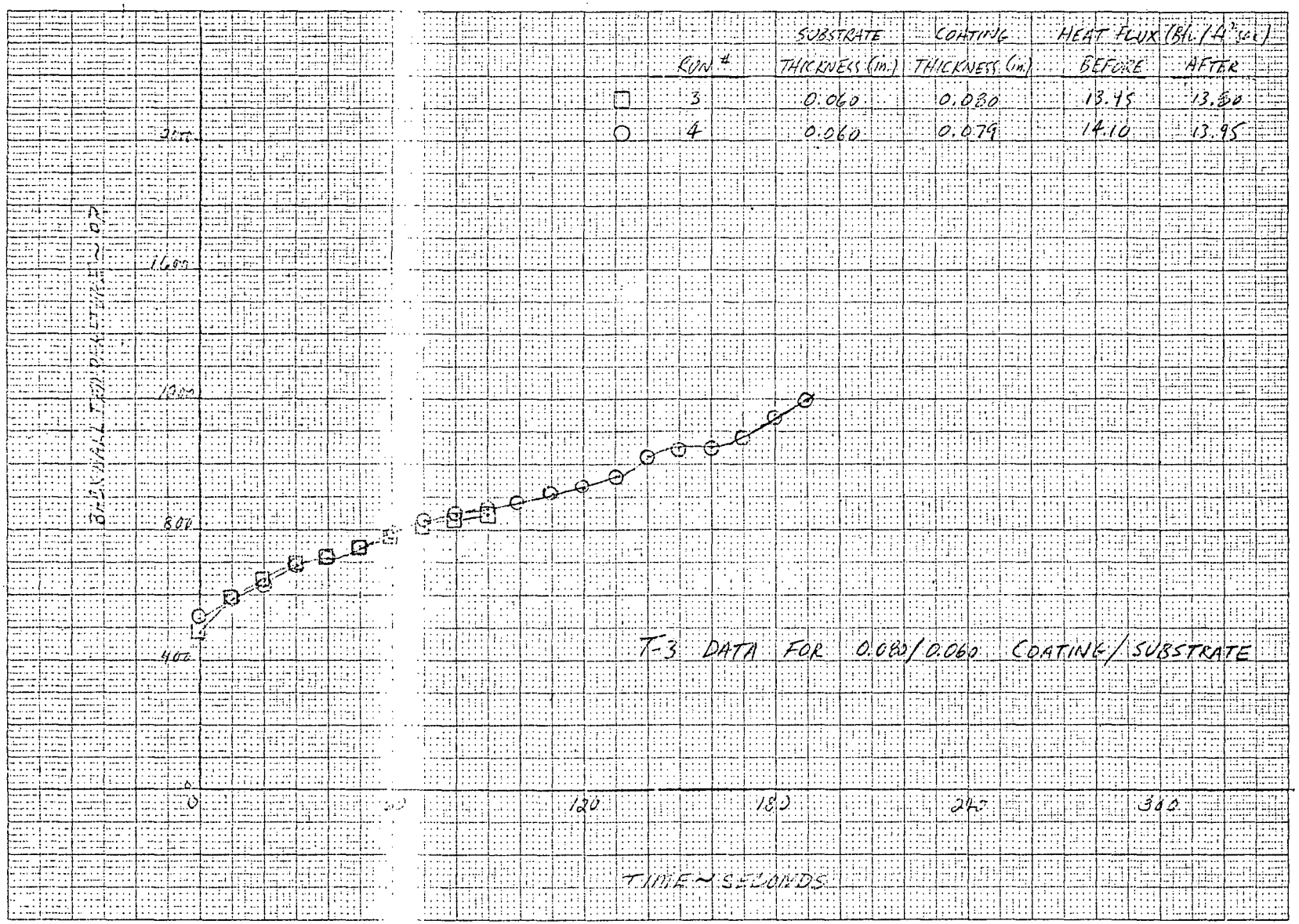
RUN #
SUBSTRATE THICKNESS (in.)
COATING THICKNESS (in.)
HEAT FLUX (Btu/ft² sec)
BEFORE
AFTER
3
0.060
0.080
13.45
13.50
4
0.060
0.079
14.10
13.95
T-3 DATA FOR 0.080/0.060 COATING/SUBSTRATE
BACK WALL TEMPERATURE ~ °F
TIME ~ SECONDS
0
120
180
240
300
400
800
1200
1600

Figure 5-4

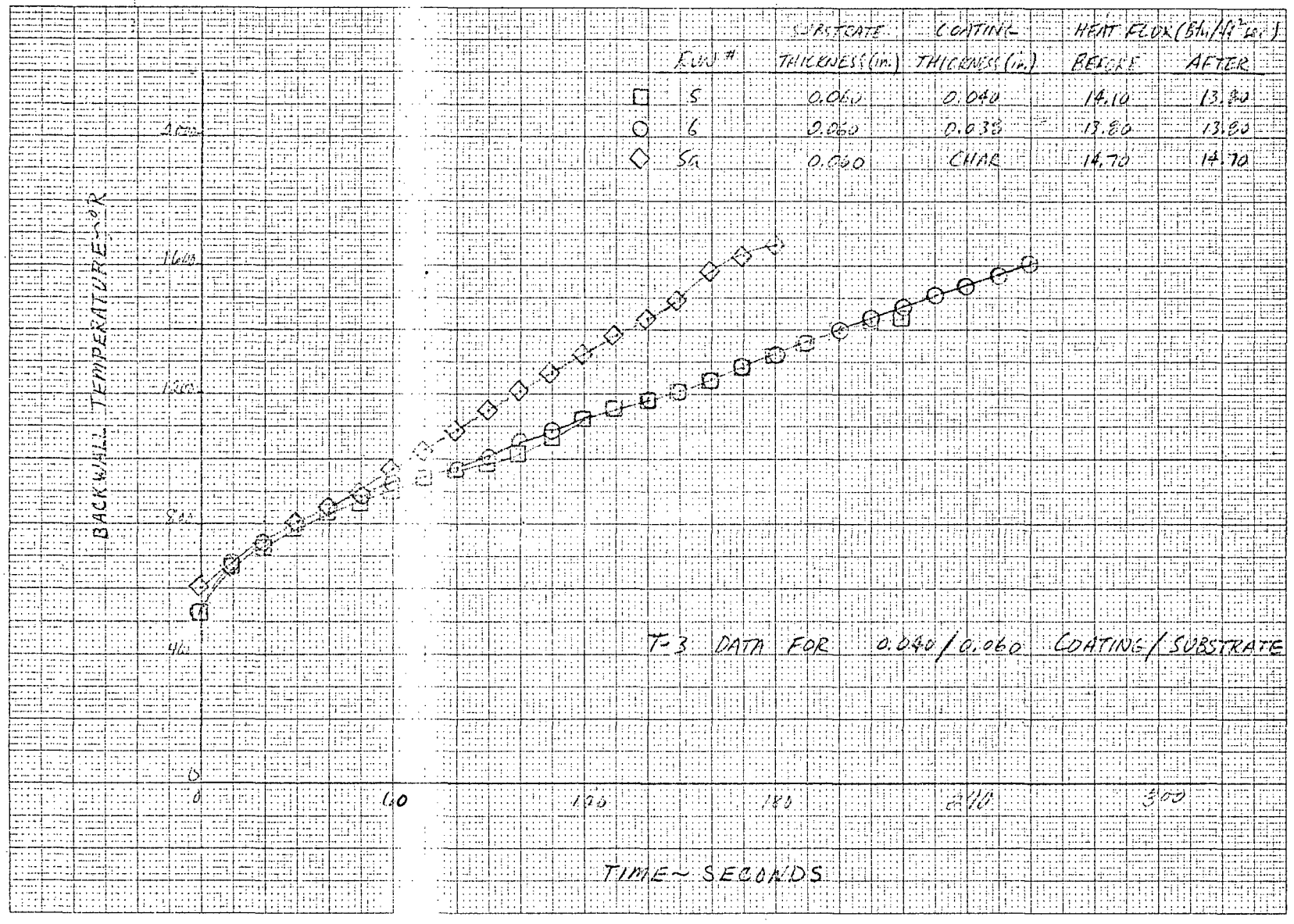
RUN #
SUBSTRATE THICKNESS (in.)
COATING THICKNESS (in.)
HEAT FLUX (Btu/ft²-sec) BEFORE
HEAT FLUX (Btu/ft²-sec) AFTER
5 0.060 0.040 14.10 13.80
6 0.060 0.033 13.80 13.80
5A 0.060 CHAR 14.70 14.70
BACKWALL TEMPERATURE °R
TIME ~ SECONDS
T-3 DATA FOR 0.040/0.060 COATING/SUBSTRATE

Figure 5-5

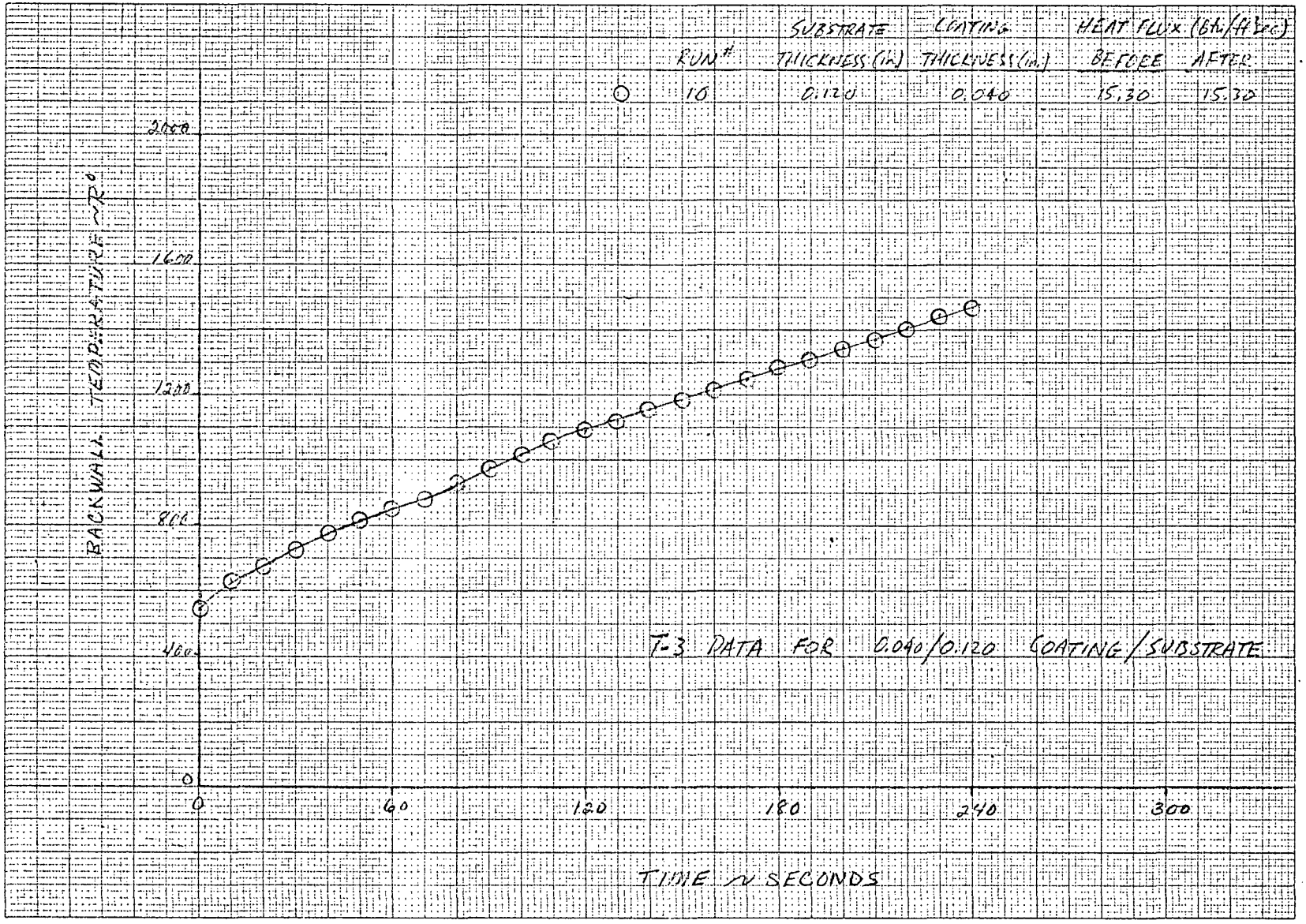
RUN #
SUBSTRATE THICKNESS (in.)
COATING THICKNESS (in.)
HEAT FLUX (Btu/ft² sec) BEFORE
AFTER
10
0.120
0.040
15.30
15.30
BACKWALL TEMPERATURE ~R°
2000
1600
1200
800
400
0
0
60
120
180
240
300
T-3 DATA FOR 0.040/0.120 COATING/SUBSTRATE
TIME ~ SECONDS

Figure 5-6

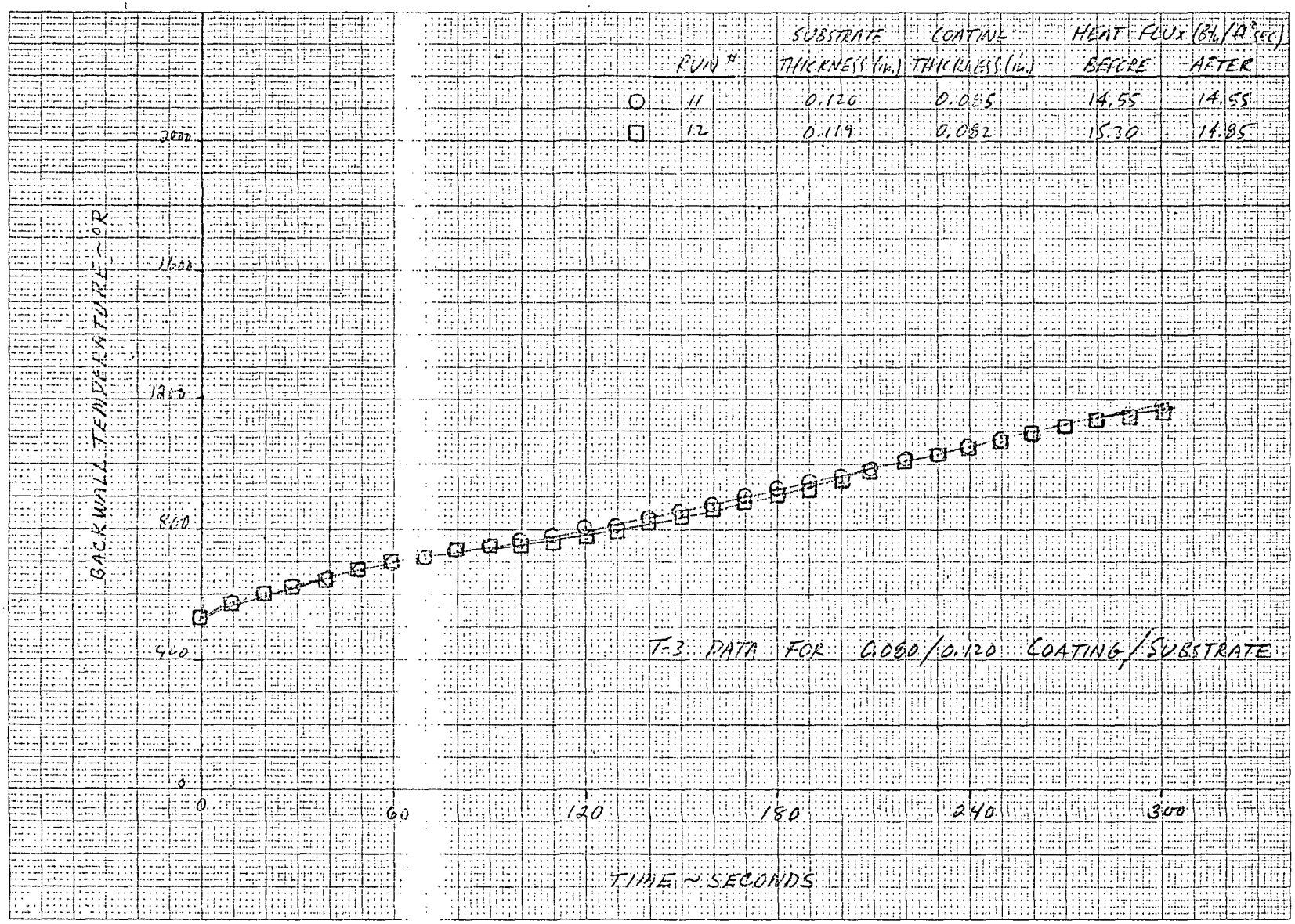
RUN #
SUBSTRATE THICKNESS (in.)
COATING THICKNESS (in.)
HEAT FLUX (Btu/ft²sec) BEFORE
HEAT FLUX (Btu/ft²sec) AFTER
○ 11 0.120 0.085 14.55 14.55
□ 12 0.119 0.082 15.30 14.85
BACKWALL TEMPERATURE ~ °R
2000
1600
1200
800
400
0
0
60
120
180
240
300
TIME ~ SECONDS
T-3 DATA FOR 0.080/0.120 COATING/SUBSTRATE

Figure 5-7

SECTION 6
COMPARISON OF PREDICTIONS WITH DATA

Using the input data discussed in Section 2 in conjunction with the TRIM code, predictions of the experimentally-measured backwall temperature histories discussed in Section 5 were carried out. By adjusting the values of three of the input parameters, optimum agreement between all predictions and data was obtained. The three parameters which were adjusted were the char heat of formation, Δh_c, the activation energy for the intumescing reaction, E_{a_B}, and the char thermal conductivity, k_c. As discussed in Section 2, each of these properties has a rather large associated uncertainty.

Figure 6-1 presents the predictions of the data for the uncoated steel substrate models. The reason for performing these predictions was to demonstrate that the uncoated steel plate response could be predicted utilizing the measured heat flux as a boundary condition and nominal values of thermophysical properties for steel. While the properties ρ, C_p, and k are known with minimal uncertainty, the surface emissivity under the test conditions was not so well defined. However, reasonable values of the emissivity, bracketed by the extreme values corresponding to a fully polished (high ϵ) and a fully oxidized (low ϵ) steel surface, lead to a reasonable match between prediction and data. This result gives confidence in the measured values of impinging heat flux obtained during the test program.

Adjustment of the parameters Δh_c and E_{a_B} was carried out for the predictions corresponding to the 0.040/0.060 coating/substrate test runs. As shown in Figure 6-2, it was found that E_{a_B} controls the initial slope and curvature of the backwall temperature response curve and Δh_c controls the level, but not the slope, of the temperature response late in time. Optimum agreement was obtained by increasing the original (Section 2) value of Δh_c from -4208.5 Btu/lbm to +2500. Btu/lbm and decreasing the original value of E_{a_B} from 20130°R to 15000°R.

The char thermal conductivity, k_c, was investigated through comparison with both the virgin and precharred 0.040/0.060 coating/substrate models. Comparison with the precharred model is shown in Figure 6-3. From this figure it was concluded that a k_c value of twice the original value was most appropriate.

Figure 6-4 shows the sensitivity of the prediction for the decomposing 0.040/0.060 coating/substrate model to variations in k_c. Consistent with the

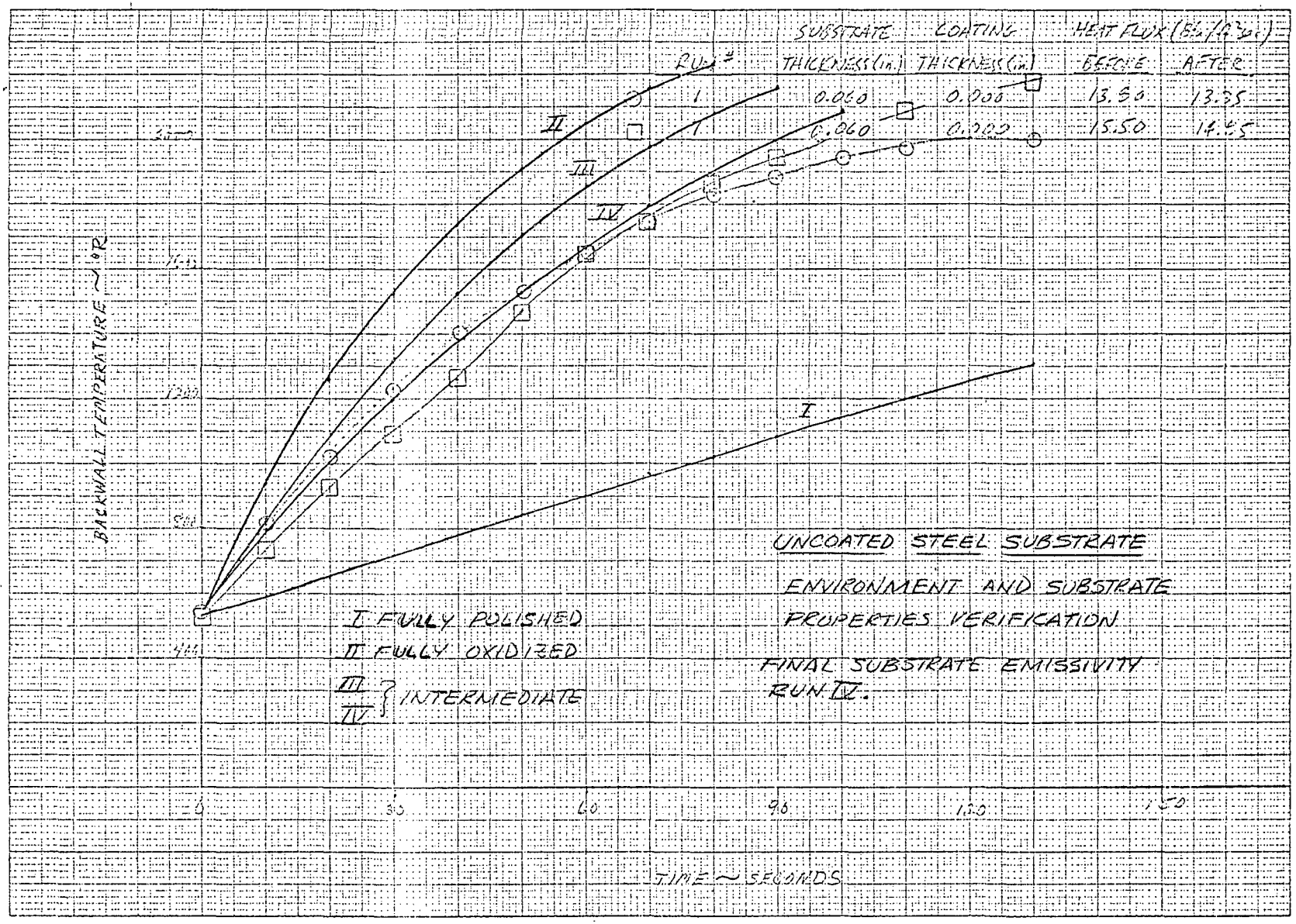
SUBSTRATE THICKNESS (in.)
COATING THICKNESS (in.)
HEAT FLUX (BTU/ft²-sec)
BEFORE
AFTER
RUN #
I 0.060 0.000 13.50 13.55
II 0.060 0.202 15.50 14.45
III
IV
BACKWALL TEMPERATURE ~ °R
TIME ~ SECONDS
UNCOATED STEEL SUBSTRATE
ENVIRONMENT AND SUBSTRATE PROPERTIES VERIFICATION
FINAL SUBSTRATE EMISSIVITY RUN IV.
I FULLY POLISHED
II FULLY OXIDIZED
III / IV } INTERMEDIATE

Figure 6-1

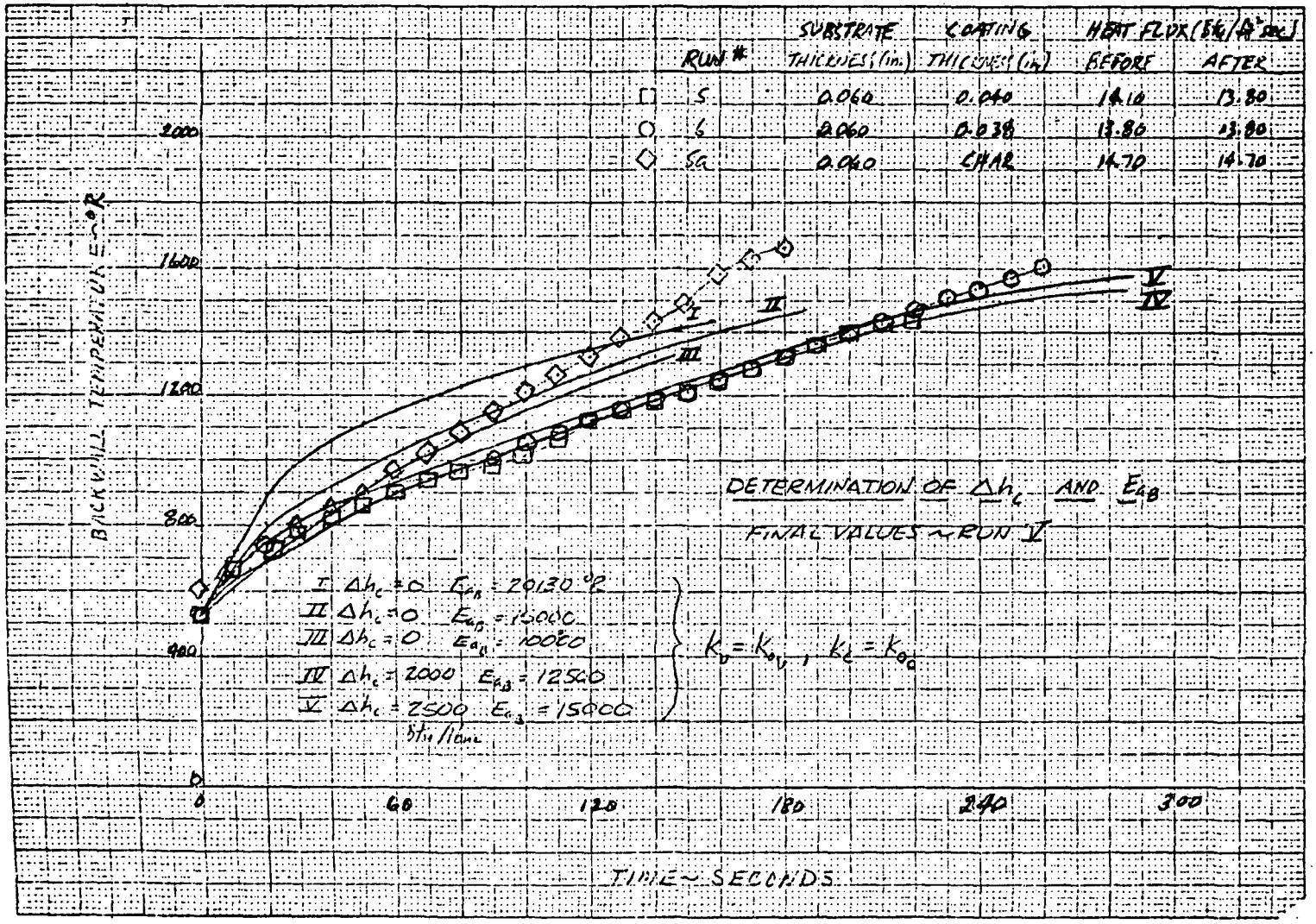
RUN #
SUBSTRATE THICKNESS (in.)
COATING THICKNESS (in.)
HEAT FLUX (Btu/ft² sec)
BEFORE
AFTER
S 0.060 0.040 14.10 13.80
6 0.060 0.038 13.80 13.80
Sa 0.060 CHAR 14.70 14.70
BACKWALL TEMPERATURE °R
2000
1600
1200
800
400
0
60
120
180
240
300
TIME ~ SECONDS
I
II
III
IV
V
DETERMINATION OF Δh_c AND E_aB
FINAL VALUES ~ RUN V
I Δh_c = 0 E_aB = 20130 °R
II Δh_c = 0 E_aB = 15000
III Δh_c = 0 E_aB = 10000
IV Δh_c = 2000 E_aB = 12500
V Δh_c = 2500 E_aB = 15000
btu/ft sec
K_v = K_aV , K_c = K_aC

Figure 6-2

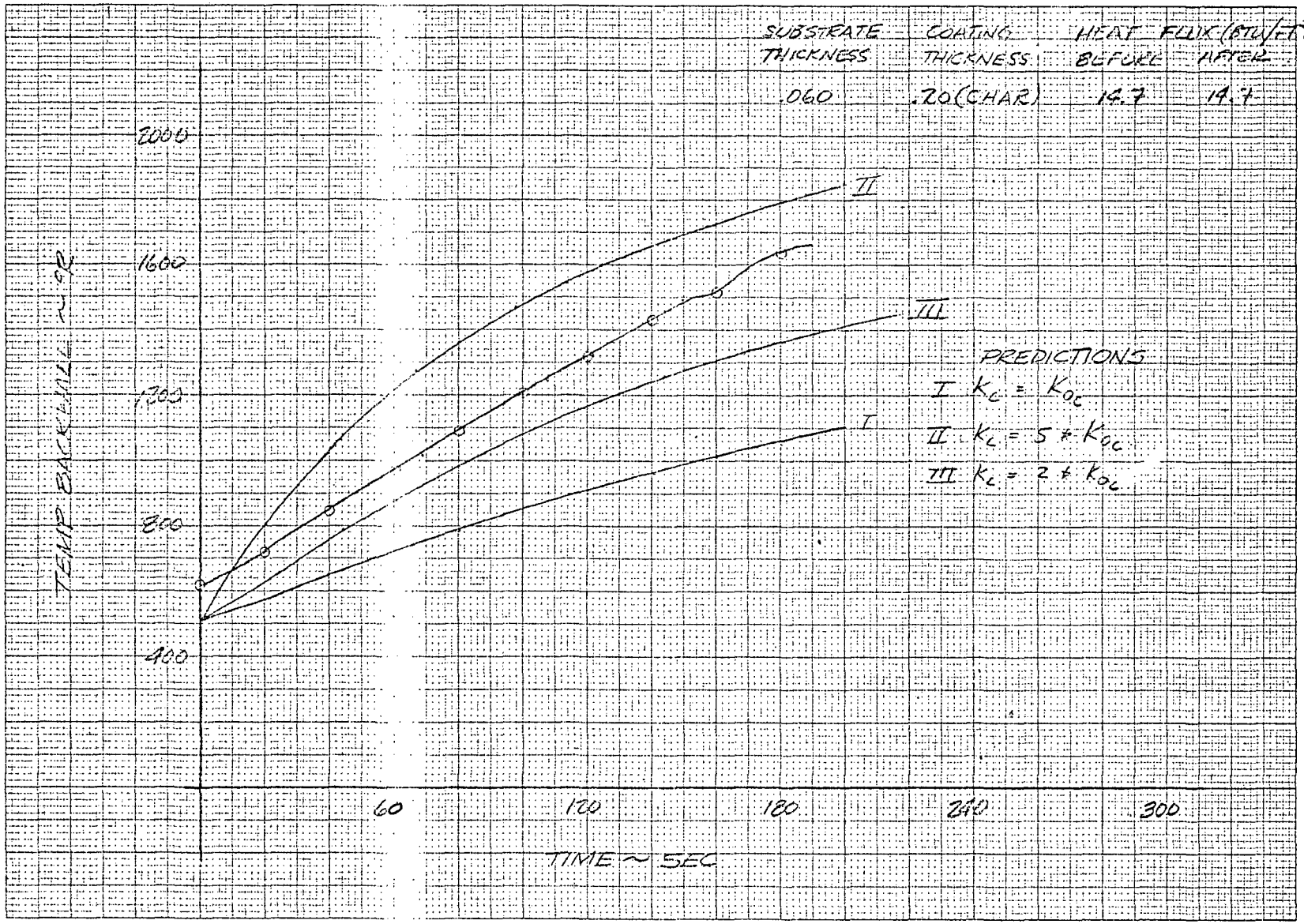
SUBSTRATE THICKNESS
COATING THICKNESS
HEAT FLUX (BTU/FT²SEC)
BEFORE
AFTER
.060
.20(CHAR)
14.7
14.7
2000
1600
1200
800
400
TEMP BACKWALL ~ °F
II
III
I
PREDICTIONS
I $K_c = K_{oc}$
II $K_c = 5 * K_{oc}$
III $K_c = 2 * K_{oc}$
60
120
180
240
300
TIME ~ SEC

Figure 6-3

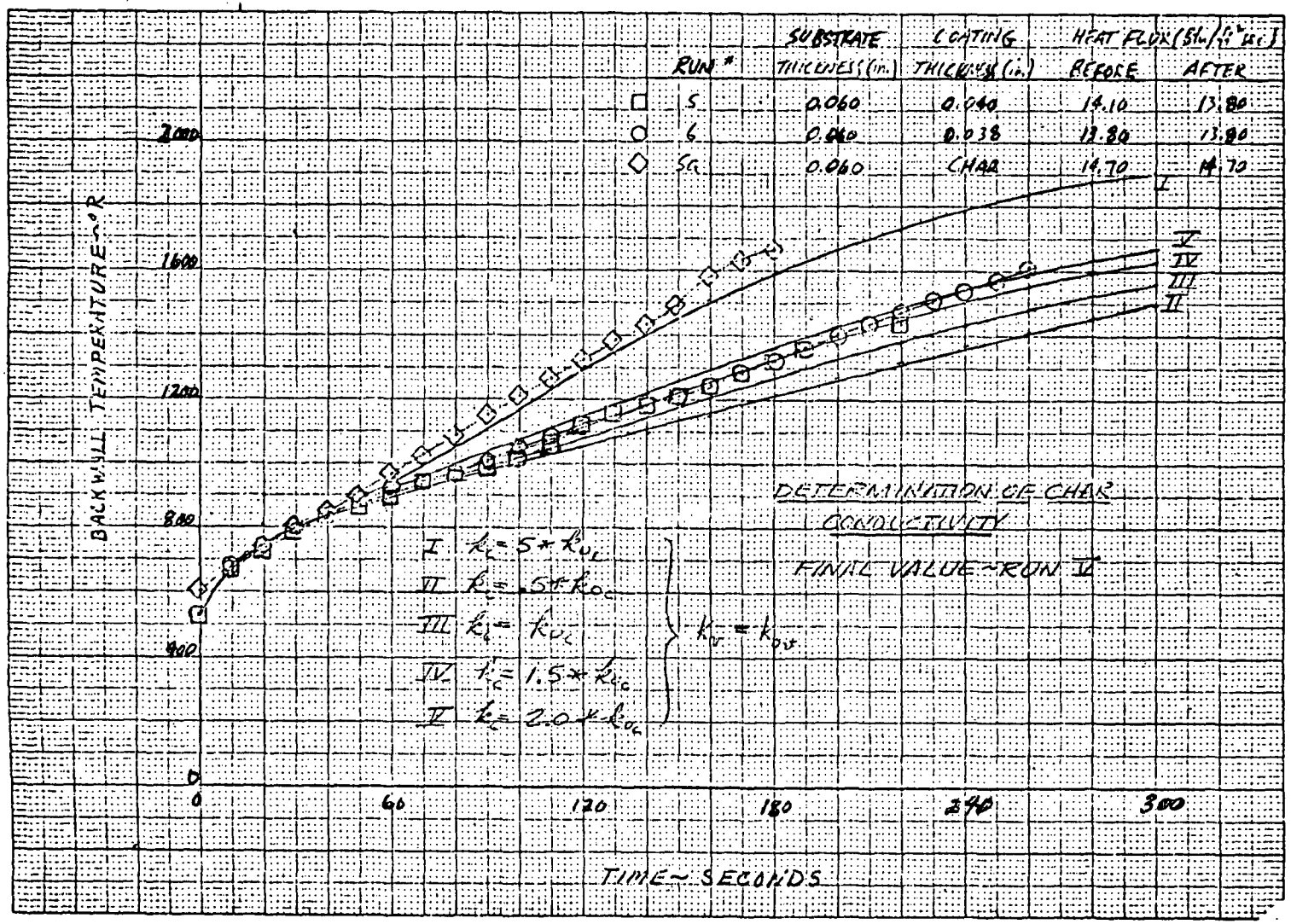
RUN #
SUBSTRATE THICKNESS (in.)
COATING THICKNESS (in.)
HEAT FLUX (Btu/in²-sec) BEFORE
HEAT FLUX (Btu/in²-sec) AFTER
□ 5 0.060 0.040 14.10 13.80
○ 6 0.060 0.038 13.80 13.80
◇ 5a 0.060 CHAR 14.70 14.70
BACK WALL TEMPERATURE °R
2000
1600
1200
800
400
0
60
120
180
240
300
TIME ~ SECONDS
I
V
IV
III
II
DETERMINATION OF CHAR CONDUCTIVITY
FINAL VALUE ~ RUN II
I $k_c = 5 * k_{v_c}$
VI $k_c = .5 * k_{v_c}$
III $k_c = k_{v_c}$
IV $k_c = 1.5 * k_{v_c}$
II $k_c = 2.0 * k_{v_c}$
$k_v = k_{v_c}$

Figure 6-4

results of Figure 6-3, it appears that a k_c value of twice the original value leads to the best agreement between prediction and data.

Figure 6-5 illustrates the sensitivity of the prediction for the decomposing 0.040/0.060 coating/substrate model to variations in k_p. From this figure, it is concluded that the original value of k_p gives the most satisfactory results.

Figures 6-6 to 6-9 present the final predictions for all test cases. It should be emphasized that the parameters Δh_c, E_{a_B}, and k_c were adjusted based on comparisons with only one of the models, that with the 0.040/0.060 coating/substrate combination. The final values thus determined, Δh_c = 2500 Btu/lbm, E_{a_B} = 15000°R, and $k_c = 2 * k_{o_c} = 0.22 \times 10^{-4}$ Btu/ft sec °R, were used unchanged in the predictions for the remaining three model configurations. In general, the early-time prediction ($\theta \leq 60$ sec) is in excellent agreement with the corresponding data, for all four cases. Of course, the prediction is in good agreement with the data at all times for the 0.040/0.060 coating/substrate case, since the model was "tuned" to this baseline case. For the remaining three models, the late-time prediction falls slightly below the corresponding experimental data.

In view of the comparisons between the final predictions and experimental data presented in Figures 6-6 to 6-9, definite uncertainty must be assigned to the overall prediction procedure, especially for the late-time predictions. For a given time after exposure to the heating environment, the predicted (absolute) backwall temperature should be viewed as being within 20 percent of the actual value. Of course, the early-time predictions are somewhat more accurate than this. On the other hand, the uncertainty associated with the predicted time to reach a specified temperature depends greatly on the slope of the temperature-versus-time curve, for late times. For the cases considered here, the maximum late-time deviation between prediction and data occurs for tests 11 and 12 (Figure 6-9), with the predicted time to reach 1000°R being about 40 percent greater than the actual time. Again, the early-time prediction for this same case and the overall predictions for the other cases are considerably better.

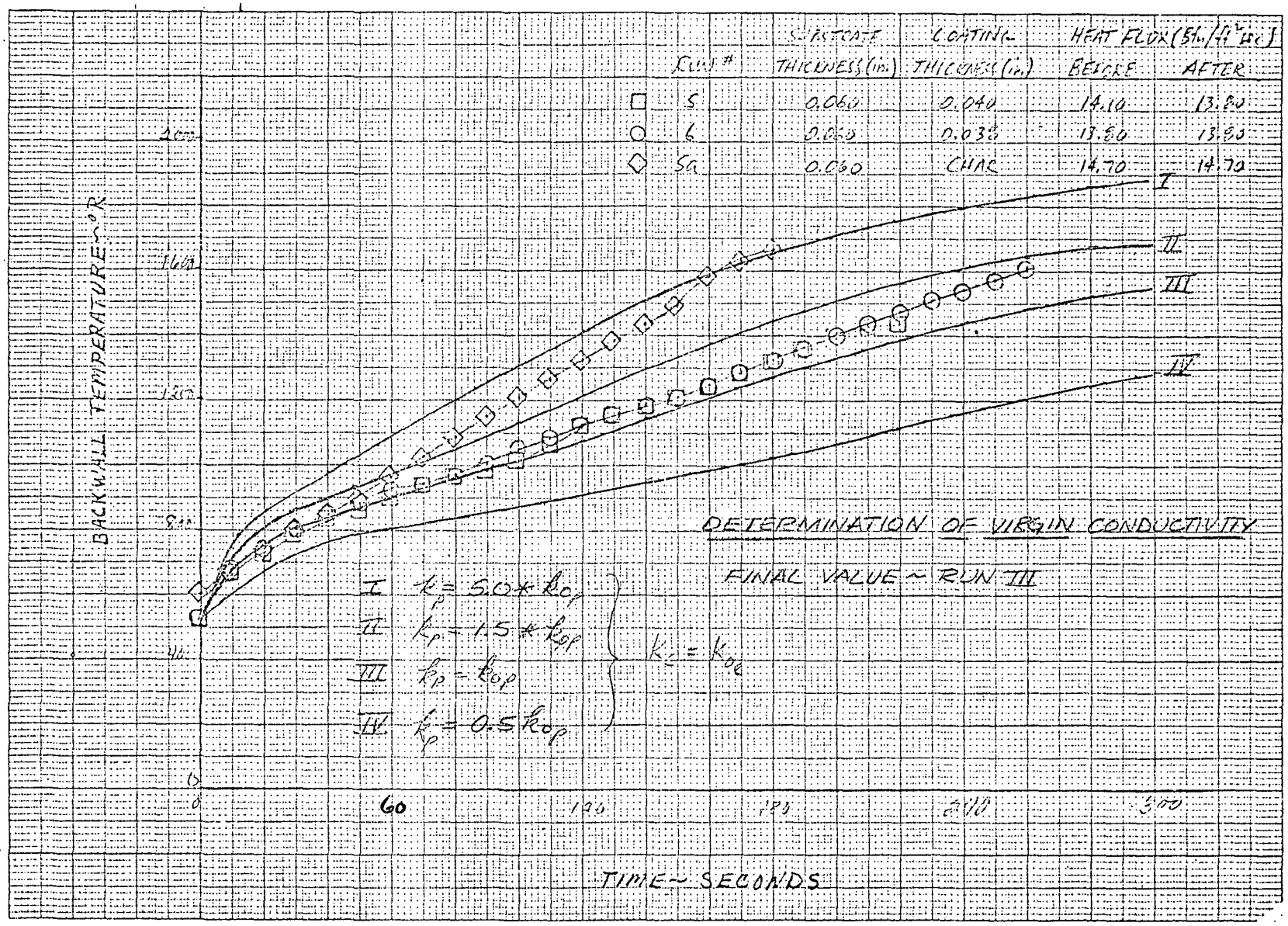
Run #
SUBSTRATE THICKNESS (in.)
COATING THICKNESS (in.)
HEAT FLUX (Btu/ft²-sec) BEFORE
HEAT FLUX (Btu/ft²-sec) AFTER
5 0.060 0.040 14.10 13.80
6 0.060 0.038 13.80 13.90
5a 0.060 CHAR 14.70 14.70
I
II
III
IV
BACKWALL TEMPERATURE ~ °R
TIME ~ SECONDS
60
DETERMINATION OF VIRGIN CONDUCTIVITY
FINAL VALUE ~ RUN III
I $k_p = 5.0 * k_{op}$
II $k_p = 1.5 * k_{op}$
III $k_p = k_{op}$
IV $k_p = 0.5 k_{op}$
$k_c = k_{oc}$

Figure 6-5

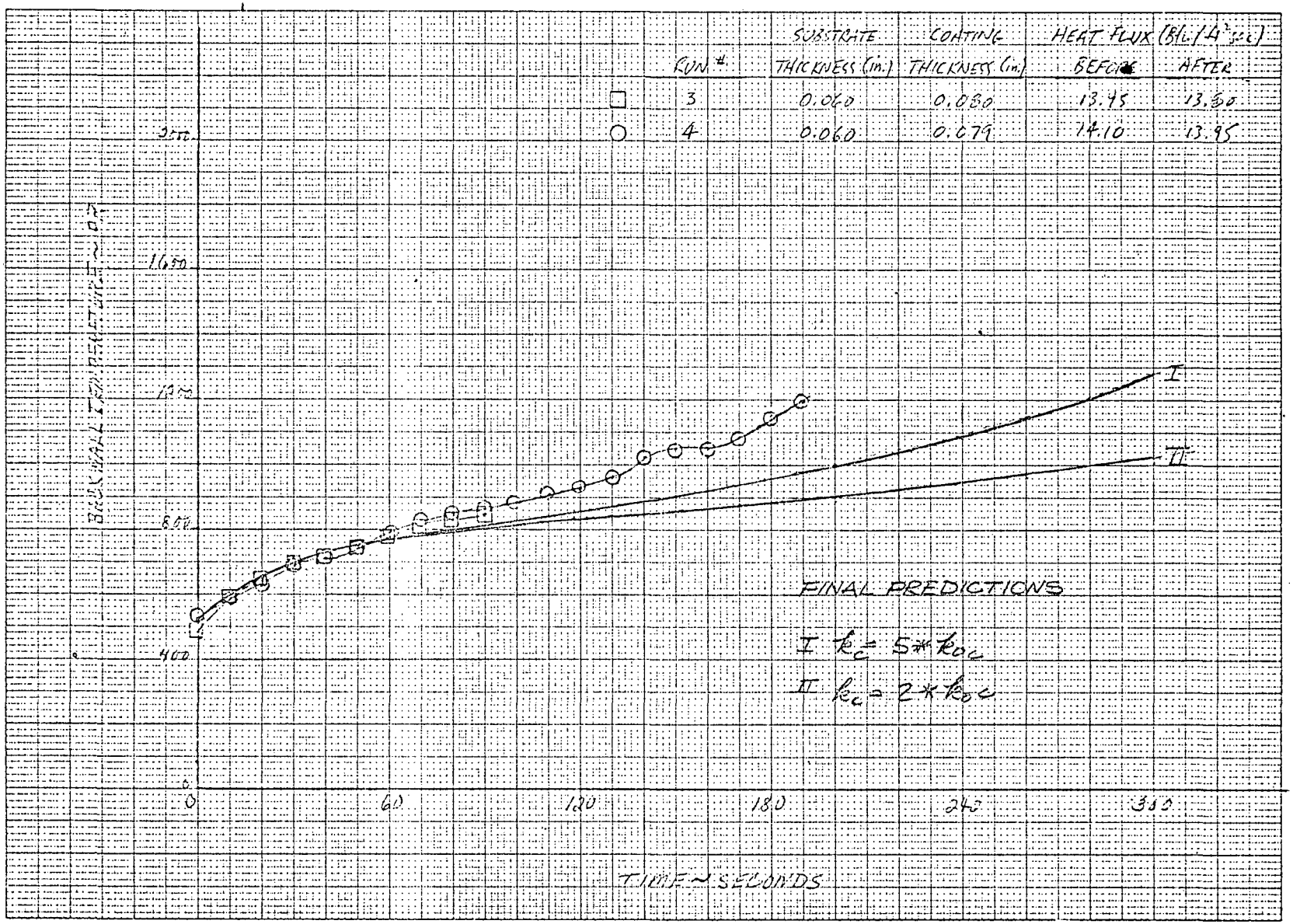
RUN #
SUBSTRATE THICKNESS (in.)
COATING THICKNESS (in.)
HEAT FLUX (Btu/ft² sec)
BEFORE
AFTER
3 0.060 0.080 13.75 13.50
4 0.060 0.079 14.10 13.95
1650
825
400
0
60
120
180
240
300
I
II
FINAL PREDICTIONS
I $k_c = 5 * k_{oc}$
II $k_c = 2 * k_{oc}$
TIME ~ SECONDS

Figure 6-6

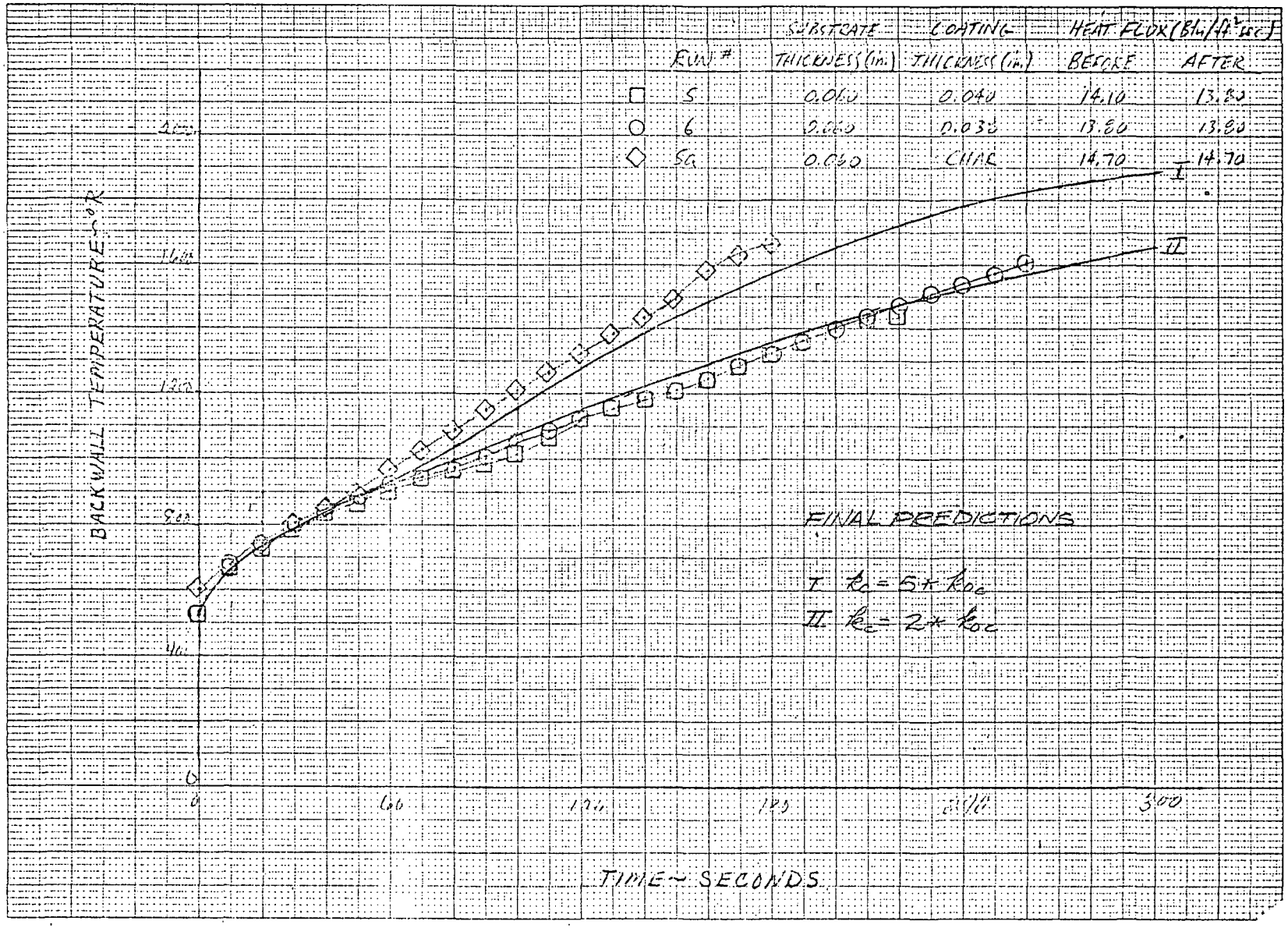
RUN #
SUBSTRATE THICKNESS (in.)
COATING THICKNESS (in.)
HEAT FLUX (BTU/FT² SEC) BEFORE
HEAT FLUX (BTU/FT² SEC) AFTER
5 0.060 0.040 14.10 13.80
6 0.060 0.035 13.80 13.80
5A 0.060 CHAR 14.70 14.70
I
II
FINAL PREDICTIONS
I $k_c = 5 * k_{oc}$
II $k_c = 2 * k_{oc}$
BACKWALL TEMPERATURE ~ °R
TIME ~ SECONDS
0
66
300

Figure 6-7

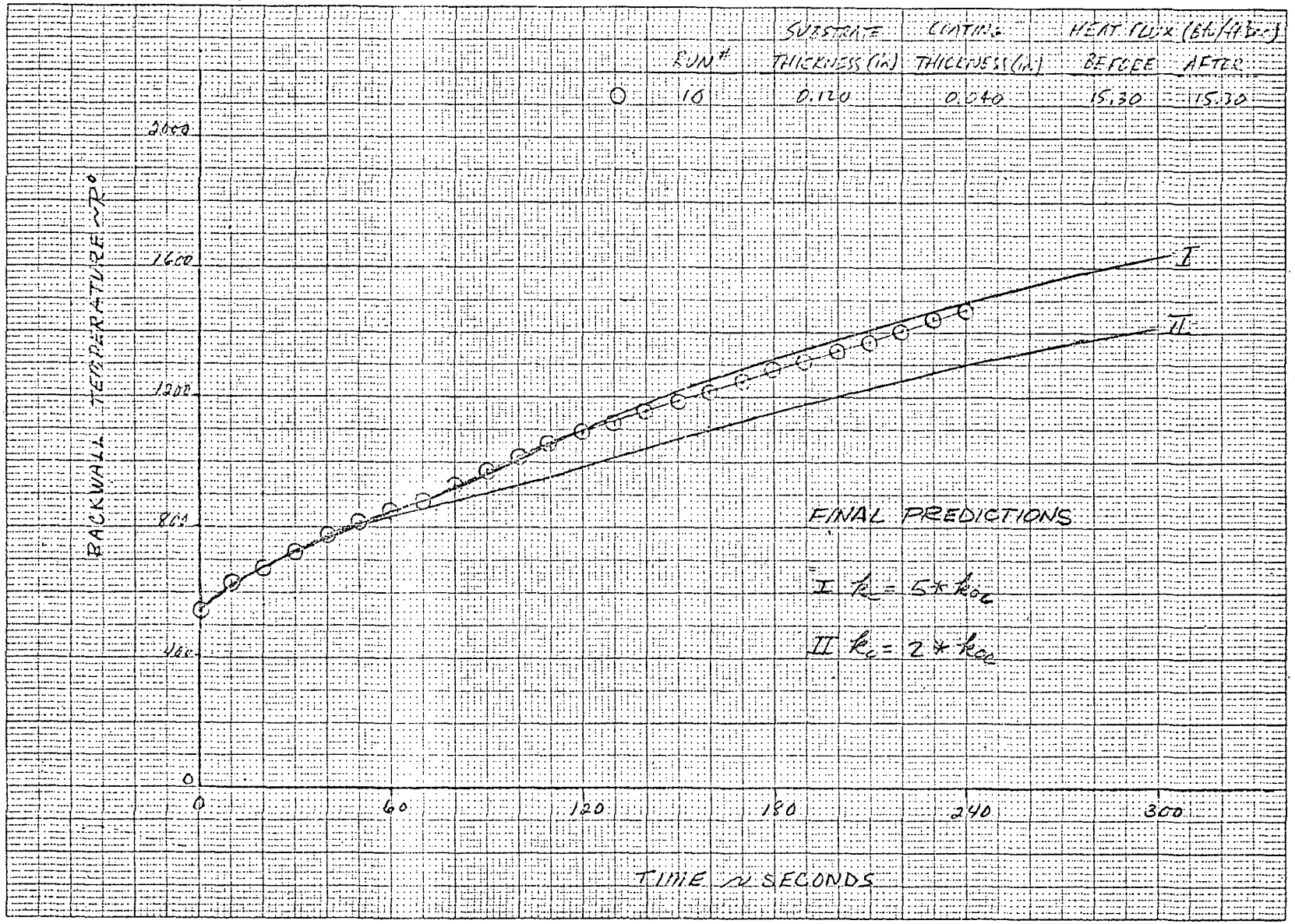
RUN #
SUBSTRATE THICKNESS (in)
COATING THICKNESS (in)
HEAT FLUX (BTU/FT²-sec)
BEFORE
AFTER
10
0.120
0.040
15.30
15.30
BACKWALL TEMPERATURE ~ F°
2000
1600
1200
800
400
0
0
60
120
180
240
300
TIME ~ SECONDS
I
II
FINAL PREDICTIONS
I $k_c = 5 * k_{oc}$
II $k_c = 2 * k_{oc}$

Figure 6-8

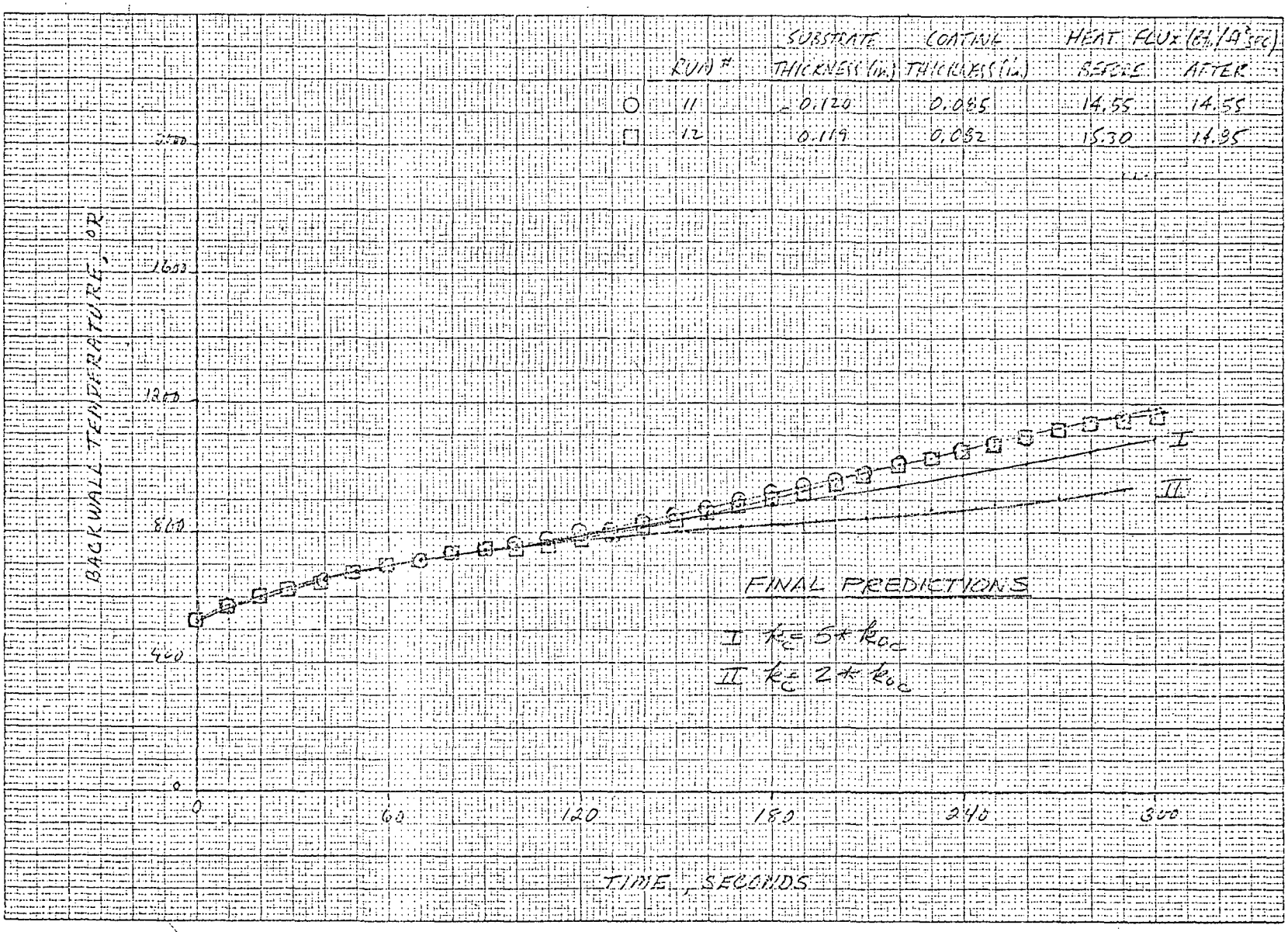
RUN #
SUBSTRATE THICKNESS (in.)
COATING THICKNESS (in.)
HEAT FLUX (Btu/ft²sec) BEFORE
HEAT FLUX (Btu/ft²sec) AFTER
○ 11 0.120 0.085 14.55 14.55
□ 12 0.119 0.082 15.30 14.95
BACKWALL TEMPERATURE, °R
1600
1200
800
400
0
0
60
120
180
240
300
TIME, SECONDS
I
II
FINAL PREDICTIONS
I $k_c = 5 * k_{0c}$
II $k_c = 2 * k_{0c}$

Figure 6-9

SECTION 7

PREDICTIONS WITH INTERMEDIATE INSULATION

An important alternative design for a thermal protection system utilizing an intumescent coating involves the installation of an inert insulation layer between the coating and the steel substrate. In this section, predictions are presented for backwall temperature history of a system utilizing an inert intermediate insulation layer.

Figure 7-1 presents the backwall temperature history predicted for six different configurations, all of which have a total original thickness for coating plus inert insulation of 0.100 in. In each case, however, the fractions of coating and insulation are different. Thermophysical properties used for the inert insulation are discussed in Section 2. They correspond to a reasonably dense (40-50 lbm/ft^3) insulation which can be applied in thin layers by spraying.

Figure 7-2 was generated from the temperature histories presented in Figure 7-1. It reveals that an optimum ratio of coating thickness to insulation thickness exists which maximizes the time to reach a specified value of the backwall temperature. Furthermore, this optimum ratio is a function of the value of the backwall temperature specified. As the specified threshold temperature increases, the optimum ratio of coating thickness to insulation thickness increases. For all temperatures of interest, this ratio is always greater than one-half.

Figure 7-3 compares the protection provided by systems with and without the intermediate insulation. In the situation where a 0.040 in insulation layer is added to a 0.060/0.060 coating/substrate system, substantial improvement in protection is realized, especially during the first two minutes of heating. Addition of a 0.020 in insulation layer to a 0.030/0.060 coating/substrate system does not lead to nearly as much improvement in protection.

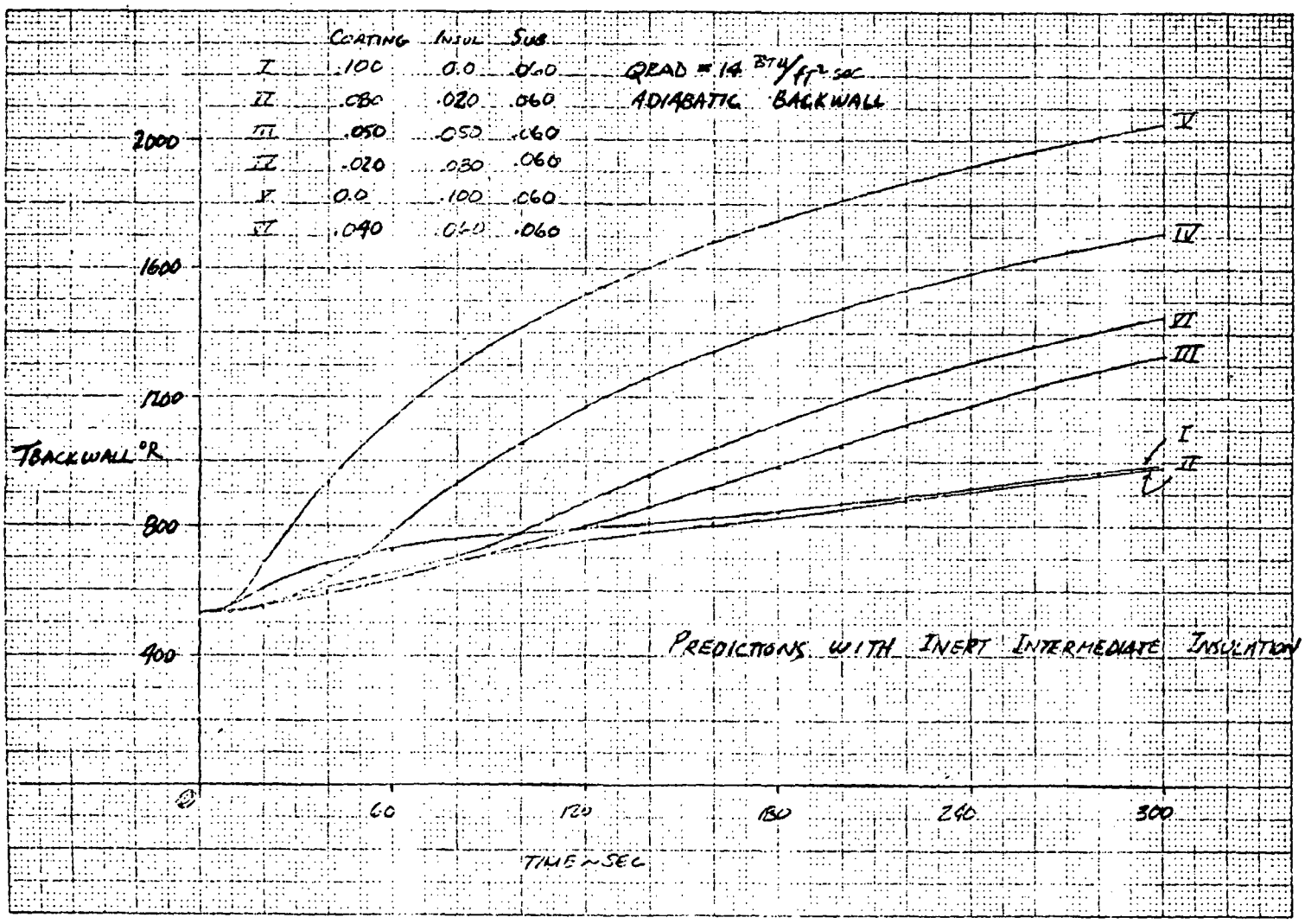
Coating Insul Sub
I .100 0.0 .060
II .080 .020 .060
III .050 .050 .060
IV .020 .030 .060
V 0.0 .100 .060
VI .090 .040 .060
QREAD = 14 BTU/ft² sec
ADIABATIC BACKWALL
2000
1600
1200
800
400
TBACKWALL °R
0
60
120
180
240
300
TIME - SEC
PREDICTIONS WITH INERT INTERMEDIATE INSULATION

Figure 7-1

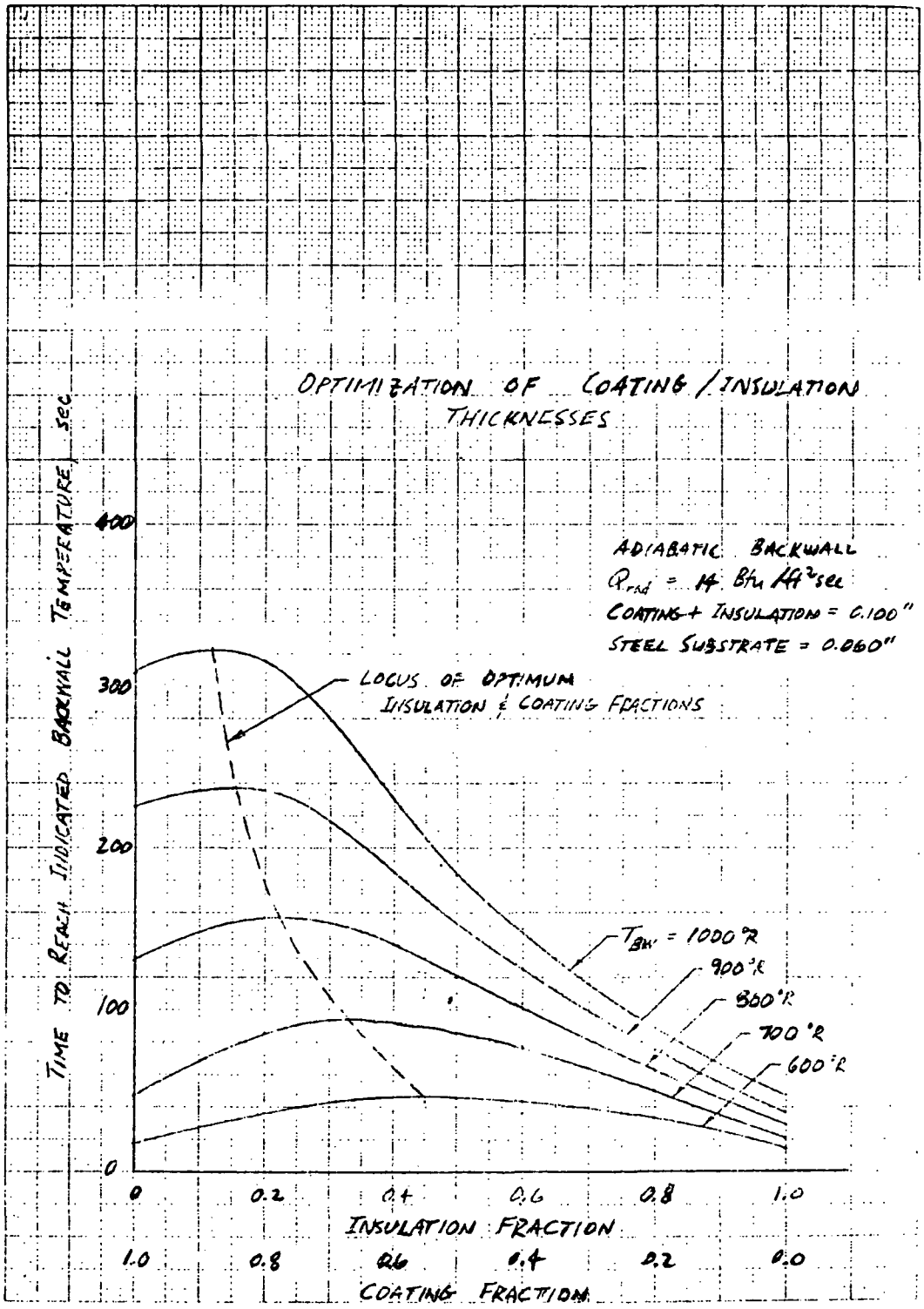
OPTIMIZATION OF COATING / INSULATION THICKNESSES
ADIABATIC BACKWALL
Q_{rad} = 14 Btu/ft²sec
COATING + INSULATION = 0.100"
STEEL SUBSTRATE = 0.060"
LOCUS OF OPTIMUM INSULATION & COATING FRACTIONS
T_{BW} = 1000°R
900°R
800°R
700°R
600°R
TIME TO REACH INDICATED BACKWALL TEMPERATURE, sec
400
300
200
100
0
0
0.2
0.4
0.6
0.8
1.0
INSULATION FRACTION
1.0
0.8
0.6
0.4
0.2
0.0
COATING FRACTION

Figure 7-2

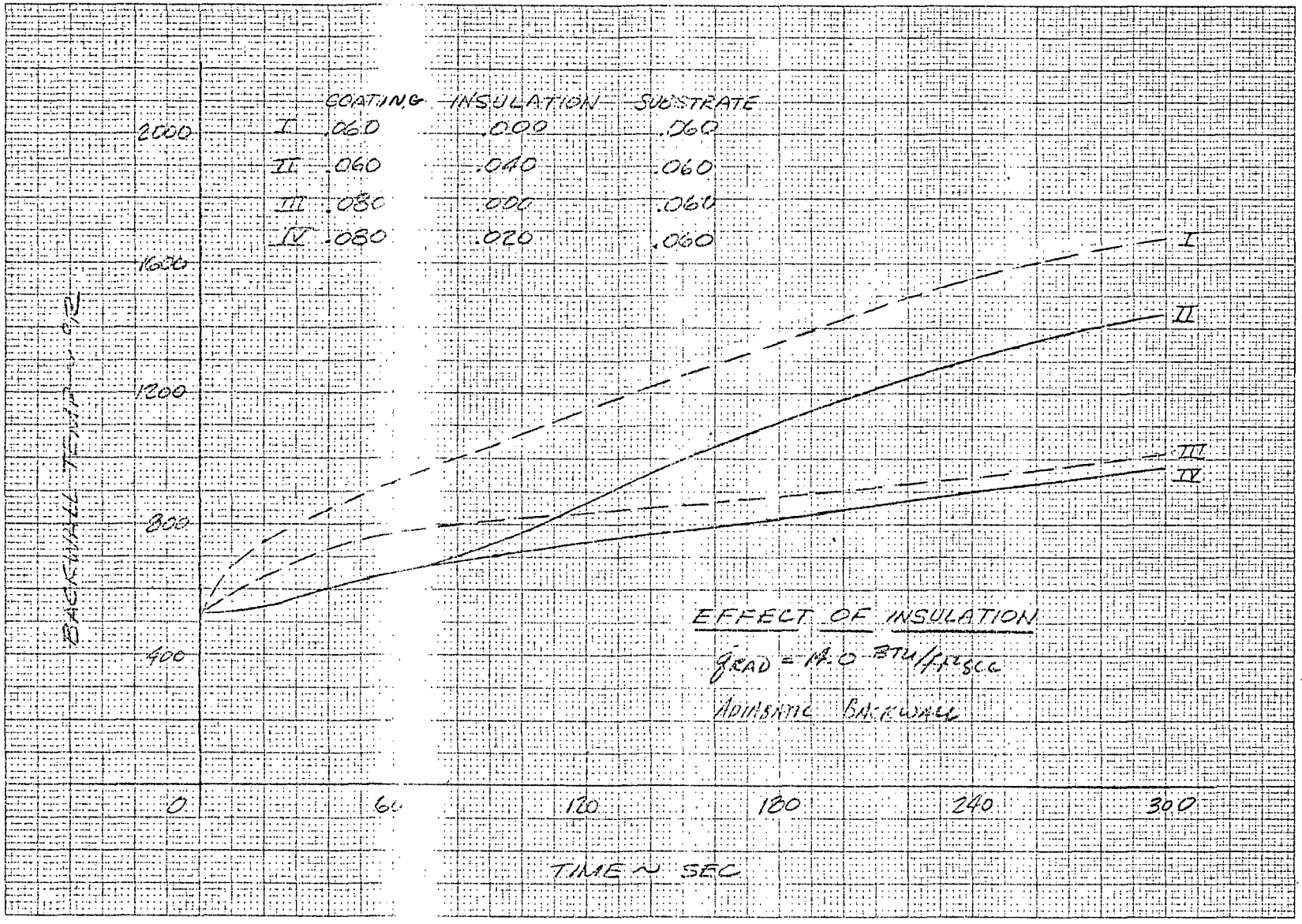
COATING INSULATION SUBSTRATE
I .060 .000 .060
II .060 .040 .060
III .080 .000 .060
IV .080 .020 .060
2000
1600
1200
800
400
0
60
120
180
240
300
I
II
III
IV
BACKWALL TEMP °R
TIME ~ SEC
EFFECT OF INSULATION
q_{RAD} = 14.0 BTU/FT²SEC
ADIABATIC BACKWALL

Figure 7-3

SECTION 8

SUMMARY AND CONCLUSIONS

The end product of this study is the Aerotherm Transient Response of Intumescing Materials (TRIM) computer program, which has been extensively validated and checked out for NASA Ames CRPO Coating 313. In the process of developing this code, the following tasks have been performed:

1. Thermophysical data for Coating 313 have been collected and reduced to a format appropriate for input to the TRIM code (Section 2).

2. A swell model has been developed and incorporated into the existing Aerotherm Charring Material Thermal Response and Ablation (CMA) code; additional code modifications associated with user convenience were also performed, and the resulting code is designated as the TRIM computer program (Section 3).

3. A sensitivity study was performed to determine the effects of uncertainties in selected input parameters on predicted backwall temperature history (Section 4).

4. Twelve Coating 313/Steel substrate models were tested in the CRPO T-3 facility, for the purpose of obtaining experimental data to be used in validating the TRIM code for Coating 313 (Section 5).

5. The TRIM code has been validated for Coating 313 on a steel substrate and exposed to typical aviation fuel fire heat fluxes, through extensive comparisons of predicted backwall temperature history with experimental data (Section 6).

6. Predictions of backwall temperature history have been made for Coating 313 applied over an intermediate inert insulation (Section 7).

A number of general conclusions can be drawn based upon the results of this study. First, use of Coating 313 over a steel substrate leads to substantial protection of heat-sensitive articles located behind the steel substrate. An uncoated 0.060 in steel plate will reach a backwall temperature of 1000°R in about 30 seconds when exposed to a nominal heat flux of 15 Btu/ft^{2}sec. Application of a 0.040 in layer to Coating 313 extends this time to roughly two minutes. Second, use of an intermediate insulation layer will generally lead to improved protection. However, an optimum ratio of coating thickness to

insulation thickness exists for each combination of impinging heat flux and threshold backwall temperature. The principal future utilization of the TRIM code will be to perform such optimization analyses, for Coating 313 in particular.

It should be emphasized that Coating 313 has been validated and "calibrated" only for Coating 313 in a typical aviation fuel fire environment. In performing this validation, the values eventually used for char heat of formation, Δh_c, and activation energy for the intumescing reaction, E_{aB}, were substantially different from the values based upon data supplied by CRPO. These two properties have a large uncertainty, and improved values are needed. One other Coating 313 property which requries further investigation is the char thermal conductivity. It appears that all remaining properties are either known with sufficient accuracy or, if they have large uncertainties, these uncertainties have only a second-order influence on the predicted backwall temperature history.

Finally, the TRIM code in its present form can be applied to the general intumescing material/arbitrary environment problem, provided the proper input data are available.

REFERENCES

1. Sawko, P. M., Fontes, E. J., and Riccitiello, S. R., "An Intumescent Coating for Improved Fuel Fire Protection of Heat Sensitive Articles," Journal of Paint Technology, Vol. 44, No. 571, August 1972, pp. 51-55.

2. Fohlen, G. M., Parker, J. A., Riccitiello, S. R. and P. M. Sawko, "Intumescence: An In-Situ Approach to Thermal Protection," presented at NASA Conference on Materials and Improved Fire Safety, Manned Space Center, Houston, Texas, May 6-7, 1970.

3. Riccitiello, S. R., Fish, R. J., Parker, J. A., and Gustafson, E. J., "Development and Evaluation of Modified Isocyaurate Foams for Low Heating Rate Thermal Protection," J. Cellular Plast., Vol. 7, No. 2, 1971.

4. Parker, J. A., Fohlen, G. M., Sawko, P. M., and Griffin, R. N., Jr., "The Use of a Salt of P-Nitroaniline as a Component for Intumescent Coatings," SAMPE Journal, August/September 1968.

5. Lamb, B., Clark, K. J., and Green, K. A., "Analysis of the Thermal Response of Parachute Fabrics in Crash Fire Environments," Aerotherm Report 74-96, February 1974.

6. "Data Reduction, Mathematical Analysis, and Mathematical Modeling in Support of Thermal Analysis Program," Aerotherm Proposal 2295, prepared for Fort Rucker, Alabama, May 17, 1972.

7. Powars, C. A. and Kendall, R. M., "User's Manual, Aerotherm Chemical Equilibrium (ACE) Comptuer Program," Aerotherm Report UM-69-7, May 1969.

8. Kendall, R. M., "An Analysis of the Coupled Chemically Reacting Boundary Layer and Charring Ablator, Part V, A General Approach to the Thermochemical Solution of Mixed Equilibrium-Nonequilibrium, Homogeneous or Heterogeneous Systems," Aerotherm Report No. 66-7, Part V, Contract NAS 9-4599, March 14, 1967.

9. "User's Manual, Aerotherm Equilibrium Surface Thermochemistry Computer Program, Version 3," AFRPL-TR-70-93, April 1970.

10. "User's Manual, Aerotherm Charring Material Thermal Response and Ablation Program," AFRPL-TR-70-92, April 1970.

11. Moyer, C. B. and Rindal, R. A., "An Analysis of the Coupled Chemically Reacting Boundary Layer and Charring Ablator, Part II, Finite Difference Solution for the Indepth Response of Charring Materials Considering Surface Chemical and Energy Balances," Aerotherm Report No. 66-7, Part II, Contract NAS 9-4599, March 14, 1967.

12. Alger, R. S. and Capener, E. L., "Aircraft Ground Fire Suppression and Rescue Systems - Basic Relationship in Military Fires, Phase I and II," AGFSRS-72-1, Tri Service System Program Office for Aircraft Ground Fire Suppression and Rescue, SMF, WPAFB, Ohio, April 1972.

13. JANAF Thermochemical Tables, The Dow Chemical Co., Midland, Michigan.

14. Eckert, E. R. G. and Drake, R. M., Jr., Heat and Mass Transfer, McGraw-Hill Book Company, Inc., New York, 1959.

15. Kays, W. M., Convective Heat and Mass Transfer, McGraw-Hill Book Company, New York, 1966.

16. Third Monthly Progress Report, Analytical Modeling of Intumescent Coating Thermal Protection System in a JP-5 Fuel Fire Environment, Aerotherm Project 7080, Contract NAS2-7709, September 11 - October 10, 1973.

17. Cagliostro, D. E., "Memorandum to S. Riccitiello," NASA Ames CRPO, July 24, 1973.

18. Goldsmith, A., Hirshhorn, H. J., and Waterman, T. E. "Thermophysical Properties of Solid Materials," Armour Research Foundation for Wright Air Development Division (WADC Technical Report 58-476) under Contract AF 33(616) 5212 Project No. 7381, Wright Patterson AFB, Ohio, November 1960.

19. "Engineer's Guide to Thermal Insulation," Vol. 71 No. 5 Materials Engineering Rheinhold Publishing Co. Stamford, Connecticut, May 1970.

20. "User's Manual, Aerotherm Transient Response of Intumescing Materials (TRIM), Aerotherm Report No. UM-74-43, April 1974.

Appendix A

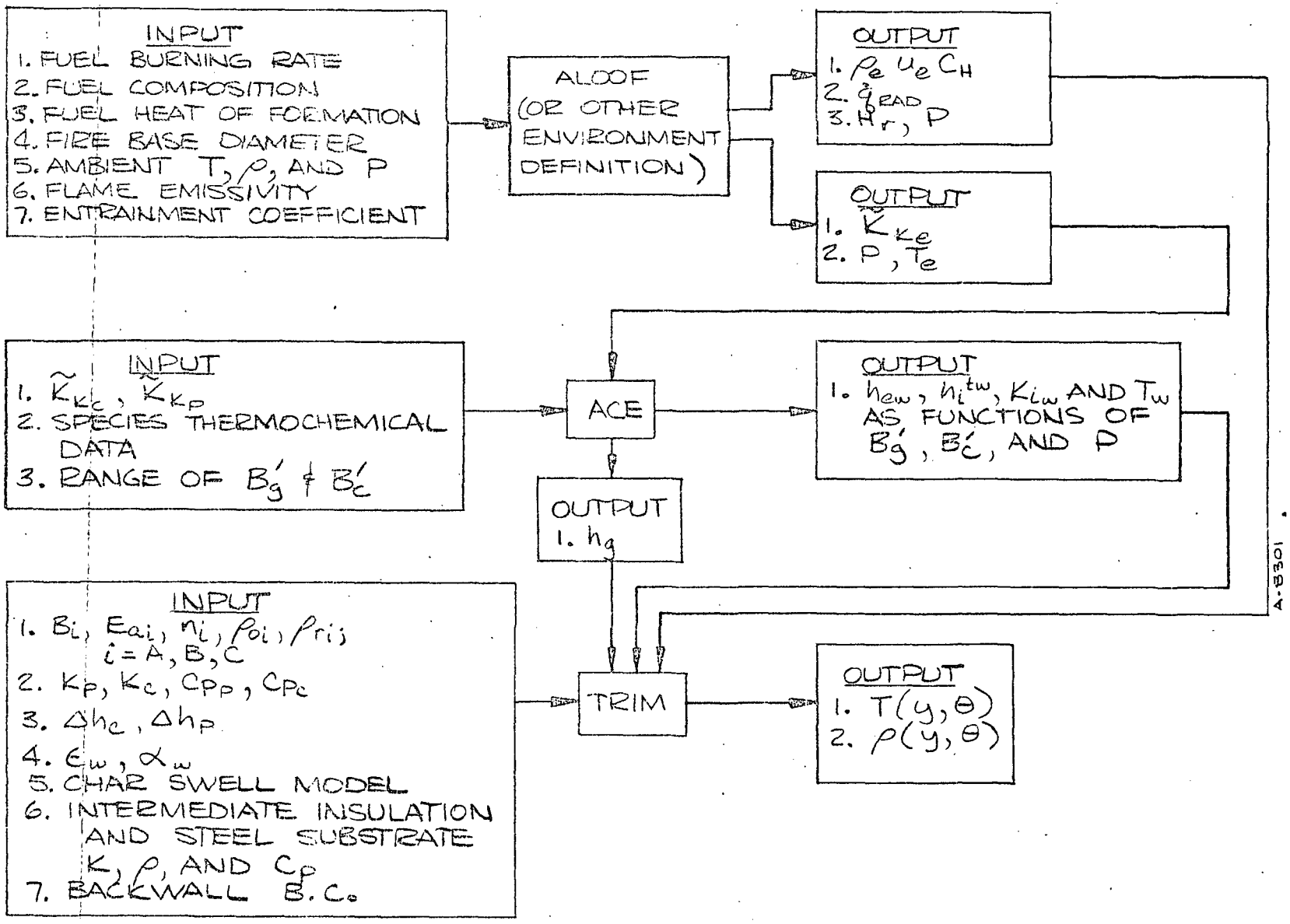

Figure A-1. Flow Diagram Showing Input and Output Data Involved In Three-Step Prediction Procedure

APPENDIX B

INCORPORATION OF THE SWELL FACTOR IN THE IN-DEPTH ENERGY EQUATION

In Section 3, the statement was made that nodal swelling affects only the conduction term in the in-depth energy equation. This fact is demonstrated rigorously in the following paragraphs.

As pointed out in Section 2.2, for the fuel-rich heating environments of interest in this study negligible thermochemical ablation of the char occurs. If, in addition, no swelling were to occur when Coating 313 decomposes, the position of its exposed surface would then remain fixed. This fact is used to simplify the following arguments, in that the in-depth energy equation is referenced to the laboratory coordinate system. It can be shown, however, that the same arguments hold for an in-depth energy equation referenced to a coordinate system moving at the thermochemical recession rate of the exposed surface.

Consider the sketch shown in Figure B-1. A one-dimensional thickness of intumescent coating is depicted. A laboratory coordinate system is attached to the fixed backwall. The y-coordinate is used to locate a point in a hypothetical nonswelling material, that is, one whose total thickness is equal to T_i at all times. The y'-coordinate system is used to locate the same point in the actual swelling material. The two coordinate systems are related by the swell factor defined by Equation (3-1):

$$\delta y' = E_f(y,\theta)\ \delta y$$

$$y'(\theta) = \int_0^y E_f(y,\theta)\ dy \qquad \text{(B-1)}$$

An energy balance can be written for the differential control volume attached to the y' coordinate system. A unit cross-sectional area is assumed. Terms contributing to the energy balance are depicted in Figure B-1. They include the time-rate-of-change of energy storage in the control volume, $\rho h \delta y'$, the conduction heat flux, $-k\ \partial T/\partial y$, and the passage of pyrolysis gas generated due to in-depth decomposition, $\dot{m}''_g h_g$. The energy balance requires that

change in energy storage = energy in - energy out

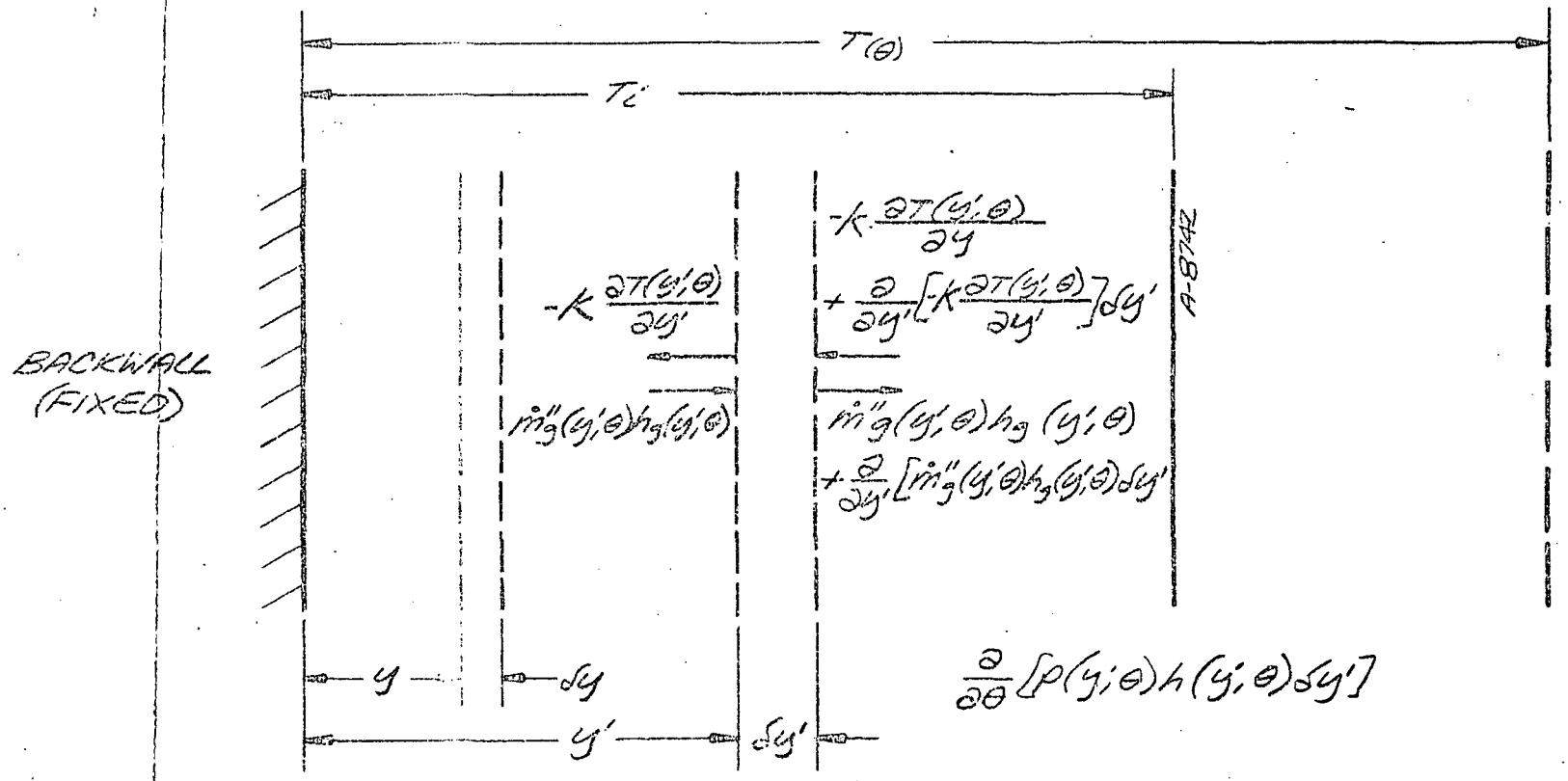

T_i = INITIAL TOTAL COATING THICKNESS

$T(\theta)$ = TOTAL THICKNESS OF PARTIALLY-DECOMPOSED, SWELLED COATING AT TIME θ.

Figure B-1. Schematic of 1-D Swelling Material with Swelling and Nonswelling Coordinate Systems

Thus,

$$\frac{\partial}{\partial\theta}[\rho(y',\theta)h(y',\theta)\delta y'] = \frac{\partial}{\partial y'}[k\frac{\partial T(y',\theta)}{\partial y'}]\delta y' + \frac{\partial}{\partial y'}[\dot{m}''_g(y',\theta)h_g(y',\theta)]\delta y' \qquad (B\text{-}2)$$

Similarly, the conservation of mass equation can be written as

$$\frac{\partial}{\partial\theta}[\rho(y',\theta)\delta y'] = \frac{\partial}{\partial y'}[\dot{m}''_g(y',\theta)]\delta y' \qquad (B\text{-}3)$$

Equations (B-2) and (B-3) will now be transformed to the y-coordinate system which, unlike the y'-coordinate system, is invariant with time. First, it is assumed that the only effect of swelling is to translate the partially-decomposed material at location y to location y'. The small amount of mechanical energy expended when the material undergoes swelling is ignored. Since the thermochemical state of the material is assumed to remain unchanged through the translation,

$$T(y',\theta) = T(y,\theta) \qquad (B\text{-}4)$$

Equation (B-4), in conjunction with the fact that both the partially-decomposed state of the material and the composition of the pyrolysis gas are unchanged through the translation, requires that

$$\begin{aligned} h(y',\theta) &= h(y,\theta) \\ h_g(y',\theta) &= h_g(y,\theta) \end{aligned} \qquad (B\text{-}5)$$

Finally, due to conservation of mass, the flux of pyrolysis gases past y is the same as that past the swelled coordinate y':

$$\dot{m}''_g\ (y',\theta) = \dot{m}''_g(y,\theta) \qquad (B\text{-}6)$$

In other words, the total amount of pyrolysis gases generated per unit time below a point in the material is independent of how that point moves when the material swells.

Incorporation of Equations (B-1) and (B-6) into Equation (B-3) gives

$$\frac{\partial}{\partial\theta}[\rho(y',\theta)\delta y'] = \frac{\partial}{\partial y}[\dot{m}''_g(y,\theta)]\delta y \qquad (B\text{-}7)$$

But, for the y-coordinate system, the conservation-of-mass equation is written as:

$$\frac{\partial}{\partial\theta}[\rho(y,\theta)\delta y] = \frac{\partial}{\partial y}[\dot{m}''_g(y,\theta)]\delta y \tag{B-8}$$

Thus,

$$\rho(y',\theta) = \frac{\rho(y,\theta)}{E_f(y,\theta)} \tag{B-9}$$

Equations (B-1), (B-5), (B-6), and (B-9) can now be used to transform Equation (B-2) into the following form:

$$\frac{\partial}{\partial\theta}[\rho(y,\theta)h(y,\theta)] = \frac{\partial}{\partial y}\left[\frac{k}{E_f(y,\theta)}\frac{T(y,\theta)}{\partial y}\right] + \frac{\partial}{\partial y}[\dot{m}''_g(y,\theta)h_g(y,\theta)] \tag{B-10}$$

where the δy's have been cancelled out of the equation. It is observed that Equation (B-10) is simply the in-depth energy equation referenced to the non-swelling y-coordinate system, with one modification. The thermal conductivity is divided by the instantaneous swell factor. It follows that the swelling process affects only the net conduction term, and with this modification a solution to the energy equation for the hypothetical nonswelling material also represents a solution to the actual swelling material. It should be reiterated, however, that in using this approach the decomposition kinetics (Section 2, Table 2-2) must also be based upon the hypothetical nonswelling material.

485 CLYDE AVENUE, MOUNTAIN VIEW, CALIFORNIA 94042

TELEPHONE (415) 964-3200 TELEX: 34-6391